FG 12

NRL Memorandum Report 3377

Final Report
Direct Laboratory Funded Program
Reliability Criteria for Advanced Structural Materials/Fast Craft and Ships

R. W. JUDY, JR., EDITOR

September 1976

NAVAL RESEARCH LABORATORY
Washington, D.C.

SECURITY CLASSIFICATION OF THIS PAGE (When Data Entered)

REPORT DOCUMENTATION PAGE

READ INSTRUCTIONS BEFORE COMPLETING FORM

1. REPORT NUMBER
NRL Memorandum Report 3377

2. GOVT ACCESSION NO.

3. RECIPIENT'S CATALOG NUMBER

4. TITLE (and Subtitle)
~~FINAL REPORT~~ – DIRECT LABORATORY FUNDED PROGRAM — RELIABILITY CRITERIA FOR ADVANCED STRUCTURAL MATERIALS/FAST CRAFT AND SHIPS

9

5. ~~TYPE OF REPORT~~ & PERIOD COVERED
Final report.

6. PERFORMING ORG. REPORT NUMBER

7. AUTHOR(s)
R. W. Judy, Jr., Editor

8. CONTRACT OR GRANT NUMBER(s)

12 163 p.

9. PERFORMING ORGANIZATION NAME AND ADDRESS
Naval Research Laboratory
Washington, D.C. 20375

10. PROGRAM ELEMENT, PROJECT, TASK AREA & WORK UNIT NUMBERS
~~NRL Problem M01-25B~~
ZF 54-544-~~002 & N65197~~-75-WR

11. CONTROLLING OFFICE NAME AND ADDRESS
Department of the Navy
Chief of Naval Material
Washington, D.C. 20360

Naval Ship Engineering Center
Center Building
Hyattsville, Maryland 20782

11

12. ~~REPORT DATE~~
Sep[redacted]976

13. NUMBER OF PAGES
162

14. MONITORING AGENCY NAME & ADDRESS(if different from Controlling Office)

14 NRL-MR-3377

15. SECURITY CLASS. (of this report)
UNCLASSIFIED

15a. DECLASSIFICATION/DOWNGRADING SCHEDULE

16. DISTRIBUTION STATEMENT (of this Report)

Approved for public release; distribution unlimited.

17. DISTRIBUTION STATEMENT (of the abstract entered in Block 20, if different from Report)

18. SUPPLEMENTARY NOTES

19. KEY WORDS (Continue on reverse side if necessary and identify by block number)

High-performance ships
Fracture
Corrosion fatigue
Stress-corrosion cracking
Composites
Adhesive bonding

20. ABSTRACT (Continue on reverse side if necessary and identify by block number)

This report summarizes the accomplishments of a three-year program to explore the materials aspects of structural integrity technology for fast craft and ships. Fast craft and ships of the future will be the first Navy experience with fleet ships where high-strength materials will be used in the seawater environment. In contrast to the customary naval structural materials, which are quite "forgiving," higher strength materials have an increased tendency for accelerated crack growth, environmental effects, and fracture; the result of this tendency will be increased safety and next

(Continues)

DD FORM 1 JAN 73 1473 EDITION OF 1 NOV 65 IS OBSOLETE
S/N 0102-014-6601

1

SECURITY CLASSIFICATION OF THIS PAGE (When Data Entered)

251 950

20. Abstract (Continued)

maintenance deficiencies in critical components until sufficient technology and experience in the correct use of such materials is gained. In the three-year program, the properties of current candidate structural materials and promising developmental materials were investigated, using general fracture mechanics methods, to evolve the technology necessary for their safe and economical use in the design of future ships. The emphasis of the program was on fracture, fatigue crack growth, and stress-corrosion cracking of metals in thin-section sizes; an additional part of the program concerned similar studies of high-strength composite materials and adhesive bonding.

CONTENTS

FINAL REPORT
DIRECT LABORATORY FUNDED PROGRAM
RELIABILITY CRITERIA
FOR ADVANCED STRUCTURAL MATERIALS/FAST CRAFT AND SHIPS

As has been the case with other weapons systems and platforms where quantum advances in performance is a primary goal, the future fleet of fast craft and ships must rely on the most advanced structural materials available to attain the desired operational requirements. Historically, development programs for new submarine structures, new aircraft involving radical departures from past configurational concepts, and spacecraft and missiles have been beset from their beginnings with materials-related problems, due to the "learning-curve" exercises that accompany the introduction of new materials. The Navy is only now entering this problem area with respect to the surface ship fleet.

Because the future fast craft fleet must rely on new materials and structural configurations to minimize structural weight, new design practices at sophistication levels well in excess of traditional methods for surface ships must be introduced, including a new set of safety and maintainability factors. Potential problems of safety and reliability for fast craft are expected to be caused by the growth of small defects to sizes which cause catastrophic failure or excessive maintenance burdens over the projected life of the ships. Problems of crack growth and fracture become more prevalent as materials of increasing yield strength are used; this is due both to the increase in sensitivity to accelerated crack growth rates due to environmental effects and a decrease in tolerance for cracks as yield strength is increased. Some problems of this type are beginning to appear early in the hydrofoil strut and foil structures, in "marinized" gas turbine power plants, and in other components of small prototype fast craft and ships, and the problems promise to become more severe as structures become larger and as ship performance requirements and operating hours are extended.

The developing methods to account for the presence of defects and their effect on structure or component life can be summarized as structural integrity (SI) technology. SI technology includes both the materials and design aspects

Note: Manuscript submitted September 10, 1976.

of predicting crack initiation and growth to critical size, including effects of variable loads and environmental effects, and has its maximum potential benefit to the Navy in giving designers the tools for materials selection, establishing design allowables, specification of quality control and fabrication practices, and defining inspection and maintenance intervals on the basis of scientifically rational principles. Further development of the field of fracture mechanics and the implementation of design procedures based on fracture mechanics principles offers the only approach to deal with crack growth and fracture problems in the fast craft and ship fleet.

This DLF program concentrated on the materials aspects of SI technology, and in particular, on materials that are potential candidates for the future fast craft and ship fleet. The principal objective was to advance and consolidate the SI technology required to establish rational reliability criteria for design of fast craft and ships, for selection and development of materials systems, and for definitions of the maturity of developmental materials for fleet usage on a large scale. Most of the emphasis was on metallic materials that are currently in use in aircraft or ships and on developmental materials which show promise for future applications; an exploratory effort in composite materials was also a part of the program.

The DLF program was organized into six major sections along technology lines, each with specific objectives as listed:

A. Fracture Mechanics Technology/Fast Fracture/Integrated Analysis Procedures

Principal Investigator: Mr. R. W. Judy, Jr.

The objective of the work in this section was intended to develop methods for characterizing fracture resistance properties of structural materials in the thickness range 2.54-1.27 cm (0.1-0.5 in.). Materials of high-strength-to-density ratio with elastic-plastic and plastic levels of fracture resistance are of primary importance for future fast craft and ships. An additional objective was to develop and validate methods for translation of materials characterization data concerning crack growth and fracture to analysis procedures which can be used for application of SI technology to current and future fast craft and ship structures.

B. Fracture Mechanics Technology/Fatigue Criteria

Principal Investigator: Mr. T. W. Crooker

The efforts in this section were directed toward development of an engineering basis for assuring that materials selected for advanced fast craft and ship applications will possess adequate resistance to fatigue crack growth encountered in service. This task was performed utilizing the framework of existing fracture mechanics technology for fatigue crack growth. The results of this work serve as the basis for establishing definitive crack growth design criteria which are necessary to assure the operational safety and reliability of fast craft and ships.

C. Fracture Mechanics Technology/Crack Growth and Electrochemical Protection

Principal Investigator: Dr. C. T. Fujii

The work of this section was to evaluate the effects of the salt water environment on the performance of structural metals for fast craft and ships, with the primary effort devoted to stress-corrosion cracking and effects of electrochemical potential. Seawater is a very aggressive corrodent for most structural alloys, and stress-corrosion-cracking problems are expected to occur frequently in many fast craft components. For this reason, the effect of seawater on the behavior of high-strength metal systems must be clearly defined to establish reliable limits of utility for their successful use.

D. Composite Materials Technology

Principal Investigators: Dr. J. V. Gauchel and Miss A. M. Sullivan

The purpose of this section was to study failure mechanisms in composites to formulate failure and design criteria specifically for these materials. Initially, an effort was made to apply existing methods of linear-elastic fracture mechanics to composites to provide a basis for comparison of properties with existing metal systems. The major thrust of the program was to identify critical conditions that comprise structural failure in typical composite structures and to define design criteria based on this information.

E. <u>Bonding Technology</u>

Principal Investigator: Dr. W. D. Bascom

The purpose of this section was to determine the relationship between the chemical composition of high-strength polymers and their mechanical and thermal properties with emphasis on their fracture toughness. These polymers, which include the epoxies, thermosetting polyesters and polyimides, are used in military aircraft and ship structures as the matrix for organic resin fiber composites and as structural adhesives. They also find use as secondary structures (e.g., housing, windows, etc.) and as components in mechanical and electronic devices (e.g., bushings, seals, gears, etc.).

F. <u>Technology Transfer</u>

This section of this report is devoted to summarizing the significant interactions of NRL personnel with other activities, wherein specialized knowledge of the subject matter was used to impact developmental programs or to disseminate the technology. This aspect of the DLF program was one of the more important contributions to the technology base.

G. <u>Bibliography</u>

<u>International Units</u>:

Because of the Department of Defense requirement for use of International Units in techical reports, values of the various parameters measured or calculated in this report are reported in these units throughout the text, with the equivalent English units in parentheses. However, most of the figures in the report were drawn using English units prior to the effective date of the directive; furthermore, many of the figures have several scales cross-referencing the parameters which can or have been correlated. To avoid an unnecessary proliferation of scales on the figures, conversion tables are presented to allow the reader to easily use either set of units. Table 1 presents the conversion factors used to constuct Tables 2 through 4, which contain the detailed conversions.

TABLE 1. CONVERSION FACTORS FOR TERMS USED IN STRUCTURAL INTEGRITY MECHANICS

<u>Distance</u>: 1 in. = 2.54 cm
1 cm = .3937 in.

<u>Stress</u>: 1 ksi = 6.8948 MPa
1 MPa = .1450 ksi

<u>Linear Elastic Fracture Mechanics</u>:

Stress Intensity K:

$$1 \text{ ksi}\sqrt{\text{in.}} = 1.0989 \text{ MPa}\sqrt{\text{m}}$$
$$1 \text{ MPa}\sqrt{\text{m}} = .910 \text{ ksi}\sqrt{\text{in.}}$$

Ratio K_I/σ_{ys}:

$$1\sqrt{\text{in.}} = 1.5937\sqrt{\text{cm}}$$
$$1\sqrt{\text{cm}} = .6275\sqrt{\text{in.}}$$

Initiation Energy $\mathcal{J}$:

$$1 \frac{\text{in.lb.}}{\text{in.}^2} = .17512 \frac{\text{KJ}}{\text{m}^2}$$

$$1 \frac{\text{KJ}}{\text{m}^2} = 5.7105 \frac{\text{in.lb}}{\text{in.}^2}$$

<u>Dynamic Tear Test Mechanics</u>:

DT Energy:

1 ft.lb. = 1.3558 Nm
1 Nm = .7376 ft.lb.

R_p

$$1 \frac{\text{ft.lb.}}{\text{in.}^{5/2}} = .01319 \frac{\text{MN.m}}{\text{m}^{5/2}}$$

$$1 \frac{\text{MN}\cdot\text{m}}{\text{m}^{5/2}} = 75.839 \text{ ft.lb.}$$

TABLE 2. ENGLISH-METRIC CONVERSION OF STRESS AND LENGTH

Stress (σ)			Length		
ksi	Value	MPa	in.	Value	cm
0	0	0	0	0	
1.45	10	68.9	.039	0.1	.254
2.90	20	138	.079	0.2	.508
4.35	30	207	.118	0.3	.762
5.80	40	276	.157	0.4	1.02
7.25	50	345	.197	0.5	1.27
8.70	60	414	.236	0.6	1.52
10.2	70	483	.276	0.7	1.78
11.6	80	552	.315	0.8	2.03
13.1	90	621	.354	0.9	2.29
14.5	100	689	.394	1.0	2.54
17.4	120	827	.787	2.0	5.08
20.3	140	965	1.181	3.0	7.62
23.2	160	1103	1.575	4.0	10.16
26.1	180	1241			
29.0	200	1379			
31.9	220	1517			
34.8	240	1655			
37.7	260	1793			
40.6	280	1931			
43.5	300	2068			
58.0	400	-			
72.5	500	-			
87.0	600	-			
101.5	700	-			
116.0	800	-			
130.5	900	-			
145.0	1000	-			

TABLE 3. ENGLISH-METRIC CONVERSION OF TERMS RELATED TO LINEAR ELASTIC FRACTURE MECHANICS

Stress Intensity K_I			Ratio K_I/σ_{ys}			Fracture Initiation Energy $\mathcal{J}$		
ksi$\sqrt{in.}$	Value	MPa$\sqrt{m}$	$(in.)^{1/2}$	Value	$(cm)^{1/2}$	$\frac{in.lb.}{in.^2}$	Value	$\frac{KJ}{m^2}$
0	0	0	0	0	0	0	0	
9	10	11	.06	.1	.16	5.7	1	.17
18	20	22	.13	.2	.32	11.4	2	.35
27	30	33	.19	.3	.48	17.1	3	.53
36	40	44	.25	.4	.64	22.8	4	.70
46	50	55	.31	.5	.80	28.6	5	.88
55	60	66	.38	.6	.96	34.3	6	1.05
64	70	77	.44	.7	1.12	40.0	7	1.23
73	80	88	.50	.8	1.27	45.7	8	1.40
82	90	99	.56	.9	1.43	51.4	9	1.58
91	100	110	.63	1.0	1.59	57.1	10	1.75
109	120	132	.75	1.2	-	114.2	20	3.50
127	140	154	.88	1.4	-	171.3	30	5.25
146	160	176	1.00	1.6	-	228.4	40	7.01
164	180	198	1.13	1.9	-	-	50	8.76
182	200	220	1.25	2.0	-	-	60	10.51
200	220	242				-	70	12.26
						-	80	14.01
						-	90	15.76
						-	100	17.51

TABLE 4. ENGLISH-METRIC CONVERSIONS FOR TERMS USED IN DYNAMIC TEAR TEST MECHANICS

DT Energy			Fracture Extension Resistance Constant R_p					
ft.-lb.	Value	Nm	$\frac{\text{ft.-lb.}}{(\text{in.})^{5/2}}$	Value	$\frac{\text{MNm}}{\text{m}^{5/2}}$	$\frac{\text{ft.-lb.}}{(\text{in.})^{5/2}}$	Value	$\frac{\text{MNm}}{\text{m}^{5/2}}$
0	0	0	0	0	0	-	160	2.11
74	100	136	75.8	1	.013	-	180	2.37
148	200	271	182	2	.026	-	200	2.64
221	300	407	228	3	.040	-	300	3.96
295	400	542	303	4	.053	-	400	5.27
369	500	678	379	5	.066	-	500	6.59
443	600	813	455	6	.79	-	600	7.91
516	700	949	531	7	.92	-	700	9.23
590	800	1085	607	8	.105	-	800	10.55
664	900	1220	682	9	.119	-	900	11.86
738	1000	1356	758	10	.13	-	1000	13.19
885	1200	1627	834	11	.15	-	1200	15.82
1033	1400	1898	910	12	.16	-	1400	18.46
1180	1600	2169	986	13	.17	-	1600	21.09
1328	1800	2440	1061	14	.18			
1475	2000	2712	1138	15	.20			
2213	3000	4067	-	20	.26			
2950	4000	5423	-	30	.40			
3688	5000	6779	-	40	.53			
4425	6000	8135	-	50	.66			
5163	7000	9491	-	60	.79			
5901	8000	10846	-	70	.92			
6638	9000	12202	-	80	1.05			
7376	10000	13558	-	90	1.19			
8851	12000	16270	-	100	1.32			
10326	14000	-	-	120	1.58			
11801	16000	-	-	140	1.85			

A. Fracture Mechanics Technology/
Fracture and Integrated Analysis Procedures

R. W. Judy, Jr., C. A. Griffis, and R. J. Goode

The application of structural integrity (SI) principles to assure the safe operation of fast craft and ships requires as a baseline a knowledge of the capability of the structure to resist failure by extensive fracture due to suddenly imposed loading. This capability is derived from the inherent resistance of the structural material to crack propagation under dynamic loading. The present state of fracture technology is that the structural behavior of metals of brittle, or plane strain, properties can be predicted with a high degree of accuracy. Applications involving the use of materials with appreciable ductility (tough materials) can only be accomplished by engineering methods rather than by analytical methods derived from first principles. Structural design procedures to prevent or control fracture extension (A1) in ductile materials are based on correlation of the appropriate materials properties with the results of structural element tests. The key to successful application of these methods to any problem is an accurate and reliable test method to characterize the fracture resistance inherent to the structural metal. Dynamic Tear (DT) test methods were evolved for this purpose and have been used in studies of aluminum, titanium, and steel in the section-size range of 0.76 to 15.2 cm (0.3 to 6.0 in.). This section presents the results of studies to develop DT test methods for characterizing the fracture resistance properties of thin-section materials in the thickness range of 0.32 to 1.27 cm (0.125 to 0.50 in.).

BACKGROUND

The DT test specimen, Fig. A1, is an edge-notched bar which is loaded dynamically in three-point bending by machines of pendulum or falling weight type. Test specimens are dimensioned according to material thickness; standard configurations for various thicknesses have been established (A2,A3). Energy to fracture the specimen at specified loading rates and temperatures is measured in standard tests. Various analysis procedures based on DT test methods have been evolved over the past several years. These include R-curve characterizations (A4-A6) and Ratio Analysis Diagram

(RAD's) for steels, aluminum alloys, and titanium alloys (A7-A9). It must be emphasized that the DT test is intended for engineering use in providing material characterizations rather than as a tool for precise scientific investigations. For this reason, every effort to simplify test procedures and to minimize test costs has been made.

In past studies (A11-A13), a relation between DT energy values and specimen cross-section dimensions has been established. The equation $E = R_p (\Delta a)^2 B^{1/2}$, where the terms are defined in Fig. A1, has been shown to apply for steels and aluminum alloys in sections above 0.76 cm (0.3-in.). The constant R_p, which is the index of material resistance to fracture, is a geometry-independent parameter. It is important to note that the equation applies only for the plastic and elastic-plastic fracture states. The plane-strain case is best handled by linear-elastic fracture mechanics. Use of the R_p parameter to measure fracture resistance allows independent analysis of mechanical constraint effects and of metallurgical effects. The lightweight, highly efficient structures expected to be used in future fast craft and ships will demand high levels of fracture resistance in thin-section structural materials. For this reason, the major effort in the fracture studies was the development of a reliable method to characterize the fracture resistance properties of such materials and to establish methods to translate these characterizations to a format useful for assessment of structural performance.

Laminated DT Specimen

A test method for characterizing thin-section materials was developed from the DT test to provide continuity between the technology developed for thicker materials. The approach to the problem was to establish that the ductile fracture equation did apply for thin-section materials of interest, using selected aluminum alloys, titanium alloys, and steels as reference materials.

The standard 1.59 cm (5/8-in.) DT specimen plan dimensions, Fig. A2, were utilized so that existing equipment could be used for the experimental part of the study. Lamination techniques, as shown in Fig. A2, were necessary to prevent specimen buckling and to provide sufficient energy to get a good measurement. Using aluminum alloy 5086-H32 in 0.32 cm (0.125-in.) thickness, it was shown that the energy-per-laminate was constant, Fig. A3, and therefore that an averaging method could be used. The next step was to establish the applicability of the ductile fracture equation by testing a matrix of specimens, varying

the thickness B and fracture length dimension Δa, for test specimens machined from 1.27 cm (0.5-in.) thick materials. This was accomplished for aluminum alloys, titanium alloys, and steels that encompassed the range of strength and fracture resistance typical of commercially available materials.

The initial experiments were conducted for aluminum alloys 5086-H32, 6061-T651, 2024-T351, and 7075-T6 using test specimen thicknesses of 0.32, 0.64, and 1.27 cm (0.125, 0.25, and 0.5-in.) (full thickness). Regression analysis of the data to determine the best values of the exponents in the equation $E = R_p \Delta a^x B^y$ showed that the exponents were approximately the same as had been determined for thicker materials, i.e., $x \simeq 2$ and $y \simeq 0.5$. The following procedure was used to demonstrate the applicability of the equation for these materials:

(a) Calculate the best value of R_p for each specimen and average the results to give a characteristic R_p for each material.

(b) Using the characteristic value of R_p for each material and the dimensions of each test specimen, calculate a predicted fracture energy for each specimen.

(c) Compare the predicted energy of step (b) with the energy measured in test.

Figure A4 is a plot of predicted energy vs. measured energy for the aluminum alloys; the close fit of the data to the 1:1 line is evidence of the applicability of the method.

The process for demonstrating the applicability of the ductile fracture equation was repeated for titanium alloys Ti-6Al-2Cb-1Ta-1Mo, Ti-6Al-4V, and Ti-6Al-6V-2Sn in 1.27 cm (0.5-in.) sections. For all of these materials, the conformance of the data to the equation was good, as indicated in Fig. A5. A similar experimental program to verify the applicability of the ductile fracture equation for thin-section steels was also conducted with two samples of HY-130 and one sample of HY-80 as the materials of interest. Figure A6 shows the good correlation of predicted energy and measured energy for these steels.

Ratio Analysis Diagram

The primary purpose of establishing the validity of the ductile fracture equation for thin-section materials was to allow use of existing analysis techniques for interpreting basic material characterization data to structural performance. For thicker-section materials, the RAD is a format

which has been verified for this purpose and which contains all of the parameters necessary for analysis involving thin-section materials.

The RAD framework is formed from the scales of yield strength vs. K_{Ic} and DT energy, Fig. A7. The most prominent features of the RAD are the limit lines and the system of lines of constant K_{Ic}/σ_{ys}. The technological-limit line represents the highest values of fracture resistance measured to date either by DT tests over the entire yield-strength range or by K_{Ic} tests in the elastic fracture range; the lower bound represents the lowest levels of fracture resistance. Reference charts of critical flaw size (A10) are provided by the system of K_{Ic}/σ_{ys} lines.

K_{Ic}/σ_{ys} ratio lines also divide the diagram into regions of expected plastic, plane-strain, and elastic-plastic behavior for given material thicknesses. The separations are determined according to thickness, as shown for the 1.27 cm (0.5-in.) section size in Fig. A7. The critical edge between plane-strain behavior and elastic-plastic behavior is the plane-strain limit, which is determined for a given metal thickness by $B = 2.5\ (K_{Ic}/\sigma_{ys})^2$. The boundary between the elastic-plastic and plastic regimes is the general-yield limit, which is given in terms of metal thickness by $B = 1.0\ (K_{Ic}/\sigma_{ys})^2$. The division of the RAD into three regions provides an engineering index of the fracture state and thereby serves to indicate the type of more detailed design approach required for each case.

The ductile-fracture equation permits entry of material properties for any metal thickness onto the RAD to determine the fracture state. This is done by adding a scale of R_p as calculated from the standard 1-in. DT energy scale. Since R_p is independent of geometry effects, section size is the only factor used to locate the elastic-plastic region on the RAD. For example, the RAD's of Figs. A8, A9, and A10 are drawn for 1.27 cm, 0.64 cm, and 0.32 cm (0.5-in., 0.25-in., and 0.125-in.) section sizes, respectively, with all the data plotted on the diagram using the R_p scale.

To illustrate the value of separating metallurgical variables and mechanical-test variables, consider the data point for the 7075-T6 alloy on Figs. A8, A9, and A10. Since R_p represents the physical properties of the metal, this point, as are all data points, is constant for all three RAD's. However, effects of section size are such that a different fracture state exists for the same material at each of the test thicknesses:

- At B = 1.27 cm (0.5-in.) (Fig. A8), the material has plane-strain properties, a level of fracture resistance that permits unstable crack extension at low elastic stress levels with minimal deformation at the crack tip.

- At B = 0.64 cm (0.25-in.) (Fig. A9), the material has elastic-plastic properties, which is a level of fracture resistance that allows unstable crack propagation at high elastic stress levels with an appreciable amount of crack-tip plasticity.

- At B = 0.32 cm (0.125-in.) (Fig. A10), the material has plastic properties, for which crack extension requires stresses over the yield strength and a higher energy expenditure to "drive" the crack.

Because the effect of section size is so important in determining the fracture state, a parameter for characterizing the fracture resistance properties of ductile materials independently of geometrical effects is essential to evolve a format for interpreting laboratory test results to structural design. Independent analyses of metallurgical aspects and mechanical aspects on the fracture properties of materials are made possible by the use of the R_p parameter associated with RAD analysis procedures.

Studies of thin-section materials, coupled with the background of experience with thicker materials, showed that a wide range of specimen configurations can be used for characterizing the fracture resistance properties of high-strength metals. Because the influence of geometry is well known, a single specimen configuration is sufficient to determine R_p. It is advantageous to use laminated specimen methods for characterization of thin-section metals because the total energy value is higher and is therefore less subject to experimental errors than are those values from tests of a single thickness and because the laminated configuration minimizes statistical variations in properties by averaging. For these reasons, the specimen design shown in Fig. A11 is recommended for DT tests of thin-section materials.

The program to verify the applicability of the ductile fracture equation and the RAD for characterization of material properties and analyses involving these characterizations was completed by a series of experiments involving large panels of aluminum to verify that the R_p values for thin section could be interpreted by the RAD format to correctly predict the behavior of the metal in structures. The test

specimens were tension loaded panels, 50.8 cm (20-in.) wide at thicknesses of 0.32 cm (0.125-in.) and 1.27 cm (0.500-in.) for each of the aluminum alloys in Table A1. Test results were largely qualitative in nature and involved measurements of failure stress relative to the yield, as well as visual observations of the fracture state. In all cases the test results confirmed projections of the behavior of the specimens that were made from the RAD. The experiments thus did verify that the technology developed for thick-section material could be applied for thinner gages.

To complete the investigation, determinations were made of the fracture resistance properties of a variety of aluminum and titanium alloys and HY-80 and HY-130 steels, as in as-rolled sections ranging between 0.25 cm (0.100-in.) and 1.27 cm (0.500-in.). Also included are results of studies of laser welds in the same materials. The alloys and mechanical properties are listed in Table A2, and the data are plotted on the RAD format in Figs. A12-A18. All of the RAD's are scaled for analysis of 1.27 cm (0.5-in.) thick material; procedures for adjustment of the ratio lines for other thicknesses are those described earlier.

Thin-Section Aluminum Alloys

Figure A12 shows data for four aluminum alloys, each in thicknesses of 0.32, 0.64, and 1.27 cm (0.125, 0.25, and 0.5-in.), as indicated by the numbers beside each data point. The materials shown are all commercial alloys and represent materials used in military applications. For example, the 7075-T6 and 2024-T351 alloys have been used extensively for aircraft applications, while the 500 series alloys shown have been used in hull structures of high-performance ships. The 7075-T6 alloy has very high-strength and fracture properties in the plane-strain region for the 1.27 cm (0.5-in.) thickness of the RAD of Fig. A12; this property is one reason that the 7000 series alloys are not utilized in marine applications. Conversely, the 5086-H116 and H32 alloys are currently used as hull structural materials for hydrofoil and surface effect ships type craft because of their weldability and because of the high degree of toughness indicated by their position high in the plastic fracture regime of the RAD. In this alloy system and in the 5456 alloy (not shown), the H116 temper or the H117 temper, which has equivalent properties, is preferred to the H32 temper to alleviate delamination in seawater which is inherent to the H32 temper.

Aluminum alloy 6061-T651 has a high degree of fracture resistance for its strength level; however, it is not

considered appropriate for marine applications because it is a heat-treated alloy and therefore weld properties approaching that of parent material cannot be attained. The 2024-T351 alloy has a strength level intermediate between 7000 and 5000 series alloys; and in addition, is resistant to stress-corrosion cracking, which has led to its use in commercial aircraft. In the alloy systems shown in Fig. A12, a considerable body of fracture data is available for thicker sections; the data for thin sections correspond very closely with this data bank. This is additional evidence that the thin-section DT test can be utilized to characterize the fracture properties of thin-gage aluminum alloys and that the RAD can be used to provide an index of expected structural performance for thin-section materials.

Thin-Section Titanium Alloys

Titanium alloys in thin-section have much to recommend their use in fast craft because of their high-strength-to-density properties and because of the backlog of information being accumulated by aircraft producers, who are using increasing quantities of various alloys on military aircraft. The Navy has had an extensive program for several years to develop a weldable titanium alloy system for applications requiring heavy-section material (thicknesses in excess of 2.54 cm (1-in.). This study concentrated on lighter gage materials, again with emphasis being placed on development of engineering test and analysis methods to facilitate the use of titanium alloys on a significant scale in fast craft.

Titanium alloy, Ti-6Al-2Cb-1Ta-1Mo (6211), is the alloy system of current interest for heavy-section applications and has been developed to the point where the alloy is available commercially in a variety of product forms. To define the properties of the commercial thin-section material, the 6211 alloy in sections ranging from 0.25 cm to 1.27 cm (0.100-in. to 0.5-in.) was characterized by the laminated DT specimen methods previously described. For titanium alloys, a reference temperature of 0°C (32°F) was used as a standard for the DT tests. This is because titanium alloys have a very gradual transition in fracture resistance with change in temperature, as opposed to many steels which have a sharp temperature transition and aluminum alloys which have little or no temperature transition. Data for the thin-section 6211 alloy are plotted on the titanium RAD in Fig. A13, which also shows the zone including data for plate materials and weld metal in thicknesses of 2.54-7.62 cm (1-3 in.). Plotting values of yield strength and R_p for the 6211 alloy in the gages indicated by the small numbers in Fig. A13 show that the strength is increased and the fracture resistance

decreased in comparison to heavier-section materials. All of the thin-section 6211 sheets had fracture resistance levels in the plastic fracture range for the 1.27 cm (0.5-in.) section. It is noted that the margin of fracture resistance for a given thickness of material is in proportion to the distance from the plane-strain limit line for that thickness. Since the plane-strain limit ratio decreases with decreasing thickness, the margin of fracture resistance for the thin-gage materials is about the same as for the thicker gages.

Fracture resistance data for two other alloy systems - Ti-6Al-4V (6-4) and Ti-6Al-6V-2.5Sn (6.6-2.5) - are shown in Fig. A14. The thickness range for these materials was 0.23 to 1.27 cm (.090 to .500-in.). The 6.4 alloy selection included materials of commercial quality (oxygen content ~0.15 wt. pct.) and ELI grade (oxygen content ~0.12 pct.), while the 6-6-2.5 alloy was commercial purity. The fracture resistance of both alloy systems corresponded to the RAD regions occupied by fracture data for thicker materials of the same composition.

Thin-Section Steels

The RAD for thin-section steels, Fig. A15, shows the data for the three samples of material used to verify the use of the laminated DT test specimen for characterizing the fracture resistance property of steels. The two samples of HY-130 appear to represent extremes of the quality range expected for HY-130. The HY-80 sample appears to be quite low in fracture resistance in comparison to the range of values previously established for this material. However, the test data were consistent in that values of R_p measured with different test specimen configurations for each sample of material were reasonably uniform. Because of the extensive backlog of test data on steels, this investigation was confined to these three materials.

Laser Welds of High-Strength Materials

A program was conducted to define the SI technology-related properties of laser welds in HY grade steels, 17-4 PH steel, and in Ti-6211 alloy. The welds were made by the United Aircraft Corporation and were all square butt fusion welds. As the technology of laser welding is largely experimental in nature, the test samples were a "best effort" basis and in reality represent the first attempt at making welds in these materials for a critical evaluation. The test materials, thicknesses, welding parameters, and comments concerning the weld quality resulting from visual and X-ray inspection are presented in Appendix A; fracture data are presented in Table A3.

Fracture resistance data for HY type steels in terms of the R_p parameter and material yield strength are shown on the RAD in Fig. A16. Zonal regions for fracture resistance of thicker-section materials of each steel type are shown for purposes of comparison; the code at the right side of Fig. A16 shows the alloy type and thickness involved for each test material. Duplicate points indicate different welding parameters. The R_p parameter was measured with a laminated specimen for the 0.64 cm (0.25-in.) thick materials and with a full-thickness specimen for the others. The fracture resistance data were somewhat lower than expected for all of the materials and might approximate the levels typical of the shielded-metal-arc process. Higher levels of fracture resistance would be expected for the GMA or GTA welding processes in the same alloy systems. It is strongly emphasized, however, that laser welding technology is still in its infancy; and that development of the technology would most likely result in properties that would be much improved over the data presented here. It can be noted that plastic levels of fracture resistance for materials in thicknesses exceeding 2.54 cm (1-in.) were attained for all of the HY grade steels.

Laser welds in 17-4 PH stainless steel were of very good quality compared to the base material properties, as shown on the RAD in Fig. A17. Laser welds of two types were investigated: (a) the as-welded properties of 2.54 cm (1-in.) thick section and (b) properties of 1.59 cm (0.625-in.) material in the H1050 temper condition. (The H1050 temper corresponds approximately to the heat treatment given struts and foils on the PHM hydrofoil, for which 17-4 PH steel is a candidate material.) A slight loss of fracture resistance resulted from the welding, as would be expected. However, the weldments were of sufficiently high quality to meet the minimum DT energy levels specified for strut/foil materials on the PHM program. (This is discussed in more detail in the section on technology transfer.)

The fracture resistance levels of laser welds in 0.64 cm (0.25-in.) thick Ti-6211 compared very favorably with the properties of parent material, as is shown in Fig. A18. The properties of two laser welds corresponded almost exactly with properties of the parent material, both of which approached the technological limit established for plate materials of thicker section.

Laser welds attempted in 1.27 cm (0.5-in.) thick aluminum alloys were unsuccessful. The welding parameters used produced a highly irregular weld bead, which was not suitable for evaluation by mechanical test methods. This problem does not indicate that laser welds cannot be made

in aluminum alloys, but it does serve as an indication that a development effort is required to produce laser welds in aluminum of acceptable quality for use in Navy applications.

HY-180 Steels

Future aircraft and fast craft and ships are developing material requirements along concurrent lines to meet the common problem of attaining maximum structural integrity with minimum structure weight. The best example of this is the proposed use of the 10Ni steel developed by the Navy as a potential submarine structural material (HY-180) for the wing carry-through structure of the B-1 bomber. The choice of the material for the Air Force program was predicated on its high inherent fracture resistance property, which was a prime parameter in development of the alloy system. In the B-1 program, a full-scale HY-180 wing carry-through structure was built and tested to demonstrate its tolerance for the growth of flaws under extreme loading conditions.

The qualities of the 10Ni steel which make it attractive for structural components that are critical to the survival of the aircraft are the same qualities that are important for critical components in large fast craft. Because of the potential need for such materials in the development of future fast craft, a survey of the properties of this alloy that pertain to the particular problems facing such craft was included in the DLF project.

Four samples of 10Ni steel were made available to NRL by the Convair Aerospace Division of General Dynamics. The samples included a forging 16.3 cm (6.4-in.) thick, a plate 8.9 cm (3.5-in.) thick, a plate 4.83 cm (1.9-in.) thick, and a 24.9 cm (9.8-in.) long weldment in 3.8 cm (1.5-in.) thick plate. All of the plate materials were processed by double vacuum (VIM-VAR) procedures, which are known to impart the highest attainable fracture resistance properties to this alloy system, as well as to others.

The DT energy values for HY-180 steels are plotted on the steel RAD in Fig. A19, which compares the materials of this study with other steel systems of interest to the Navy. One of the products of past Navy research is the delineation of the chain of materials of highest quality (optimum strength/toughness) that is associated with double vacuum processing. The chain of material property data zones indicates that alloying elements control strength and that cleanliness (processing) controls fracture properties. The zone coded "10-8-12" is Navy data for 2.54 cm (1-in.) thick plate of the nominal HY-180 composition.

Data for the B-1 bomber program are represented by the cross-hatched zone shown on the RAD in Fig. A19. This zone lies in the region of elastic-plastic and plastic properties for the 2.54 cm (1-in.) thickness of the analysis, which implies that brittle fracture is not expected for any of the materials in 2.54 cm (1-in.) thickness. At a greater thickness fracture might become a problem area, even though the K_{Ic}/σ_{ys} value is high. For thinner sections, the potential for fracture diminishes, since larger flaws and stresses in excess of the material yield strength are required for fracture.

For applications involving a need for high-strength, tough materials on weight critical structures, the HY-180 steel offers attractive properties; however, much would hinge on the properties related to environmental crack growth.

Verification of FM for SCC

The value of using fracture mechanics (FM) test methods to define the resistance of structural metals to stress-corrosion cracking (SCC) and to fracture stems from the capability to translate K numbers that describe material properties to physical parameters - stress and crack size - that are readily understood by designers. The translation capability is in the form of equations of the type $K/\sigma_{ys} = \alpha\, \sigma/\sigma_{ys} \sqrt{a}$, where a = crack size, σ/σ_{ys} = stress level relative to yield, and α = geometry dependent constant. One of these is the surface flaw equation which describes a part-through crack in a tensile stress field, $[(K_I/\sigma_{ys})^2 = 1.21\ (\sigma/\sigma_{ys})^2\ \pi a/Q]$, where Q is a constant related to flaw shape and σ/σ_{ys}; this equation is widely used because natural flaws usually occur in this configuration. The applicability of the equation has been proven for brittle fracture by laboratory experiments and by analysis of service failures. Because of its general applicability, the surface-flaw equation has been utilized to construct analytical diagrams, such as the plot of crack depth vs. ratio, Fig. A20, and has been used to define the significance of K_{Ic}/σ_{ys} ratio lines on the RAD.

It is considered a reasonable extrapolation of fracture mechanics technology to use the surface-flaw equation for the case of SCC by substituting the parameter K_{Iscc} in the equation; the recently developed three-part RAD for analysis of SCC is based on this assumption. In this application, the K_{Iscc} parameter is used to predict the flaw size/stress level necessary for the onset of crack growth due to SCC. The objective of this investigation was to experimentally determine whether values of K_{Iscc} measured by cantilever-bend

tests (see section on FM Technology/Crack Growth and Electrochemical Protection) could be used to predict the stress level/flaw size combination necessary to cause crack growth from a surface crack.

The materials selected were 17-4 PH steel in the H1050 temper and SAE 4340 steel because the SCC properties of both were well known. Large panels having known surface crack geometries were tested according to a schedule designed to demonstrate the accuracy of the surface-flaw equation. The first step was to apply a stress-intensity level just below that calculated to be necessary for crack growth in a salt-water environment (i.e., just below K_{Iscc}) for a reasonable time period to establish that no crack growth would occur. Following this, the stress intensity was raised a small amount to a value just above that necessary to cause crack growth. All calculations for the tensile panels were made with the surface-flaw equation using characteristic K_{Iscc} values determined in previous studies by cantilever-bend type specimens. To obtain variations in the K_{Iscc} ratio, the conditions of cathodic coupling were varied in the 17-4 PH steel; the same effect was attained in the 4340 steel by heat treating the specimens to different yield strengths.

Two test specimen configurations were used, as shown in Fig. A21. Part-through flaws were machined in each specimen by EDM procedures followed by fatiguing in bending to maximize crack-tip acuity. In tests of 17-4 PH, where specimens were cathodically coupled to aluminum, zinc, or magnesium, the electrode size was chosen so that wetted areas of specimen and of electrode were approximately equal. The stresses on the specimens were measured by strain gages, while crack growth was monitored by a strain-gaged beam clip gage and by strain gages at the tip of the original crack. Calculations for test purposes were made with the best estimates of crack depth. Final calculations were made with the crack dimensions (machined notch plus fatigue crack) measured at the completion of the test for each specimen.

Results of the test program are shown in Table A4 and in Figs. A22-27. Figure A22 is a plot of K_{Iscc} or K_{sc} (the K_{sc} term represents a test where the specimen failure was due to a mechanism other than slow crack growth) vs. yield strength to show the variables introduced into the program. The titanium data are from earlier investigations and are included to indicate the completeness of the survey.

The experimental work for 17-4 PH steel is summarized on the crack-depth ratio plot in Fig. A23. This plot is a

convenient format to show the relation between the three parameters of interest - ratio K_I/σ_{ys}, which is the material property of interest, flaw size, which is shown as a/Q (flaw size normalized by shape parameter) on the left-hand scale and as absolute flaw size on the right-hand scales, and applied stress, σ_N/σ_{ys}. As shown in the code, the end points of the cross-hatched bars indicate the imposed test conditions, the no-fracture point is on the left and the point where the specimen failed is on the right. The arrow representing the characteristic K_{Iscc}/σ_{ys} ratio should fall between the end points for a successful test to verify the applicability of the equation. All of the test specimens except three met this condition; in two cases the specimen failed because the initial applied K level exceeded the K_{Iscc}/σ_{ys} ratio due to inaccurate estimates of the crack depth. The third specimen (a/Q of 0.3) maintained a K/σ_{ys} above the K_{Iscc}/σ_{ys} at the initial load but failed at the first load increment. Since the differences in applied stress and K/σ_{ys} were small, and since another specimen of nearly the same K_{Iscc}/σ_{ys} and a/Q failed as predicted, this result is not considered anomalous.

Results for 4340 steel and for titanium are presented in Figs. A24 and A25, respectively. The 4340 steel was included to get a combination of high-strength and low K_{Iscc} values. Both tests were at low relative stress levels, one specimen having a small flaw and the other having a large flaw. Both of the tests were considered to verify the applicability of the surface flaw equation. The titanium results of Fig. A25 were not a part of the DLF investigation but are included to indicate the completeness of the verification effort. The two points at $K_{Iscc}/\sigma_{ys} = 0.3$ are for alloy Ti-7Al-2Cb-1Ta, which is very sensitive to SCC; both of these gave very good confirmation of the equation. The point at K_{sc}/σ_{ys} ratio 1.59 $\sqrt{cm}$ (1.0 $\sqrt{in.}$) is for alloy Ti-6Al-2Cb-1Ta-1Mo in 50.8 cm (2-in.) thick section; this alloy appeared to be immune to SCC from both cantilever and surface-flawed panel tests. However, the surface flaw equation gave very good correlation with cantilever-bend predictions, even though the thickness of the specimens in both tests was not large enough to satisfy plane-strain requirements.

To show the agreement of test results from cantilever-bend tests and surface-cracked tensile panel tests, the data are plotted as one vs. the other in Fig. A26. As with the preceding plots, the length of the bar connecting "no-growth" and "growth" points indicated the applied K_I/σ_{ys} ratio in the surface-flawed specimen tests. The intersection of the 1:1 correspondence line with the bar is the K_{Iscc}/σ_{ys}

value for the particular material; the "growth" point should therefore fall on the line or to the right of it to verify the surface flaw equation, as was the case for all tests.

A summary of the test data is shown in Fig. A27 to illustrate the areas of the crack-depth-ratio chart that have been verified for engineering use in predicting initiation of SCC crack growth. The verification is reasonably complete for the entire diagram; the most obvious data voids are at the combination of large crack sizes and K_{Iscc}/σ_{ys} values in the range of 0.64-1.27 $\sqrt{cm}$ (0.4-0.8 $\sqrt{in.}$) and at stress levels in the range of 1.27-1.59 $\sqrt{cm}$ (0.8-1.0 $\sqrt{in.}$) for all crack sizes and K_{Iscc}/σ_{ys} values. Some of these combinations are expected to be covered in future work.

SUMMARY

The primary objective of this effort was to develop test methods and engineering analysis procedures to describe the fracture resistance levels that are of interest for construction of the future fleet of fast craft and ships. Such craft are expected to be highly sensitive to the weight of basic components and therefore will utilize high-strength materials, which will cause an increased sensitivity to fracture. In developing an understanding of the fracture process in thin-section materials, an attempt was made to characterize a group of metals representing the range of current commercial alloys as well as some exotic materials for specialized applications.

These objectives were met by the development of test methods based on the Dynamic Tear test, using a technique of laminating specimens and application of an equation relating specimen dimensions and total energy to a parameter - R_p - which is descriptive of the inherent resistance of a material to fracture extension. Much of the experimental program was devoted to demonstrating the validity of the equation, which had been derived in earlier studies of thick-section materials, to the thinner, high-strength materials. An additional experimental effort was given to demonstrating that the R_p values could be projected to assess structural performance in a general fashion through the use of Ratio Analysis Diagram procedures. It was noted that the minimum acceptable level of fracture resistance for Navy ship structures and components is non-brittle, or plastic fracture. Finally, the test methods and analysis procedures were used to characterize the behavior of several steels, aluminum alloys, and titanium alloys of potential interest for future fast craft and ships. Included in this survey were samples of laser welds in several of the project materials, with the caveat that the laser welding technology has not matured

REFERENCES

A1. R. W. Judy, Jr., "Review of Principles for Assurance of Structural Integrity," NRL Memorandum Report 2501, Sept. 1972.

A2. E. A. Lange, P. P. Puzak, and L. A. Cooley, "Standard Method for the 5/8-Inch Dynamic Tear Test," NRL Report 7159, Aug. 27, 1970.

A3. P. P. Puzak and E. A. Lange, "Standard Method for the 1-Inch Dynamic Tear Test," NRL Report 6851, Feb. 13, 1969.

A4. W. S. Pellini and R. W. Judy, Jr., "Significance of Fracture Extension Resistance (R-Curve) Factors in Fracture-Safe Design for Nonfrangible Metals," Welding Research Council Bulletin 157 (1970) and NRL Report 7187, Oct. 19, 1970.

A5. R. J. Goode and R. W. Judy, Jr., "Fracture Extension Resistance (R-Curve) Features of Nonfrangible Aluminum Alloys," NRL Report 7262, June 11, 1971.

A6. R. W. Judy, Jr. and R. J. Goode, "Fracture Extension Resistance (R-Curve) Concepts for Fracture-Safe Design with Nonfrangible Titanium Alloys," NRL Report 7313, Aug. 16, 1971.

A7. W. S. Pellini, "Advances in Fracture Toughness Characterization Procedures and in Quantitative Interpretations to Fracture-Safe Design for Structural Steels," Welding Research Council Bulletin 130, May 1968, and NRL Report 6713, Apr. 3, 1968.

A8. R. W. Judy, Jr., R. J. Goode, and C. N. Freed, "Fracture Toughness Characterization Procedures and Interpretations to Fracture-Safe Design for Structural Aluminum Alloys," NRL Report 6871, Mar. 31, 1969, and Welding Research Council Bulletin 140, May 1969.

A9. R. J. Goode, R. W. Judy, Jr., and R. W. Huber, "Procedures for Fracture Toughness Characterization and Interpretations to Failure-Safe Design for Structural Titanium Alloys," Welding Research Council Bulletin 134, Oct. 1968, and NRL Report 6779, Dec. 5, 1968.

A10. W. S. Pellini, "Criteria for Fracture Control Plans," NRL Report 7406, May 11, 1972.

REFERENCES

A1. R. W. Judy, Jr., "Review of Principles for Assurance of Structural Integrity," NRL Memorandum Report 2501, Sept. 1972.

A2. E. A. Lange, P. P. Puzak, and L. A. Cooley, "Standard Method for the 5/8-Inch Dynamic Tear Test," NRL Report 7159, Aug. 27, 1970.

A3. P. P. Puzak and E. A. Lange, "Standard Method for the 1-Inch Dynamic Tear Test," NRL Report 6851, Feb. 13, 1969.

A4. W. S. Pellini and R. W. Judy, Jr., "Significance of Fracture Extension Resistance (R-Curve) Factors in Fracture-Safe Design for Nonfrangible Metals," Welding Research Council Bulletin 157 (1970) and NRL Report 7187, Oct. 19, 1970.

A5. R. J. Goode and R. W. Judy, Jr., "Fracture Extension Resistance (R-Curve) Features of Nonfrangible Aluminum Alloys," NRL Report 7262, June 11, 1971.

A6. R. W. Judy, Jr. and R. J. Goode, "Fracture Extension Resistance (R-Curve) Concepts for Fracture-Safe Design with Nonfrangible Titanium Alloys," NRL Report 7313, Aug. 16, 1971.

A7. W. S. Pellini, "Advances in Fracture Toughness Characterization Procedures and in Quantitative Interpretations to Fracture-Safe Design for Structural Steels," Welding Research Council Bulletin 130, May 1968, and NRL Report 6713, Apr. 3, 1968.

A8. R. W. Judy, Jr., R. J. Goode, and C. N. Freed, "Fracture Toughness Characterization Procedures and Interpretations to Fracture-Safe Design for Structural Aluminum Alloys," NRL Report 6871, Mar. 31, 1969, and Welding Research Council Bulletin 140, May 1969.

A9. R. J. Goode, R. W. Judy, Jr., and R. W. Huber, "Procedures for Fracture Toughness Characterization and Interpretations to Failure-Safe Design for Structural Titanium Alloys," Welding Research Council Bulletin 134, Oct. 1968, and NRL Report 6779, Dec. 5, 1968.

A10. W. S. Pellini, "Criteria for Fracture Control Plans," NRL Report 7406, May 11, 1972.

TABLE A1. PROPERTIES OF ALUMINUM ALLOY SHEET MATERIALS FOR STRUCTURAL ELEMENT FRACTURE TESTS

Alloy	Thickness (cm)	Thickness (in.)	Yield Strength (MPa)	Yield Strength (ksi)	R_p $\left(\frac{MN \cdot m}{m^{5/2}}\right)$	R_p $\left(\frac{ft.-lb.}{in.^{5/2}}\right)$
7075-T6	.32	.125	518	75.1	.13	9.6
	1.27	.500	527	76.4	.16	12.0
2024-T351	.32	.125	386	56.0	.42	32.0
	1.27	.500	328	47.6	.71	54.0
6061-T651	.32	.125	254	36.8	.48	36.5
	1.27	.500	294	42.6	1.02	77.0
5086-H32	.32	.125	235	34.1	.83	63.0
	1.27	.500	210	30.5	1.48	112.0

TABLE A1. PROPERTIES OF ALUMINUM ALLOY SHEET MATERIALS FOR STRUCTURAL ELEMENT FRACTURE TESTS

Alloy	Thickness		Yield Strength		R_p	
	(cm)	(in.)	(MPa)	(ksi)	$\left(\frac{MN \cdot m}{m^{5/2}}\right)$	$\left(\frac{ft.-lb.}{in.^{5/2}}\right)$
7075-T6	.32	.125	518	75.1	.13	9.6
	1.27	.500	527	76.4	.16	12.0
2024-T351	.32	.125	386	56.0	.42	32.0
	1.27	.500	328	47.6	.71	54.0
6061-T651	.32	.125	254	36.8	.48	36.5
	1.27	.500	294	42.6	1.02	77.0
5086-H32	.32	.125	235	34.1	.83	63.0
	1.27	.500	210	30.5	1.48	112.0

TABLE A2. PROPERTIES OF THIN-SECTION METALLIC MATERIALS FOR FAST CRAFT AND SHIP APPLICATIONS

Alloy		Thickness (cm)	Thickness (in.)	Yield Strength (MPa)	Yield Strength (ksi)	R_p $\left(\frac{MN \cdot m}{m^{5/2}}\right)$	R_p $\left(\frac{ft.-lb.}{in.^{5/2}}\right)$
Aluminum							
7075-T6		1.26	.498	527	76.4	NA	NA
		.65	.255	512	74.2	.13	9.5
		.33	.130	518	75.1	.13	9.6
2024-T351		1.26	.496	328	47.6	.71	54
		.65	.257	315	45.7	.57	43
		.33	.130	386	56.0	.42	32
6061-T651		1.27	.500	294	42.6	1.02	77
		.65	.257	288	41.7	.66	50
		.34	.132	254	36.8	.49	37
5086-H32		1.24	.490	210	30.5	1.48	112
		.68	.266	225	32.6	1.41	107
		.32	.127	235	34.1	.83	63
5086-H116		1.27	.500	213	30.9	2.11	160
		.56	.222	261	37.8	1.31	99
		.48	.188	235	34.1	1.46	111
		.30	.120	235	34.1	.90	68
Steels							
HY-130		1.27	.500	911	132.2	13.66	1036
HY-130		1.27	.500	1049	152.2	5.80	440
HY-80		1.27	.500	770	111.7	3.09	234
Titanium							
Ti-6Al-2Cb-1Ta-0.8Mo		.254	.100	843	122.2	1.27	96
		.318	.125	829	120.2	1.56	118
		.478	.188	891	129.2	2.30	174
		.635	.250	868	125.9	2.40	182
		.953	.375	871	126.3	2.16	164
		1.270	.500	878	127.4	2.08	158
Ti-6Al-4V	CP*	.229	.090	923	133.9	.73	55
	ELI†	.229	.090	967	140.3	.84	64
	ELI	.318	.125	967	140.2	1.48	112
	ELI	.318	.125	967	140.2	1.20	91
	ELI	.635	.250	936	135.7	2.14	162
	CP	1.270	.500	996	144.4	.65	49
	ELI	1.270	.500	943	136.8	1.82	138
Ti-6Al-6V-2.5Sn (CP)		.229	.090	1069	155.0	.86	65
		.318	.125	1122	162.7	.26	20
		.635	.250	1078	156.3	.36	27
		1.270	.500	1039	150.7	.53	40

*Commercial Purity (oxygen content >0.15%)
†Extra Low Interstitial (oxygen content <0.13%)

TABLE A3A. MECHANICAL PROPERTIES OF LASER WELDS (International Units)

Alloy	Code		Thickness B (cm)	Tensile Properties σ_{ys} (MPa)	σ_{ts} (MPa)	RA (%)	El. (%)	R_p $\left(\frac{MN\cdot m}{m^{5/2}}\right)$
HY-80	U-55	N-12	.64	633	732	66	19	1.17
		N-13		634	746	64	19	3.18
HY-100	U-58	N-33A	1.58	734	873	70	19	4.01
		N-33B		763	873	69	19	5.62
		N-34A		758	761	12	4	4.45
		N-34B		745	751	13	4	5.70
HY-100	U-61	N-15	.64	734	813	61	21	1.81
		N-18		729	815	61	18	2.44
HY-130	U-98	N-91A	1.27	1031	1098	63	16	5.38
		N-91B		1034	1095	62	16	6.17
		N-92A		1033	1093	64	17	6.03
		N-92B		1033	1093	64	17	5.91
HY-130	U-99	N-45	2.54	965	1044	62	17	3.83
		N-37		993	1022	8	3	5.20
17-4 PH (as welded)	U-69I	N-35	2.54	795	898	64	17	7.14
		N-41		769	880	65	20	4.45
17-4 PH (H-1050)	U-69H	N-11B1	1.58	1050	1076	12	6	2.49
		N-11B2		1046	1065	13	4	3.34
		N-31A		1029	1037	8	2	3.40
		N-31B		1029	1047	12	3	2.99
Ti-100 (Ti-6Al-2Cb-1Ta-1Mo)	R-32	N-19	.64	865	925	12	9	2.33
		N-20		886	939	11	8	2.56

TABLE A3B. MECHANICAL PROPERTIES OF LASER WELDS
(English Units)

Alloy	Code		Thickness B (in.)	σ_{ys} (ksi)	σ_{ts} (ksi)	RA (%)	El. (%)	R_p $\frac{\text{ft.-lb.}}{\text{in.}^{5/2}}$
HY-80	U-55	N-12	0.25	91.8	106.2	66	19	89
		N-13		92.0	108.2	64	19	241
HY-100	U-58	N-33A	0.625	106.5	126.6	70	19	304
		N-33B		110.6	126.6	69	19	426
		N-34A		109.9	110.4	12	4	337
		N-34B		108.1	108.9	13	4	432
HY-100	U-61	N-15	0.25	106.1	118.0	61	21	137
		N-18		105.8	118.2	61	18	185
HY-130	U-98	N-91A	0.50	149.6	159.3	63	16	408
		N-91B		150.0	158.8	62	16	468
		N-92A		149.8	158.5	64	17	457
		N-92B		149.8	158.5	64	17	448
HY-130	U-99	N-45	1.00	140.0	151.4	62	17	290
		N-37		144.0	147.9	8	3	394
17-4 PH (as-welded)	U-69I	N-35	1.00	115.3	130.3	64	17	541
		N-41		111.6	127.7	65	20	337
17-4 PH (H-1050)	U-69H	N-11B1	0.625	152.3	156.1	12	6	189
		N-11B2		151.7	154.4	13	4	253
		N-31A		149.2	150.4	8	2	258
		N-31B		149.2	151.8	12	3	227
Ti-100 (Ti-6Al-2Cb-1Ta-1Mo)	R-32	N-19	0.25	125.5	134.1	12	9	177
		N-20		128.5	136.2	11	8	194

TABLE A4A. RESULTS OF SCC TESTS WITH SURFACE FLAWED PANELS
(International Units)

	Material Properties			Tensile Panel Test Results								
					Initial Flaw			No Growth		Growth		
Material	σ_{ys} (MPa)	K_{Iscc}* (MPa$\sqrt{m}$)	K_{Iscc}/σ_{ys} ($\sqrt{cm}$)	Thickness (cm)	a (cm)	2c (cm)	a/2c -	K_I (MPa$\sqrt{m}$)	K_I/σ_{ys} ($\sqrt{cm}$)	K_I (MPa$\sqrt{m}$)	K_I/σ_{ys} ($\sqrt{cm}$)	Coupled to
17-4 PH steel H1050	1103	42	0.15	1.65	0.22	0.54	0.40	43	0.15	49	0.18	Zn
	1103	89	0.32	1.65	0.37	1.67	0.22	84	0.30	95	0.34	Al
	1103	42	0.15	1.65	0.19	0.41	0.45	-	-	44	0.16	Zn
	1103	42	0.15	1.68	0.31	1.07	0.29	43	0.15	59	0.21	Zn
	1103	30	0.11	1.65	0.24	0.64	0.38	-	-	36	0.13	Mg
	1217	97	0.34	2.54	0.45	1.63	0.28	92	0.33	104	0.37	Al
	1117	113	0.41	2.54	0.75	4.29	0.17	92	0.33	116	0.41	Open
	1117	42	0.15	2.54	0.94	5.00	0.19	46	0.16	57	0.20	Mg
	1103	93	0.33	2.54	0.75	4.29	0.17	92	0.33	116	0.41	Open
	1103	49	0.18	2.54	0.94	5.00	0.19	46	0.16	57	0.20	Mg
4340 Steel	1427	20	0.05	2.54	1.01	5.01	0.20	-	-	21	0.06	-
	1407	20	0.05	1.27	0.36	1.35	0.2	16	0.04	22	0.06	-
Ti-7Al-2Cb-1Ta	710	34	0.09	2.54	0.46	1.60	0.11	29	0.16	34	0.19	-
	710	34	0.09	2.54	0.46	4.93	0.09	-	-	34	0.19	-
Ti-6Al-2Cb-1Ta-1Mo	696	127	0.72	5.08	1.40	5.59	0.27	111	0.63	126	0.71	-

*Value determined with cantilever bend specimens

TABLE A4B. RESULTS OF SCC TESTS WITH SURFACE-FLAWED PANELS
(English Units)

Material	Material Properties: σ_{ys} (ksi)	K_{Iscc}* (ksi$\sqrt{\text{in.}}$)	K_{Iscc}/σ_{ys} ($\sqrt{\text{in.}}$)	Tensile Panel Test Results: Thickness (in.)	Initial Flaw: a (in.)	2c (in.)	a/2c	No Growth: K_I (ksi$\sqrt{\text{in.}}$)	K_I/σ_{ys} ($\sqrt{\text{in.}}$)	Growth: K_I (ksi$\sqrt{\text{in.}}$)	K_I/σ_{ys} ($\sqrt{\text{in.}}$)	Coupled to
17-4 PH steel H1050	160	38	0.24	0.65	0.085	0.212	0.40	39	0.24	45	0.28	Zn
	160	81	0.51	0.65	0.147	0.659	0.22	78	0.48	88	0.34	Al
	160	38	0.24	0.65	0.073	0.161	0.45	-	-	40	0.25	Zn
	160	38	0.24	0.66	0.124	0.421	0.29	39	0.24	54	0.34	Zn
	160	27	0.17	0.65	0.096	0.253	0.38	-	-	33	0.21	Mg
	162	88	0.54	1.0	0.178	0.640	0.28	84	0.52	93	0.59	Al
	162	103	0.64	1.0	0.294	1.690	0.17	84	0.52	106	0.65	Open
	162	38	0.24	1.0	0.372	1.970	0.19	42	0.26	52	0.32	Mg
	160	85	0.53	1.0	0.294	1.690	0.17	84	0.52	106	0.65	Open
	160	45	0.28	1.0	0.372	1.970	0.19	42	0.26	52	0.32	Mg
4340 steel	207	18	0.09	1.0	0.400	1.972	0.20	-	-	19	0.09	-
	204	18	0.09	0.5	0.141	0.531	0.27	15	0.07	20	0.10	-
Ti-7Al-2Cb-1Ta	103	31	0.30	1.0	0.18	0.63	0.11	26	0.25	31	0.30	-
	103	31	0.30	1.0	0.18	1.94	0.09	-	-	31	0.30	-
Ti-6Al-2Cb-1Ta-1Mo	101	116	1.15	2.0	0.55	2.20	0.27	101	1.00	115	1.14	-

*Value determined with cantilever bend specimens

APPENDIX A-1

SUMMARY OF WELD CHARACTERISTICS

Plate	Material	Laser Power, kW	Weld Speed ipm	Comments
N- 1	U61	10.0	80	Good top bead, weak underbead, x-ray good, slight warp
N- 2	"	"	"	Good top bead, slight warp, x-ray good
N- 3	"	10.6	70	Good top bead, slight warp, x-ray good
N- 4	"	"	"	Good top bead, slight warp, w-ray good
N- 5	U55	10.7	"	Weak underbead, slight discoloration, x-ray good
N- 6	"	"	"	Weak underbead, slight discoloration, x-ray good
N- 7	"	"	"	Good bead, x-ray good
N- 8	"	"	"	Slight discoloration, slight warp, some lower surface spatter, x-ray good
H- 9-1	U98	11.6	30	Some discoloration and spatter, slight bead taper, x-ray gross porosity
N- 9-2	"	"	"	Slight drop through, some joint mismatch. x-ray smaller scale porosity than in N-9-1
N-10-1	"	"	"	Slightly irregular and discolored bead, start-stop defects, x-ray distributed porosity, some clear zones

Plate	Material	Laser Power, kW	Weld Speed ipm	Comments
N-10-2	"	"	"	Cleaner than N-10-1, end defects, x-ray good
N-11	U55	10.0	70	Weak underbead, slight warp and spatter, x-ray good
N-11B	U69H	13,6.4	30,60	Good bead, x-ray root bead porosity
N-12	U55	10.0	60	Good bead, x-ray good
N-12B	U69H	13,6.4	30,60	Good bead, x-ray distributed porosity
N-13	U55	10.0	60	Good bead, slight discoloration, x-ray porosity in about 1/2 weld length
N-14	"	"	50	Good bead, slight discoloration, x-ray one small pore
N-15	U61	"	70	Weak underbead, slight discoloration, x-ray good
N-16	"	"	60	Good top bead, lower bead irregular, slight warp, x-ray shows lower bead irregularity
N-17	"	"	50	Good bead, x-ray good
N-18	"	"	40	Good bead, slight taper, x-ray good
N-19	R-32	"	67	Good top bead, weak underbead, no x-ray
N-20	"	"	"	Good top bead, weak underbead, no x-ray

Plate	Material	Laser Power, kW	Weld Speed ipm	Comments
N-21	"	"	55	Excellent bead, x-ray good
N-22	"	"	"	Undercut at end of weld (plate separation)
N-23	"	"	45	Good bead, slight undercut
N-24	"	"	"	Good bead, slight undercut, x-ray one pinhole
N-25	"	"	50	Bead on plate, trace of oxidation on lower surface, x-ray one pore
N-26	"	12.0	60	Bead on plate into butt weld (sample forwarded to NRL prior to x-ray)
N-27	U98	12.0	35	Narrow underbead, cold shut defect, x-ray pores (probably at bead root)
N-28	"	"	30	Good underbead, x-ray 6 large pores
N-29	U98	12.0	27	Good bead, slight discoloration, x-ray a few small pores
N-30	"	"	24	Good bead, broad weld zone
N-31	U69H	10.0	50	Wide top bead (evidence of plasma formation), x-ray gross porosity
N-32	"	"	40	Good bead, x-ray fine-grained bead root porosity

Plate	Material	Laser Power, kW	Weld Speed ipm	Comments
N-33	U58	"	35*	Wide bead, irregular, plate mismatch, x-ray traces of porosity
N-34	"	"	45*	Good bead, start defect lask of fusion
N-35	U69I	"	30*	Good bead, x-ray fine-grained root bead porosity
N-36	"	"	25*	Good bead, x-ray fine-grained root bead porosity (aligned pores look like incomplete fusion)
N-37	U99	"	25*	Good top bead, incomplete penetration
N-38	"	"	20*	Good top bead, incomplete penetration
N-39	U69I	13.0	25*	Good top bead, shield damaged during weld, incomplete penetration
N-40	"	"	"	Good top bead, shield damaged during weld, incomplete penetration
N-41	"	12.0	30*	Tapered bead, x-ray root bead and distributed porosity
N-42	"	"	27*	Good bead, x-ray root bead porosity
N-43	"	"	""	Irregular bead, x-ray distributed porosity
N-44	"	"	""	Good bead, x-ray some porosity

* denotes dual pass weld

Plate	Material	Laser Power, kW	Weld Speed ipm	Comments
N-45	U99	"	25*	Slight mismatch, one end undercut, x-ray root-bead porosity
N-46	"	"	"	Slight mismatch, one end undercut, x-ray root bead porosity

* denotes dual pass weld

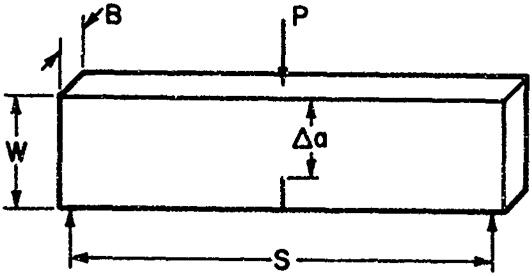

ENERGY = $R_P\ B^X\ \Delta a^Y$

WHERE R_P = CONSTANT

STANDARD SPECIMENS

B		Δa		W		S	
(IN.)	(CM)	(IN.)	(CM)	(IN.)	(CM)	(IN.)	(CM)
0.63	1.6	1.125	2.9	1.625	4.1	6.5	16.5
1.0	2.5	3	7.6	4.75	12.1	16	41

Fig. A1 — Illustration of Dynamic Tear Test specimen

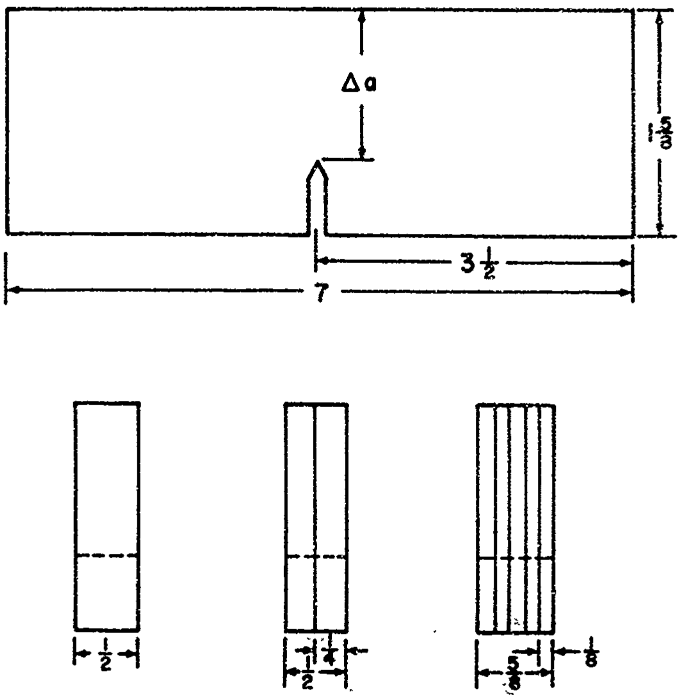

Fig. A2 — Configuration of specimens used for studies of thin-section materials. (Conversion factor: 1 in. = 2.54 cm.)

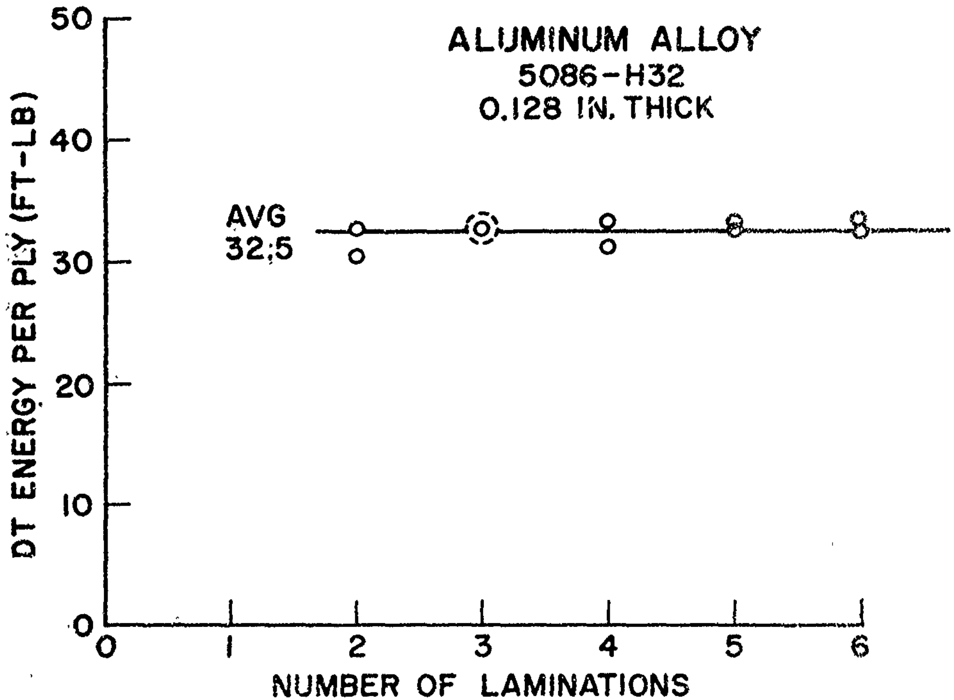

Fig. A3 — Illustration of the applicability of the specimen lamination technique for DT tests of thin-section materials. (Conversion factors: 1 in. = 2.54 cm, 1 ft-lb = 1.356 Nm.)

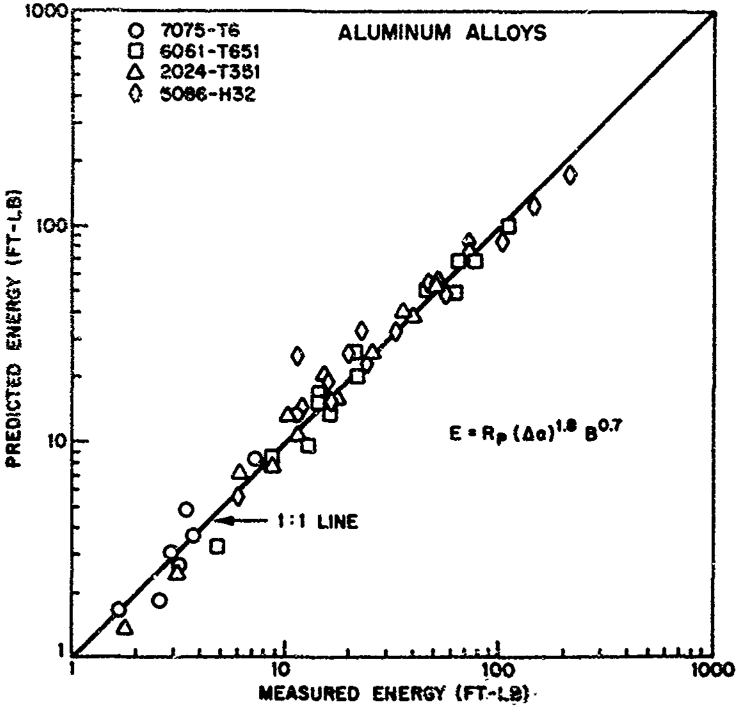

Fig. A4 — Comparison of measured energy values with energy values predicted by the equation for aluminum alloys. (Conversion factor: 1 ft-lb = 1.356 Nm.)

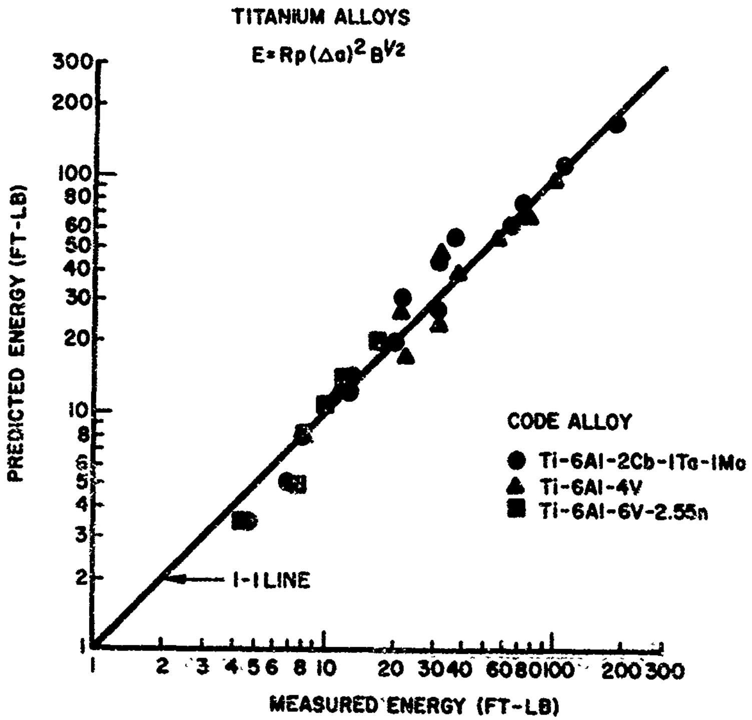

Fig. A5 — Comparison of measured energy values with predicted energy values for three titanium alloys. (Conversion factor: 1 ft-lb = 1.356 Nm.)

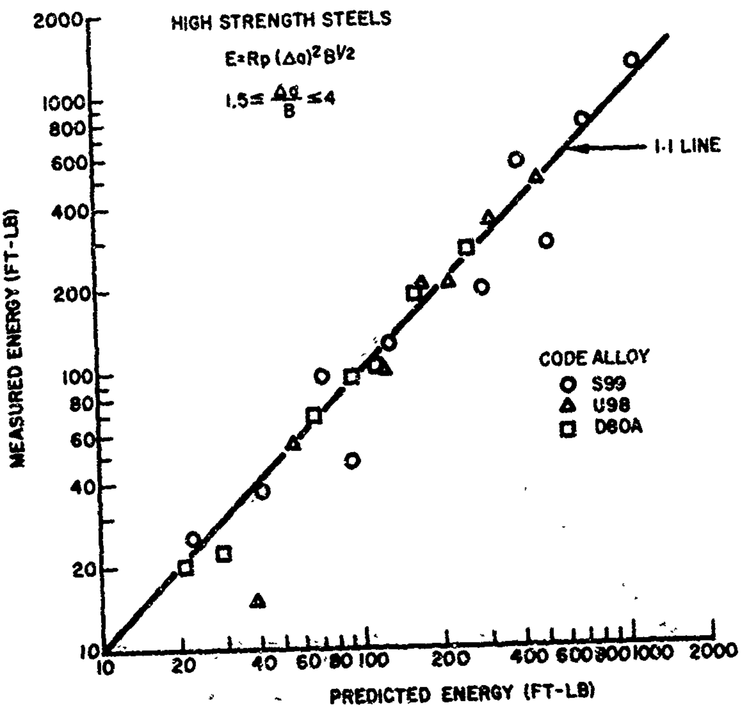

Fig. A6 — Comparison of measured energy values with predicted energy values for three steels. (Conversion factor: 1 ft-lb = 1.356 Nm.)

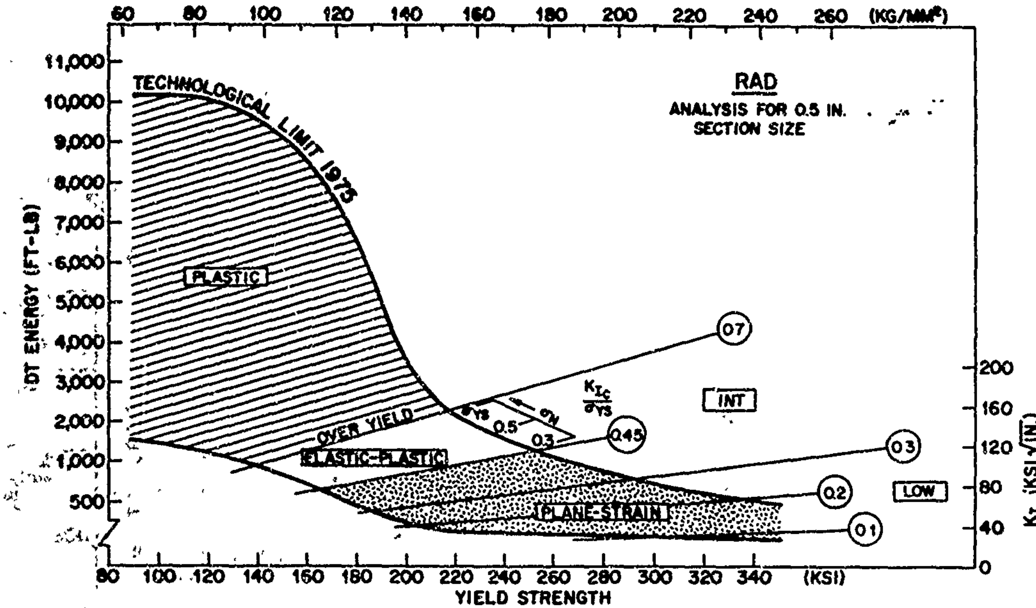

Fig. A7 — Ratio Analysis Diagram format for high-strength metals. (Conversion factors: 1 ft-lb = 1.356 Nm, 1 ksi$\sqrt{\text{in.}}$ = 1.099 MPa$\sqrt{\text{m}}$, 1 ksi = 6.895 MPa.)

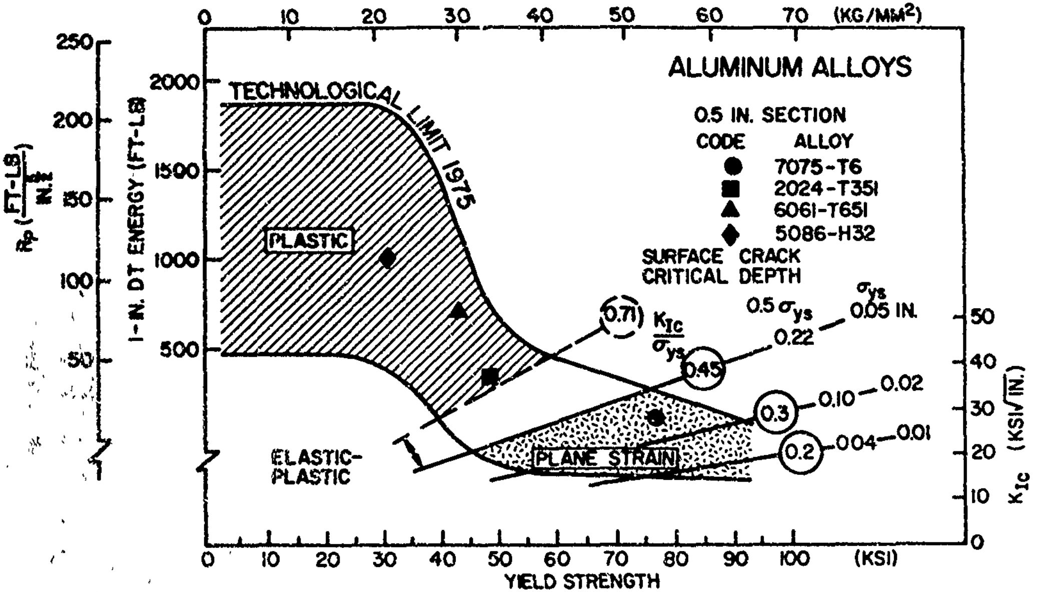

Fig. A8 — Ratio Analysis Diagram for the 0.5-in. section size. The 7075-T6 alloy is in the plane-strain region at this thickness. (Conversion factors: 1 ft-lb = 1.356 Nm, 1 ksi$\sqrt{\text{in.}}$ = 1.099 MPa$\sqrt{\text{m}}$, 1 ksi = 6.895 MPa.)

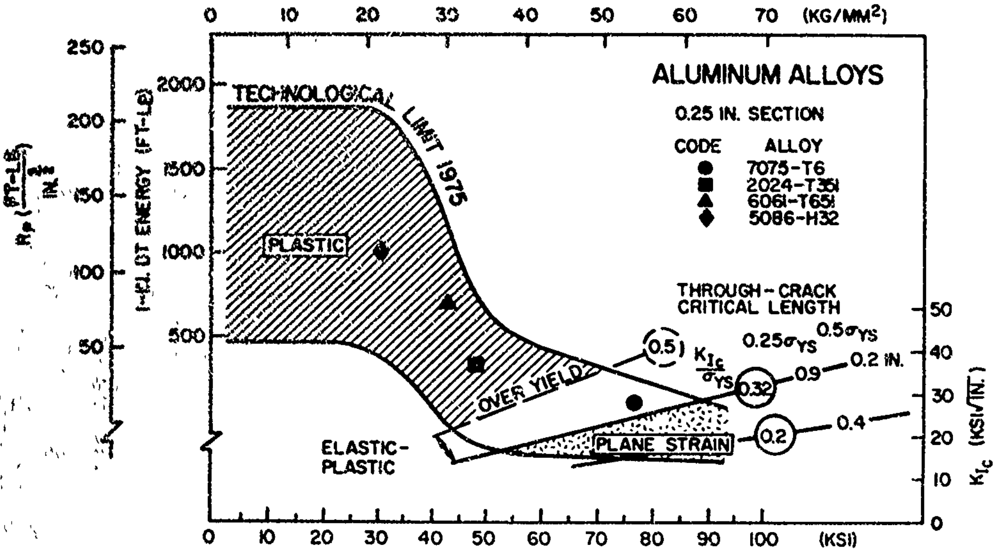

Fig. A9 — Ratio Analysis Diagram for 0.25-in. section size. The 7075-T6 alloy is in the elastic-plastic region at this thickness. (Conversion factors: 1 ft-lb = 1.356 Nm, 1 ksi$\sqrt{in.}$ = 1.099 MPa$\sqrt{m}$, 1 ksi = 6.895 MPa.)

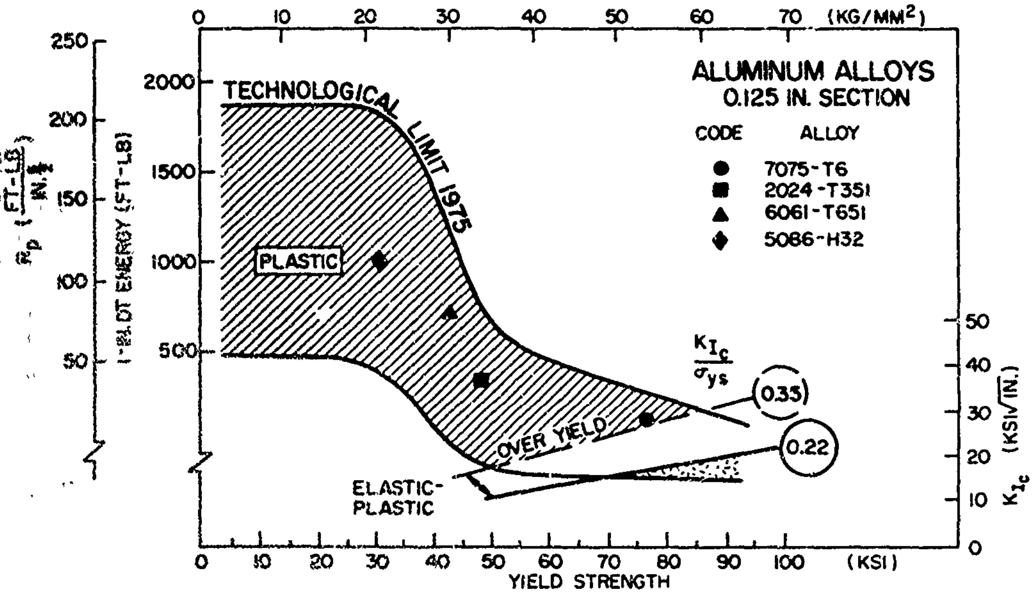

Fig. A16 — Ratio Analysis Diagram for 0.125-in. section size. The 7075-T6 alloy is in the plastic region. (Conversion factors: 1 ft-lb = 1.356 Nm, 1 ksi$\sqrt{in}$ = 1.099 MPa$\sqrt{m}$, 1 ksi = 6.895 MPa.)

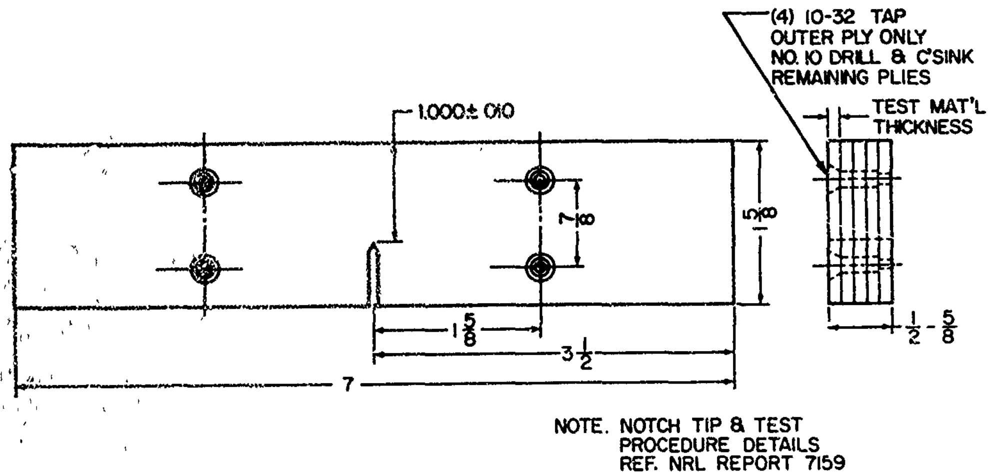

Fig. A11 — Recommended standard specimen configuration for DT tests of thin-section materials. (Conversion factor: 1 in. = 2.54 cm.)

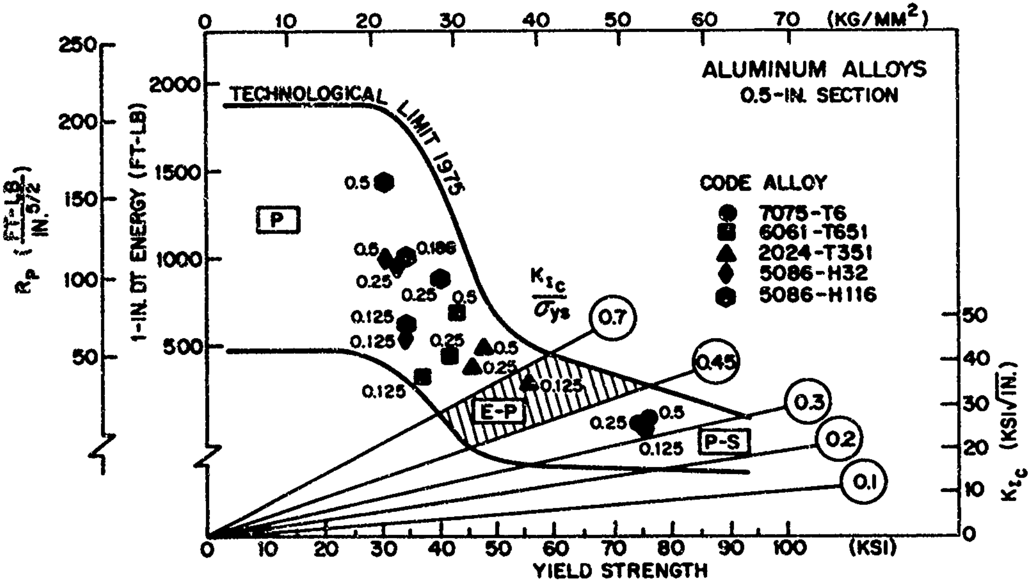

Fig. A12 — RAD for aluminum showing properties of commercial alloys in sections ranging from 0.125 to 0.500 in., as indicated by the small numbers on the plot. (Conversion factors: 1 ft-lb = 1.356 Nm, 1 ksi$\sqrt{in.}$ = 1.099 MPa$\sqrt{m}$, 1 ksi = 6.895 MPa, 1 in. = 2.54 cm.)

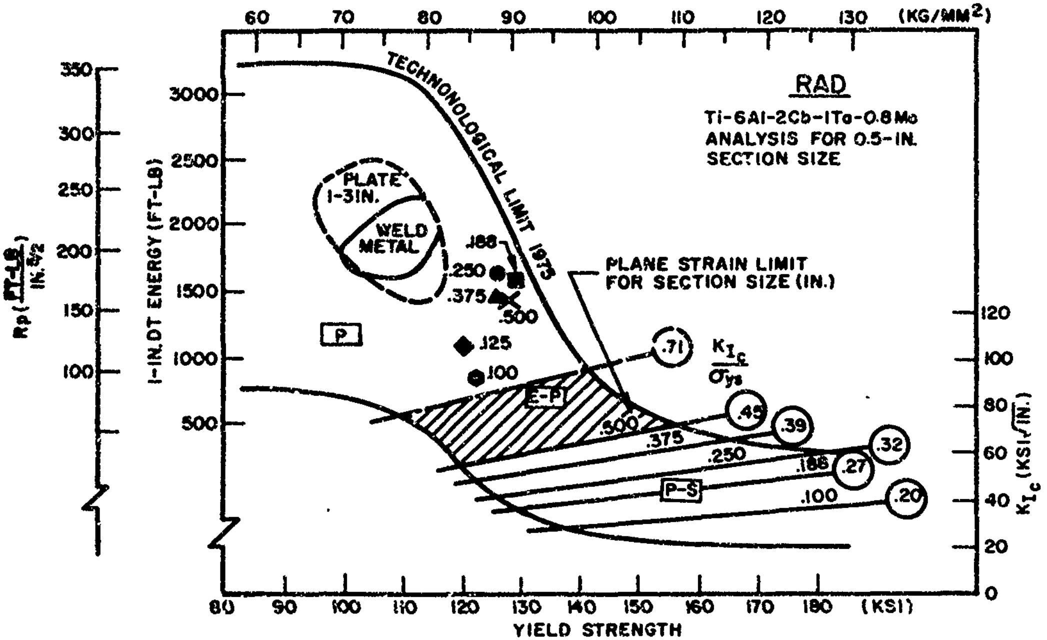

Fig. A13 — RAD for titanium alloys showing comparison of properties of thin-section alloy Ti-6Al-2Cb-1Ta-1Mo with data for heavy-section plate and weld metal of the same composition. The small numbers are the thickness in inches. (Conversion factors: 1 ft-lb = 1.356 Nm, 1 ksi$\sqrt{in.}$ = 1.099 MPa$\sqrt{m}$, 1 ksi = 6.895 MPa, 1 in. = 2.54 cm.)

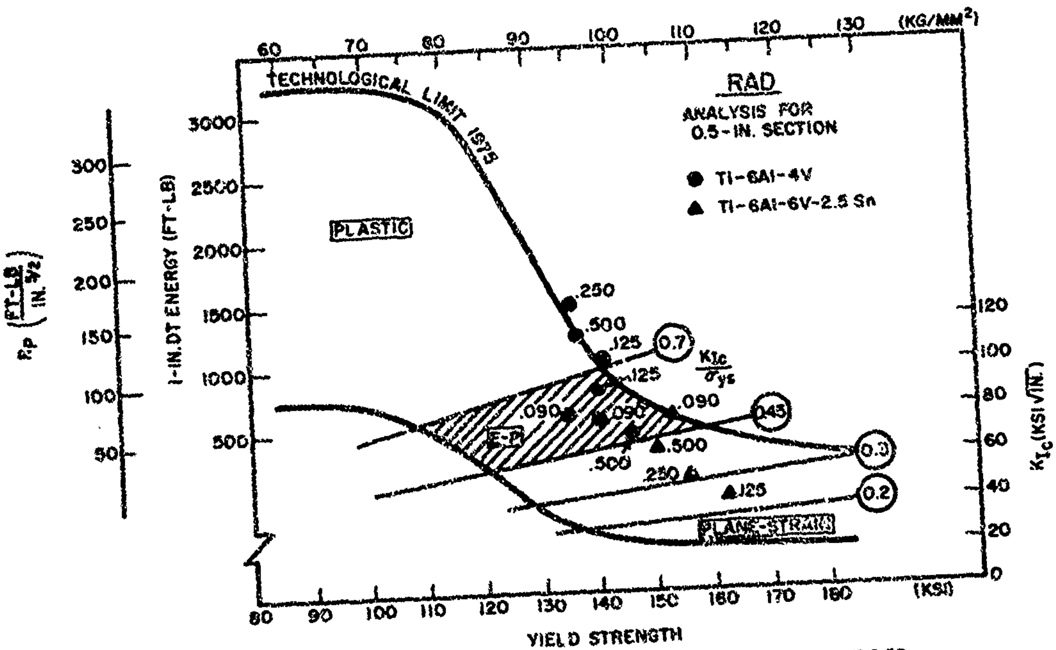

Fig. A14 — RAD showing properties of titanium alloys Ti-6Al-4V and Ti-6Al-6V-2.5Sn in the thin-section sizes shown by the small numbers. (Conversion factors: 1 ft-lb = 1.356 Nm, 1 ksi$\sqrt{\text{in.}}$ = 1.099 MPa$\sqrt{\text{m}}$, 1 ksi = 6.895 MPa, 1 in. = 2.54 cm.)

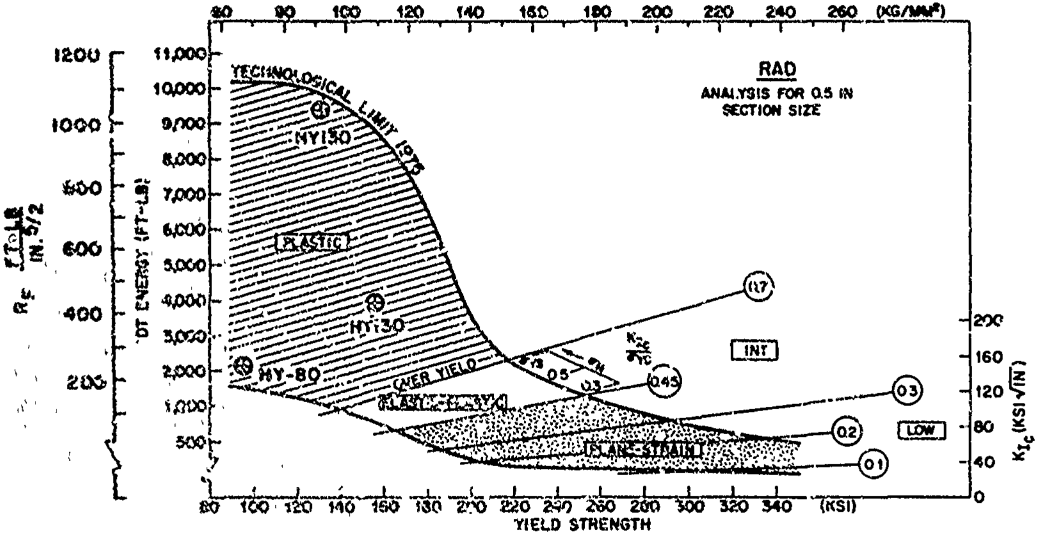

Fig. A15 — Steel RAD showing properties of samples of HY-80 and HY-130 in 0.5-in. thickness. (Conversion factors: 1 ft-lb = 1.356 Nm, 1 ksi$\sqrt{in.}$ = 1.099 MPa$\sqrt{m}$, 1 ksi = 0.895 MPa, 1 in. = 2.54 cm.)

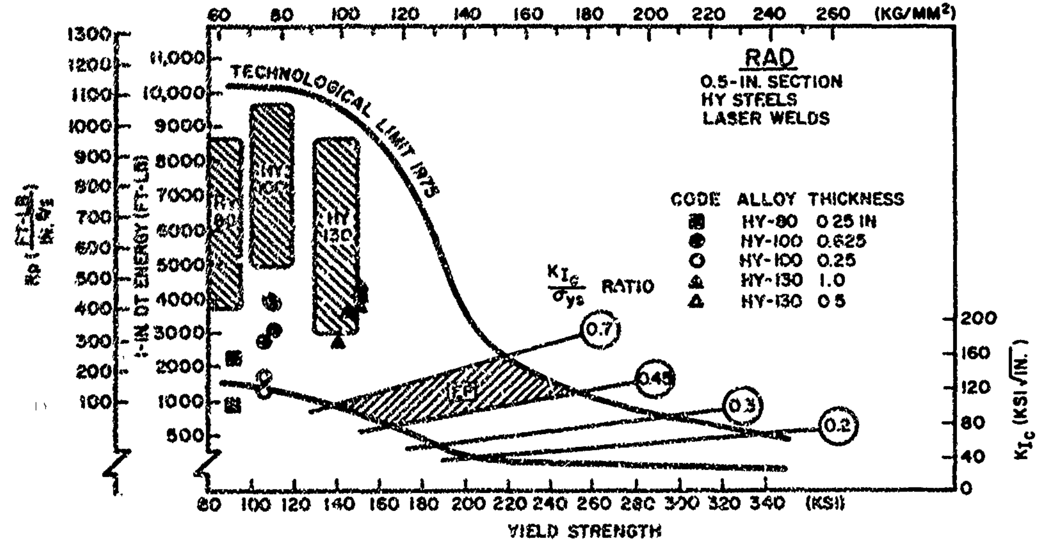

Fig. A16 — Properties of laser welds in HYgrade steels in comparison to properties of plate materials in thicker section. The laser welds of this study are approximately equivalent to shielded-metal-arc welds in the same alloys. (Conversion factors: 1 ft-lb = 1.356 Nm, 1 ksi$\sqrt{in.}$ = 1.099 MPa$\sqrt{m}$, 1 ksi = 6.895 MPa, 1 in. = 2.54 cm.)

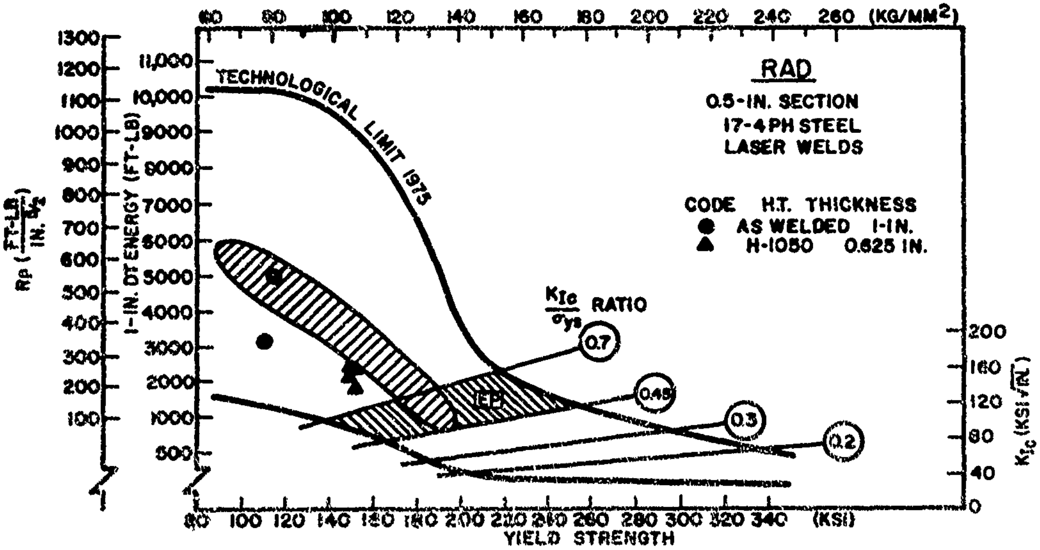

Fig. A17 — Properties of laser welds in 17-4 PH steel compared to properties of base metal (cross-hatched zone). The laser weld properties in this material are very good, as they approach base metal properties. (Conversion factors: 1 ft-lb = 1.356 Nm, 1 ksi$\sqrt{in.}$ = 1.099 MPa$\sqrt{m}$, 1 ksi = 6.895 MPa, 1 in. = 2.54 cm.)

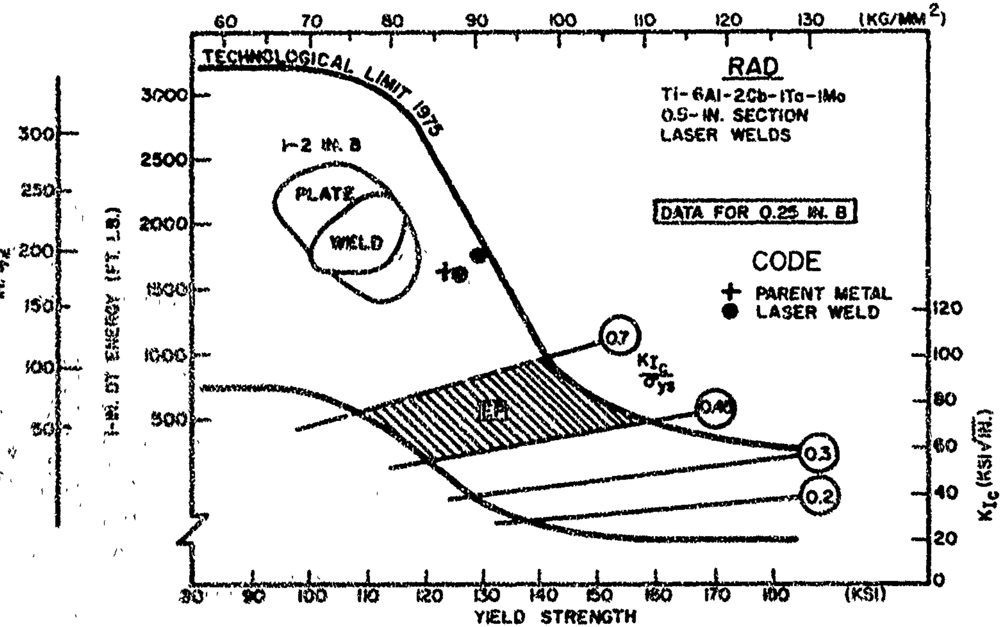

Fig. A18 — Properties of laser welds in Ti-6Al-2Cb-1Ta-1Mo. As shown by the code, the properties of the laser welds approximate that of the parent material. (Conversion factors: 1 ft-lb = 1.356 Nm, 1 ksi$\sqrt{in.}$ = 1.099 MPa$\sqrt{m}$, 1 ksi = 6.895 MPa, 1 in = 2.54 cm.)

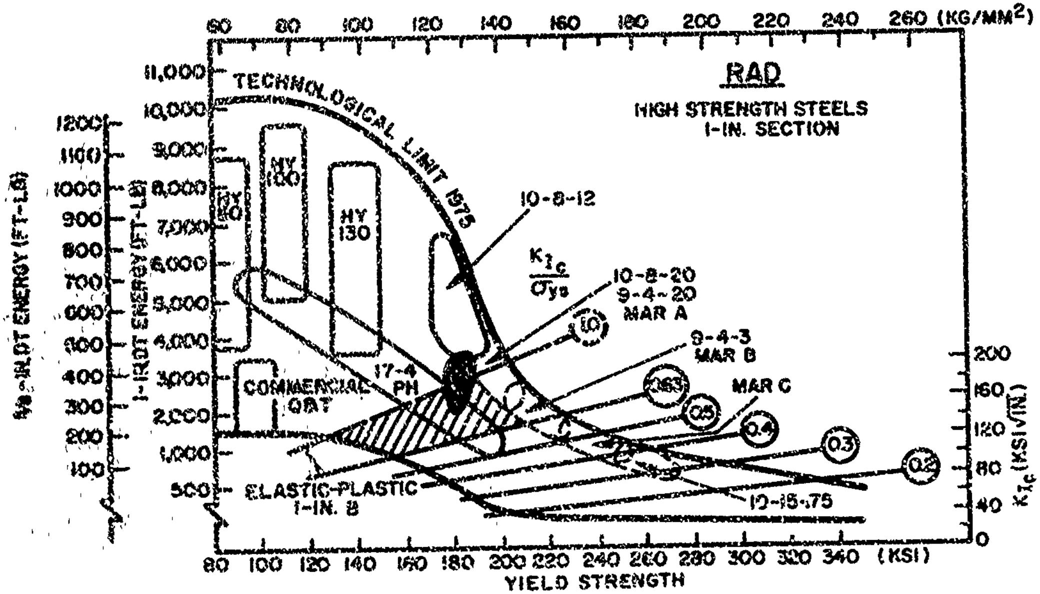

Fig. A19 — Fracture resistance of plate, forging, and weld metal in 10Ni steel used on B-1 bomber program. The cross-hatched zone includes properties of all product forms. Data for other steel types are shown for comparison. (Conversion factors: 1 ft-lb = 1.356 Nm, 1 ksi$\sqrt{\text{in.}}$ = 1.099 MPa$\sqrt{\text{m}}$, 1 ksi = 6.895 MPa, 1 in. = 2.54 cm.)

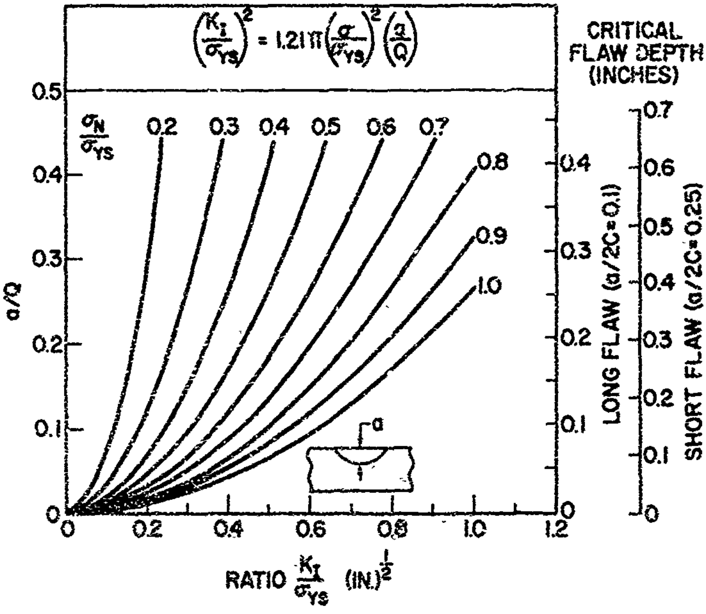

Fig. A20 — Flaw size diagram constructed from the surface flaw equation shown at the top of the diagram. The equation relates stress (σ/σ_{ys}), flaw size (a/Q), and ratio (K_{Ic}/σ_{ys} and K_{Iscc}/σ_{ys}). (Conversion factors: 1 in. = 2.54 cm, $1\sqrt{\text{in.}} = 1.594\sqrt{\text{cm.}}$)

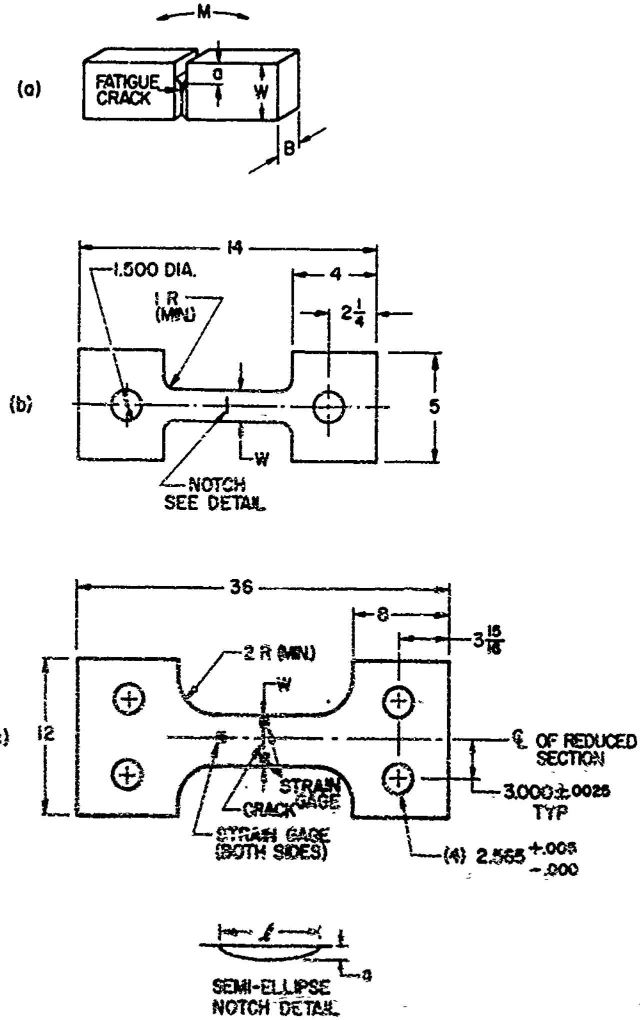

Fig. A21 — Geometry of tensile loaded part-through-cracked (PTC) test specimens. (Conversion factor: 1 in. = 2.54 cm.)

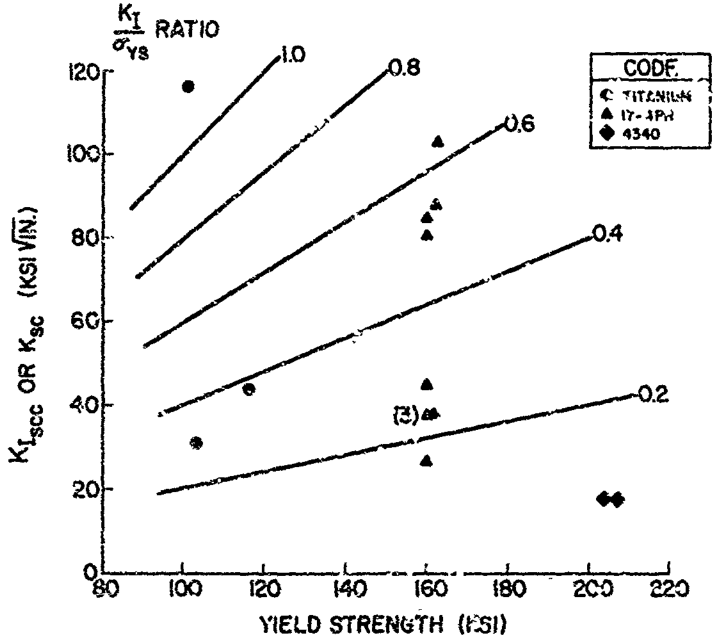

Fig. A22 — Plot of K_{Iscc} vs. yield strength illustrating range of values investigated for verification of the capability of the surface flaw equation to predict the onset of crack growth. (Conversion factors: 1 ksi = 6.895 MPa, 1 ksi$\sqrt{in.}$ = 1.099 MPa$\sqrt{m}$.)

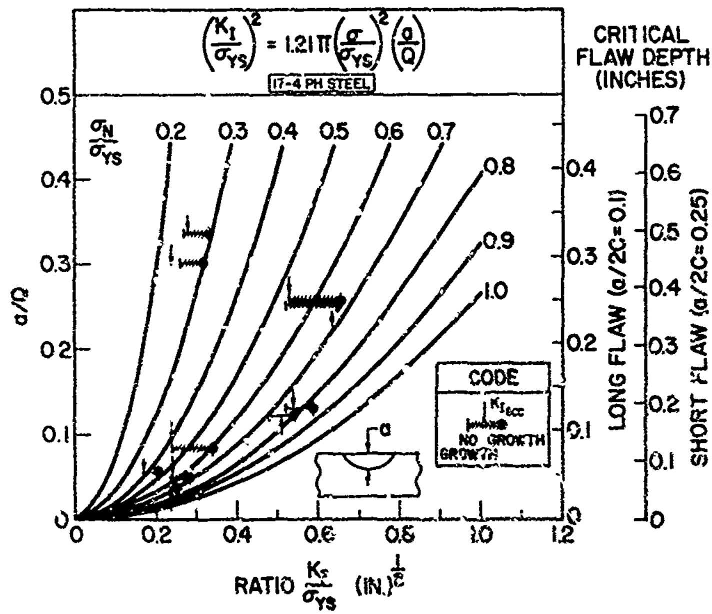

Fig. A23 — Data from test of PTC specimens of 17-4 PH steel. The ends of the bars correspond to externally imposed test conditions. (Conversion factors: $1\sqrt{\text{in.}} = 1.594\sqrt{\text{cm}}$, 1 in. = 2.54 cm.)

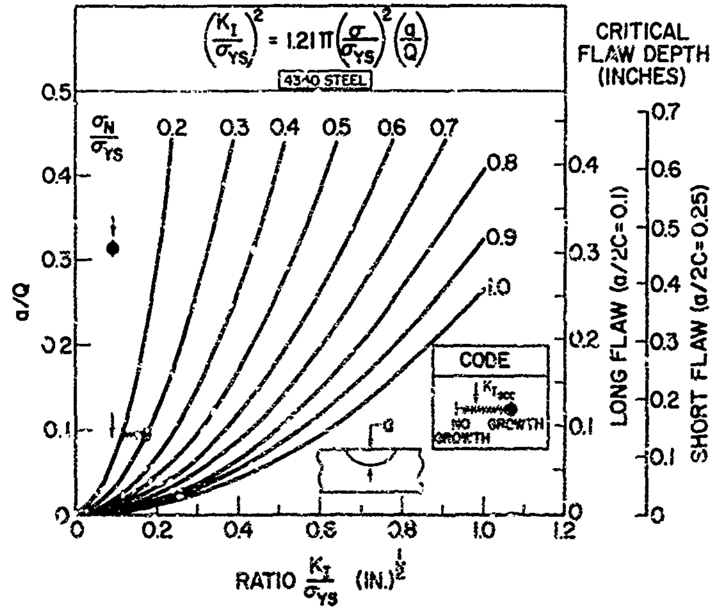

Fig. A24 — Results of tests of PTC specimens of 4340 steel. (Conversion factors: $1\sqrt{in.} = 1.594\sqrt{cm}$, 1 in. = 2.54 cm.)

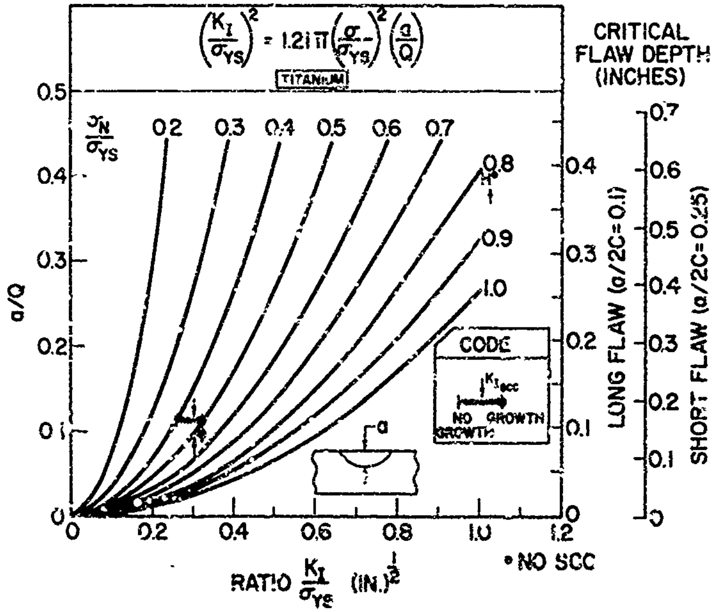

$$\left(\frac{K_I}{\sigma_{YS}}\right)^2 = 1.21\pi\left(\frac{\sigma}{\sigma_{YS}}\right)^2\left(\frac{a}{Q}\right)$$

Fig. A23 — Results of early experiments with titanium alloys using PTC type specimens. Note that the 2-in.-thick specimen of Ti-6211 at the top did not exhibit SCC crack growth, but the fracture mechanics prediction of failure was accurate. (Conversion factors: $1\sqrt{in.} = 1.594\sqrt{cm}$, 1 in. = 2.54 cm.)

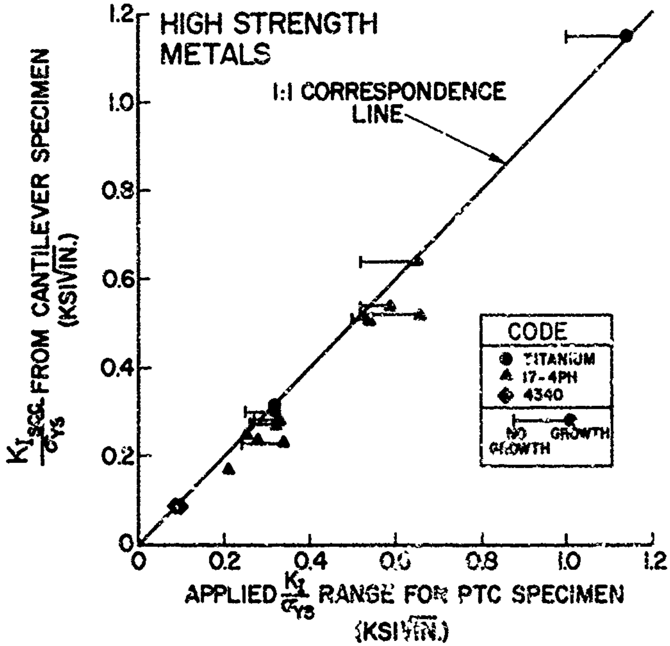

Fig. A26 — Comparing results of experiments with cantilever-bend and PTC specimens on the basis of the K_I/σ_{ys} ratio. K_{Iscc} is the point of intersection of the 1:1 line with the bar joining "no-growth" and "growth" conditions. (Conversion factors: 1 ksi$\sqrt{in.}$ = 1.099 MPa-$\sqrt{m}$.)

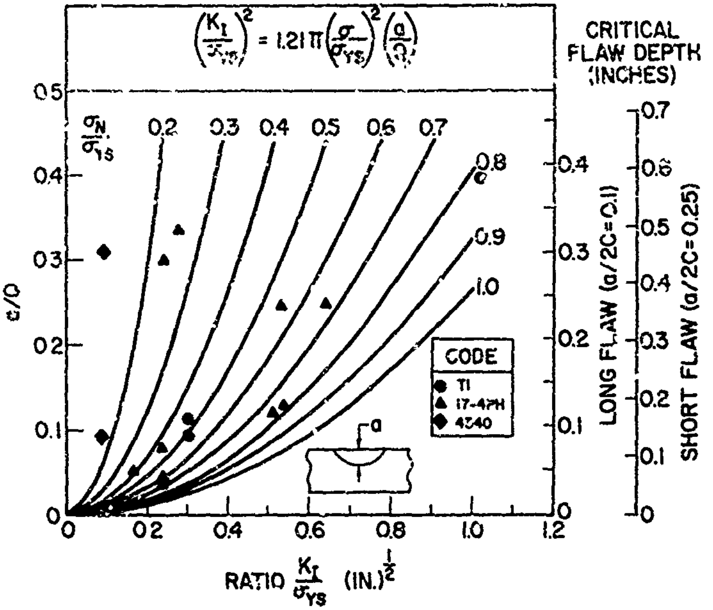

Fig. A27 -- Summary plot showing regions of flaw-size diagram that have been verified for predicting onset of SCC crack growth. (Conversion factors: $1\sqrt{in.} = 1.594\sqrt{cm}$, 1 in. = 2.5 cm.)

B. Fracture Mechanics Technology/Fatigue Criteria

T. W. Crooker

High-performance surface ship structures involve the use of materials under circumstances which incur a serious risk of fatigue damage: high strength-to-density alloys, complex structural configurations, cost-conscious fabrication, highly aggressive service environments and repeated loading stresses generated by unavoidable structure/environment force interactions. Metal fatigue will pose a long-term threat to the integrity and reliability of these structures and thus demands careful consideration from the earliest design concept stages through the development of life-cycle operation and maintenance criteria. The establishment of fatigue design criteria and the selection of materials within the framework of such criteria will play a vital role in preventing fatigue failures in high-performance ship structures. A pioneer effort in pursuit of these goals is currently underway for the PHM strut/foil structure system using, in part, data generated under this program. This section presents the results of a broad range of fatigue and corrosion-fatigue studies conducted to develop the fatigue technology base for a selection of candidate alloys for high-performance ship applications.

BACKGROUND

Work aimed at establishing a rational means of dealing with fatigue crack propagation began in the aircraft industry during the 1950's, in response to the widely publicized British Comet aircraft failures plus other lesser known instances of aircraft structural fatigue. A 1960 conference on the problem in Cranfield, England revealed a significant amount of research had been initiated, but no common analytical basis had yet emerged (B1). However, in a highly significant paper published in 1963 (B2), Paris and Erdogan proposed that the fracture mechanics crack-tip stress-intensity factor (K) could successfully serve as the primary variable in describing fatigue crack growth rate (da/dN). This widely heeded paper still continues to both stimulate and focus fatigue technology.

Once the basic engineering approach to fatigue crack propagation using fracture mechanics began to evolve, the

extension of these studies into the realm of corrosion-fatigue began to occur. Early studies of corrosion-fatigue using fracture-mechanics-type precracked specimens began in the mid-1960's, and by 1971 a significant portion of a major symposium on corrosion-fatigue was devoted to fracture mechanics oriented crack propagation studies (B3).

Since 1971, major developments have occurred in the application of fatigue crack propagation technology. Formalized requirements for the use of crack growth rate data in materials selection and in structural design have been instituted or are being contemplated by several influential organizations. The U.S. Air Force presently requires that the structural integrity of airplanes be demonstrated through the implementation of fatigue and fracture control plans which utilize fatigue crack propagation analyses (B4). The U.S. Navy is currently developing a similar approach towards the design of high-performance surface ships (B5).

The studies performed under this program were intended to further develop the fracture mechanics technology base necessary for implementation of modern structural integrity concepts. Data generated under this program have been utilized in the fatigue design criteria for the PHM 17-4 PH strut/foil system by the Boeing Company and also in the structural integrity plan for the PHM HY-130 strut/foil system by the Grumman Aerospace Corporation.

FATIGUE CRACK PROPAGATION CHARACTERISTICS OF 17-4 PH STEELS

High-strength precipitation hardening (PH) stainless steels are among the candidate materials for application in new high-performance surface ships. Such sophisticated applications will require a far more comprehensive knowledge of the mechanical characteristics of these materials than presently exists. The study reported here was undertaken to develop basic engineering information on the cyclic crack-growth behavior of 17-4 PH stainless steels. The 17-4 family of PH stainless steels represents a highly complex and incompletely understood alloy system. The mechanical properties of 17-4 PH steels can vary widely, depending upon processing and heat treatment (B6,B7). This investigation resulted in data on and interpretation of cyclic crack growth in samples of 17-4 PH steels of interest for potential application in naval structures. Both macroscopic fracture-mechanics cyclic crack-growth test results and microscopic electron fractography interpretations are presented.

Description of Materials

Two 12.7 mm (0.50 in.)-thick rolled plates of 17-4 PH stainless steel were studied, a vacuum-melted (VM) sample in

the H1050 condition and an argon-oxygen melted (AOM) sample in the H1050 and H1150 conditions. Chemical compositions of the two plates are given in Table B1. Rough-cut specimen blanks were solution treated at 1038°C (1900°F) for 1 hr. in an argon atmosphere, followed by an oil quench. Machined specimens were then aged in an air atmosphere at either 566 or 621°C (1050 or 1150°F) for 4 hrs., followed by air cooling. Mechanical properties of the heat-treated materials are shown in Table B2.

Experimental Procedures

Fatigue crack growth rate (FCGR) tests were conducted on each of the three materials studied. Single-edge-notch (SEN) tension specimens 12.1 mm (0.475 in.)-thick, shown schematically in Fig. B1a, were employed in the FCGR tests. Crack propagation in these specimens occurred in the T-L orientation (B8). The proportions of these specimens and the stress-intensity formulation utilized in calculating ΔK values were obtained from Ref. B9. Fatigue crack growth rate tests were conducted on a closed-loop fatigue machine in ambient laboratory air at a frequency of 5 Hz. Observations of crack length were made optically at approximately 15X using a Gaertner traveling microscope. Specimens of each material were tested at various stress ratios (minimum stress-intensity factor/maximum stress-intensity factor = R). Ratios of 0.04, 0.40, 0.67, and 0.80 were studied. Duplicate specimens were tested in each case, and all FCGR curves reported include data from two specimens. One specimen was first tested under constant load, then a second specimen was step-loaded with the load increased incrementally after each 0.25 cm (0.100 in.) of crack growth.

Tensile tests were conducted on 0.907 cm (0.357 in.) diameter specimens taken from the SEN specimens following FCGR testing. Fracture-toughness values were obtained from 1.59 cm (5/8-in.) Dynamic Tear specimens, Fig. B1b, tested at ambient laboratory temperature in accordance with Ref. B10.

Replicas were made to determine the mode of cyclic crack propagation across the spectrum of stress-intensity ranges examined. These replicas were made from cellulose acetate films which were stripped from the fatigue fracture surfaces (at the midthickness positions), shadowed with platinum, and then deposited with a carbon backing. Visual estimates of percentages of the constituent microfracture modes were made by thoroughly examining each replica.

Results

The fracture-mechanics, cyclic crack growth results are presented in Fig. B2a,b,c. These are logarithmic plots of crack growth rate da/dN vs. crack-tip stress-intensity factor range ΔK for each of the three materials studied. In each case, the minimum ΔK values reported were near 11 $MPa\sqrt{m}$ (10 $ksi\sqrt{in.}$), and several R values are included. Tests were continued to the maximum stress-intensity level at which optical observation of cyclic crack growth could be maintained for each combination of material and stress ratio studied. Tests were terminated either, because of the occurrence of fracture, or because of experimental difficulties in monitoring full-slant shear-mode cracks which were known to have irregular crack front shapes. The significant features of these results are the variation in da/dN values shown as a function of material variables (processing and heat treatment) and the varying sensitivities to R. For any given set of values of ΔK and R, da/dN values can vary by as much as a factor of five due to metallurgical effects. Also, for any of the materials studied, da/dN values at any level of ΔK can vary widely in response to variations in R, especially for higher levels of ΔK.

The DT fracture test results are plotted in Fig. B3, which is a modification of the Ratio Analysis Diagram (RAD) for steels (B11). This cumulative plot of fracture toughness vs. yield strength is useful in the present work for comparing the relative strengths and toughness values of the three materials studied to one another, as well as to the overall range of fracture toughness values measured in extensive prior testing of steels. The results from the 1.59 cm (5/8-in.) Dynamic Tear (DT) Test were plotted in Fig. B3 using procedures outlined in Ref. B12. It can be seen that for the three materials studied, processing exerts a greater influence on toughness than does heat treatment. Both of the AOM materials studied are of low toughness, whereas the VM material exhibited significantly greater toughness.

A wide range of fracture mechanisms was detected from the fatigue surfaces of the specimens examined, including striations (STR), microvoid coalescence (MVC), and micro-cleavage (CLE). Since cleavage is a particularly low-energy mode of crack extension and is associated with poor resistance to crack growth, both in fracture and in stress-corrosion cracking, considerable significance is placed on its occurrence under conditions of cyclic crack growth. An example of micro-cleavage observed in the AOM H1050 material is shown in a stereographic pair of electron fractographs in Fig. B4. It is worth noting that the occurrence of CLE was virtually confined to the AOM H1050 material and its

occurrence, along with the associated accelerated crack growth rates, could be suppressed either through processing or heat-treatment variations.

DISCUSSION

Fracture Results

The fracture results, which indicate a very distinct beneficial effect of vacuum melting, are in excellent agreement with the much more extensive fracture studies on 17-4 PH steels conducted by Judy et al. (B6). Beneficial purity effects on fracture toughness resulting from vacuum melting are well recognized in steels and are the principal factor in determining metal quality "corridors" on the RAD (B11). It should be pointed out that the AOM material does not appear amenable to significant improvement in fracture toughness through variation in heat treatment and falls among the least fracture-resistant steels available at the respective yield-strength levels studied (B6).

Cyclic Crack Growth Results

Several investigations have shown that cyclic crack growth, as measured in terms of da/dN values as a function of ΔK, is remarkably invariant in a broad selection of steels (principally martensitic), ranging in yield strength from intermediate to ultrahigh levels (B13-B15). Conversely, other investigators have shown significant and systematic variations in da/dN values in similar types of steels which can be related to macromechanical properties or heat treatment (B7, B16-B18). However, these previous investigations of cyclic crack growth in steels have tended, for the most part, to limit the loading conditions to R values near zero (zero-to-tension), and to make relatively few fractographic observations as a means of explaining variations (or the lack thereof) in behavior. Thus, an incomplete and somewhat confusing picture of cyclic crack growth behavior in high-strength steels exists.

Recent investigations conducted in Great Britain have begun to remedy this void in our knowledge of cyclic crack-growth behavior of metallic materials (B19-B23). The findings of these separate investigations largely support the observations of this study of 17-4 PH steels.

The da/dN vs. ΔK results shown in Fig. B2 indicate distinct differences in the cyclic crack-growth characteristics of the three 17-4 PH steels studied. Several salient observations are as follows: First, for virtually any combination of ΔK and R, the H1050 VM material exhibits lower crack growth

rates than does the H1050 AOM material. This can be regarded as a beneficial purity effect and is in agreement with the findings of Evans et al. (B19). Second, heat treating the AOM material to the lower yield-strength H1150 temper significantly improves the cyclic crack-growth resistance at the low R value (0.04), as compared to the H1050 AOM material at the same R value, and results in da/dN values comparable to the VM material despite significant differences in fracture toughness between the AOM H1150 and VM H1050 materials. However, at higher R values, the lower toughness H1150 AOM material develops significantly higher da/dN values than does the H1050 VM material. This finding is in general agreement with the results of Rack and Kalish (B7). Third, each material exhibits a significant dependence of da/dN on R, which is most pronounced in the lower toughness materials; and, this R-factor dependence diminishes with decreasing ΔK. In fact, there is a tendency for convergence of nearly all the curves at ΔK levels near 11 MPa$\sqrt{m}$ (10 ksi$\sqrt{in.}$). These observations agree, at least in part, with the findings of most of the British investigations cited in Refs. B19-B23.

In recent years, numerous FCGR laws which account for stress-ratio effects have been formulated. However, attempts to normalize each of the sets of data shown in Figs. B2a,b, and c into a unified format were unsuccessful. Obviously, in a situation where metallurgical factors exert such a pronounced effect on cyclic crack growth behavior, no single law based on continuum mechanics principles will successfully describe such varied behavior. Rather, an understanding of micro-mechanistic events is necessary.

Fractographic Results

As shown above, both the VM and AOM steels in the H1150 condition exhibit a growth rate dependence on R, although the dependence is greater in the case of the AOM plate. And for a given value of R, the crack propagation rate is higher for the AOM plate. Electron fractography reveals that this difference in behavior between the two plates correlates with the propensity toward cleavage as a mode of cyclic crack extension. For example, at R = 0.04, the AOM-H1050 steel exhibits 2-5% CLE for ΔK levels from 31.9 to 133 MPa$\sqrt{m}$ (29 to 121 ksi$\sqrt{in.}$). At R = 0.67, however, much more CLE appears, viz., a constant level of 15-20% for ΔK ranges of 16.5 to 38.5 MPa$\sqrt{m}$ (15 to 35 ksi$\sqrt{in.}$). On the other hand, the VM-H1050 steel exhibits no cleavage at R = 0.04, over the whole spectrum of ΔK levels examined; at R = 0.67, just a trace of CLE (1%) appears at ΔK levels from 25.3 to 87.9 MPa$\sqrt{m}$ (23 to 80 ksi$\sqrt{in.}$). Thus, the incidence of CLE appears to coincide with the poorer crack-growth-rate

resistance of the AOM plate. The greater propensity toward cleavage in the AOM plate might be related to the greater percentage of δ-ferrite in the microstructure.

When AOM steel was aged at a higher temperature to obtain the H1150 condition, cleavage was completely suppressed as a mode of crack extension, for $R = 0.04$, and the crack growth rates were reduced significantly to levels less than or equal to those for the VM steel in the H1050 condition. This improvement might be related to the increased formation of reverted austenite in going from the H1050 to the H1150 condition in the AOM steel, or to the alteration of some feature of the precipitation-hardening mechanism, e.g., the magnitude of the coherency strains. For cyclic crack growth at $R = 0.67$, a trace of CLE (1-2%) did appear at all ΔK levels examined, from 18.7 to 51.6 $MPa\sqrt{m}$ (17 to 47 $ksi\sqrt{in.}$), just as it did in the case of the VM steel in the H1050 condition.

While microcleavage is not uncommon as a mode of cyclic crack propagation in alloys of various families, the nature of its occurrence in the present case is enigmatic in one respect, viz., that the percent CLE appears to be independent of ΔK over wide ranges of ΔK. This finding contrasts with that for the H900 condition of a 17-4 PH steel studied by Hack and Kalish (B7), who reported that percent CLE increased with ΔK. While it has been reported for other alloys that the percent CLE decreases with increased ΔK (B24,B25), this is the first known instance where the percent CLE appears independent of ΔK, for a given value of R. Much further work may be required for a full understanding of this behavior.

SUMMARY AND CONCLUSIONS

Fatigue crack propagation rates (da/dN) in ambient laboratory air have been obtained as a function of stress-intensity factor range (ΔK) for an argon-oxygen melted steel in the H1050 and H1150 conditions, and for a vacuum-melted steel in the H1050 condition. These growth rates were determined for stress-intensity factor ratios $R = 0.04$, 0.40, 0.67, and 0.80. Modes of crack extension were determined by electron fractography to elucidate differences in crack-growth-rate behavior. Cleavage appears as a mode of cyclic crack propagation in this family of steels, to the detriment of cyclic crack-growth resistance. In particular, it was found that:

(a) the amount of cleavage appears to be independent of ΔK over a wide spectrum of ΔK levels.

(b) the amount of cleavage (as well as the associated cyclic crack propagation rates) increases significantly with R.

(c) heat treatment can be adjusted to minimize the appearance of cleavage.

(d) slight variations in alloy processing serve to eliminate cleavage.

CORROSION-FATIGUE CRACK PROPAGATION CHARACTERISTICS OF SELECTED HIGH-STRENGTH MARINE ALLOYS

Crack propagation in high-strength alloys, caused by the combined forces of fatigue and corrosion, represents a potentially serious threat to the service capabilities of high-performance surface ship structures. The application of fracture mechanics principles to fatigue has permitted researchers to study crack propagation under strictly defined crack tip mechanical conditions which duplicate structural service. Studies conducted under this program at NRL's Marine Corrosion Research Laboratory located in Key West, Florida have added a new degree of service simulation to corrosion-fatigue studies by conducting crack propagation tests in flowing natural seawater. This added degree of service simulation, which is provided by the natural marine environment, is of particular importance in the characterization of new alloys being developed for application in critical, high-performance structures.

Description of Materials

The materials studied under this phase of the program included the three 17-4 PH steels described in the previous section plus HY-130 steel, Ti-6Al-2Cb-1Ta-0.8Mo and 5456-H116 aluminum alloy. The tensile properties of these materials are given in Tables B2 and B3.

Experimental Procedures

Tests were conducted using single-edge-notch (SEN) cantilever specimens. Details of the test specimen geometry are shown in Fig. B5. Fracture mechanics stress-intensity factors were calculated using the Kies' equation (B26). The specimens were oriented with the edge crack parallel to the final rolling direction, in the ASTM designated T-L orientation (B8).

Cycling was performed under constant maximum load, zero-to-tension, (R = 0), at frequencies of either 10 or 1 cpm. Unfortunately, the control system of the test machines did

not permit load-time waveform control, an important parameter in corrosion-fatigue testing (B27). However, for comparison purposes, the waveform can be considered to be approximately triangular.

Fatigue specimens were tested in natural seawater at the NRL Marine Corrosion Research Laboratory in Key West, Florida. Natural seawater was taken directly from the ocean and immediately passed through a polyurethane enclosure cell, placed around the specimen test section, in a single-pass mode at a flow rate of ca. 200 ml/min. The corrosion cell had a plexiglas viewing area for optical observation of crack growth. Measurement of the fatigue-crack length was performed by a slide-mounted optical micrometer focused on the root surface of one side-groove of the specimens.

Electrochemical potentials were applied by means of a potentiostat device. Potentials were measured versus an Ag/AgCl reference electrode. The freely corroding potentials of the various materials studied are given in Table B4

Results

The results of this phase of the program are shown in Figs. B6 through B11. These figures are logarithmic plots of crack growth rate (da/dN) vs. stress-intensity factor range (ΔK) for the six materials included in this phase of the program. Each plot includes a reference curve generated in a laboratory ambient air environment (relative humidity ~50 percent) plus data generated in flowing natural seawater under freely corroding conditions and under various applied electrochemical potentials. All data shown are for a 10 cpm triangular load-time wave form unless otherwise noted. Several of the air environment reference curves include higher frequency data from other phases of this study or from previous studies and are shown for confirmation purposes. Specifically, the HY-130 air environment data are reported in reference B28, and some of the 17-4 PH air environment data are reported in reference B29 under another phase of this program. Also, one curve of potentiostated seawater data for the HY-130 material was obtained at a frequency of 1 cpm.

A wide variety of responses to seawater and electrochemical potential were noted among the six materials.

(i) no effect of either seawater or potential (Ti-6Al-2Cb-1Ta-0.8Mo)

(ii) deleterious effect of seawater with no effect of potential (vacuum melted 17-4 PH steel)

(iii) deleterious effect of seawater with beneficial effect of potential (5456-H116 aluminum)

(iv) deleterious effect of seawater with deleterious effect of potential (argon-oxygen melted 17-4 PH steels)

(v) deleterious effect of seawater and potential with a further deleterious effect of reduced cyclic frequency (HY-130 steel)

The magnitudes of the seawater-induced accelerations in crack growth rates varied from negligible to an order of magnitude, with the greatest accelerations tending to occur under lower-amplitude cycling conditions.

DISCUSSION

The highly varied effects of natural seawater and electrochemical potential on fatigue crack growth rates observed in this study have important implications for the use of these materials in high-performance naval ship structures. Particular emphasis should be placed on the results obtained for HY-130 and 17-4 PH steels, owing to the deleterious nature of the effects observed and immediacy of these materials to Navy programs. Specifically, the seriously deleterious effects of seawater, electrochemical potential and reduced cyclic frequency observed in these materials relate directly to actual service conditions. Despite new developments in coating systems, these materials do suffer direct contact with seawater. Electrochemical potentials of the sign and magnitude included in this study are encountered with these materials as the result of unintentional coupling between dissimilar metals (such as steel foils and an aluminum hull) or as the result of the intentional use of sacrificial anodes to suppress pitting and crevice corrosion. Low cyclic frequency loading (~10 to 1 cpm) is also encountered in the actual service loading of these materials. The results of this study clearly indicate each of these factors to be a potential problem area in the application of these high-strength marine alloys to high-performance ship structures.

However, the results obtained on the nonferrous titanium and aluminum alloys are more promising. The results for Ti-6Al-2Cb-1Ta-0.8Mo showing no effect of either seawater or potential suggest that this alloy may be a very attractive candidate material for applications involving corrosion-fatigue. Also, the results for 5456-H116 aluminum showing only a modest deleterious effect of seawater and a beneficial effect of potential suggest that electrochemistry may offer a means of protecting this material against corrosion-fatigue.

SUMMARY AND CONCLUSIONS

Corrosion-fatigue crack propagation studies were conducted on a selected group of high-strength marine alloys in flowing natural seawater at various controlled levels of electrochemical potential. The materials studied included: HY-130 steel, vacuum melted 17-4 PH steel in the H1050 temper, argon-oxygen melted 17-4 PH steel in the H1050 and H1150 tempers, Ti-6Al-2Cb-1Ta-0.8Mo and 5456-H116 aluminum alloy. The results are presented in terms of a da/dN-ΔK fracture mechanics format. These results have shown that:

(a) The corrosion-fatigue response of these alloys to natural seawater and electrochemical potential varies widely depending upon the particular alloy. Effects range from negligible to seriously deleterious.

(b) Generally, the high-strength steels (HY-130 and 17-4 PH) currently committed to Navy programs are among the most seriously affected by corrosion-fatigue.

(c) The nonferrous marine alloys (Ti-6Al-2Cb-1Ta-0.8Mo and 5456-H116 aluminum) exhibited very promising responses to the conditions of corrosion-fatigue utilized in this program.

B13. R. C. Bates and W. G. Clark, Jr., "Fractography and Fracture Mechanics," ASM Trans. 62, No. 2, 380-389 (June 1969).

B14. J. M. Barsom, E. J. Imhof, and S. T. Rolfe, "Fatigue-Crack Propagation in High Yield-Strength Steels," Eng. Fracture Mech. 2, No. 4, 301-317, June 1971.

B15. T. W. Crooker, "Fatigue and Corrosion-Fatigue Crack Propagation in Intermediate-Strength Aluminum Alloys," ASME Trans. 95, Ser. H, No. 3, 150-156 (July 1973).

B16. G. A. Miller, "The Dependence of Fatigue-Crack Growth Rate on the Stress Intensity Factor and the Mechanical Properties of Some High-Strength Steels," ASM Trans. 61, No. 3, 442-448 (Sept. 1968).

B17. A. A. Anctil and E. B. Kula, "Effect of Tempering Temperature on Fatigue Crack Propagation in 4340 Steel," <u>Effects of Environment and Load History on Fatigue Life, ASTM STP 462, American Society for Testing and Materials</u>, pp. 297-317, 1970.

B18. J. F. Throop and G. A. Miller, "Optimum Fatigue Crack Resistance," <u>Achievement of High Fatigue Resistance in Metals and Alloys, ASTM STP 467, American Society for Testing and Materials</u>, pp. 154-168, 1970.

B19. P. R. V. Evans, N. B. Owen, and B. E. Hopkins, "The Effect of Purity on Fatigue Crack Growth in a High-Strength Steel," Eng. Fracture Mech. 3, No. 4, pp. 463-473 (Dec. 1971).

B20. S. Pearson, "The Effect of Mean Stress on Fatigue Crack Propagation in Half-Inch (12.7 mm) Thick Specimens of Aluminum Alloys of High and Low Fracture Toughness," Eng. Fracture Mech. 4, No. 1, pp. 9-24 (March 1972).

B21. C. E. Richards and T. C. Lindley, "The Influence of Stress Intensity and Microstructure on Fatigue Crack Propagation in Ferritic Materials," Eng. Fracture Mech. 4, No. 4, 951-978 (Dec. 1972).

B22. R. O Ritchie and J. F. Knott, "Mechanisms of Fatigue Crack Growth in Low Alloy Steel," Acta Met. 21, 639-648 (May 1973).

B23. R. O. Ritchie and J. F. Knott, "Micro Cleavage Cracking During Fatigue Crack Propagation in Low Strength Steel," Mater. Sci. Eng. 14, No. 12, 7-14 (1974).

B13. R. C. Bates and W. G. Clark, Jr., "Fractography and Fracture Mechanics," ASM Trans. 62, No. 2, 380-389 (June 1969).

B14. J. M. Barsom, E. J. Imhof, and S. T. Rolfe, "Fatigue-Crack Propagation in High Yield-Strength Steels," Eng. Fracture Mech. 2, No. 4, 301-317, June 1971.

B15. T. W. Crooker, "Fatigue and Corrosion-Fatigue Crack Propagation in Intermediate-Strength Aluminum Alloys," ASME Trans. 95, Ser. H, No. 3, 150-156 (July 1973).

B16. G. A. Miller, "The Dependence of Fatigue-Crack Growth Rate on the Stress Intensity Factor and the Mechanical Properties of Some High-Strength Steels," ASM Trans. 61, No. 3, 442-448 (Sept. 1968).

B17. A. A. Anctil and E. B. Kula, "Effect of Tempering Temperature on Fatigue Crack Propagation in 4340 Steel," <u>Effects of Environment and Load History on Fatigue Life, ASTM STP 462, American Society for Testing and Materials</u>, pp. 297-317, 1970.

B18. J. F. Throop and G. A. Miller, "Optimum Fatigue Crack Resistance," <u>Achievement of High Fatigue Resistance in Metals and Alloys, ASTM STP 467, American Society for Testing and Materials</u>, pp. 154-168, 1970.

B19. P. R. V. Evans, N. B. Owen, and B. E. Hopkins, "The Effect of Purity on Fatigue Crack Growth in a High-Strength Steel," Eng. Fracture Mech. 3, No. 4, pp. 463-473 (Dec. 1971).

B20. S. Pearson, "The Effect of Mean Stress on Fatigue Crack Propagation in Half-Inch (12.7 mm) Thick Specimens of Aluminum Alloys of High and Low Fracture Toughness," Eng. Fracture Mech. 4, No. 1, pp. 9-24 (March 1972).

B21. C. E. Richards and T. C. Lindley, "The Influence of Stress Intensity and Microstructure on Fatigue Crack Propagation in Ferritic Materials," Eng. Fracture Mech. 4, No. 4, 951-978 (Dec. 1972).

B22. R. O Ritchie and J. F. Knott, "Mechanisms of Fatigue Crack Growth in Low Alloy Steel," Acta Met. 21, 639-648 (May 1973).

B23. R. O. Ritchie and J. F. Knott, "Micro Cleavage Cracking During Fatigue Crack Propagation in Low Strength Steel," Mater. Sci. Eng. 14, No. 12, 7-14 (1974).

B24. A. Yuen, S. W. Hopkins, G. R. Leverant, and C. A. Rau, "Correlations between Fracture Surface Appearance and Fracture Mechanics Parameters for Stage II Fatigue Crack Propagation in Ti-6Al-4V," Met. Trans. 5, No. 8, 1833-42 (1974).

B25. K. R. L. Thompson and J. V. Craig, "Fatigue Crack Growth Along Cleavage Planes in an Aluminum Alloy," Met. Trans. 1, 1047-49 (1970).

B26. J. A. Kies, H. L. Smith, H. E. Romine and H. Bernstein, "Fracture Testing of Weldments," Fracture Toughness Testing and its Applications, ASTM STP 381, American Society for Testing and Materials, p. 328, 1965.

B27. J. M. Barsom, "Effect of Cyclic Stress Form on Corrosion Fatigue Crack Propagation Below K_{Iscc} in a High Yield Strength Steel," Corrosion Fatigue, National Association of Corrosion Engineers, p. 424, 1972.

B28. A. M. Sullivan and T. W. Crooker, "Analysis of Fatigue-Crack Growth in a High-Strength Steel - Part 1: Stress Level and Stress Ratio Effects at Constant Amplitude," ASME Paper No. 75-WA/PVP-22.

B29. T. W. Crooker, D. F. Hasson and G. R. Yoder, "A Fracture Mechanics and Fractographic Study of Fatigue-Crack Propagation Resistance in 17-4 PH Stainless Steels," NRL Report 7910, July 17, 1975.

TABLE B1. CHEMICAL COMPOSITIONS BY ELEMENT (Wt. Pct.)

Melt	Cr	Ni	Cu	C	Mn	P	S	Si	N	Cb	Ta	Co
AOM	15.84	4.26	3.36	0.032	0.32	0.02	0.017	0.60	-	0.22	0.01	-
VM	15.81	4.47	3.34	0.046	0.26	0.02	0.008	0.53	0.016	0.28	0.01	0.04

TABLE B2. MECHANICAL PROPERTIES

Melt	Condition	DT Energy (Nm)	DT Energy (ft.-lb.)	σ_{ys} (MPa)	σ_{ys} (ksi)	σ_{uts} (MPa)	σ_{uts} (ksi)	El. (%)	RA (%)	Hardness R_c
AOM	H1050	149	110	1124	163.0	1178	170.8	12.5	47.2	36.8
AOM	H1150	169	125	931	135.0	1025	148.6	14.2	48.0	32.5
VM	H1050	651	480	1059	153.6	1105	160.3	16.0	62.0	34.3

TABLE B3. MECHANICAL PROPERTIES

Material	σ_{ys} (MPa)	σ_{ys} (ksi)	σ_{uts} (MPa)	σ_{uts} (ksi)	El. (%)	RA (%)
HY-130	1015	147.2	1054	152.9	18.8	20.0
Ti-6Al-2Cb-1Ta-0.8Mo	789	114.5	865	125.5	12.0	27.6
5456-H116 Al	214	31.1	371	53.8	22.7	20.0

TABLE B4. FREELY CORRODING POTENTIALS VERSUS Ag/AgCl

Material	HY-130	17-4 PH VM	17-4 PH AOM	5456-H116 Al	Ti-6Al-2Cb-1Ta-0.8Mo
Potential (mv)	-665	-300	-200	-950	-300

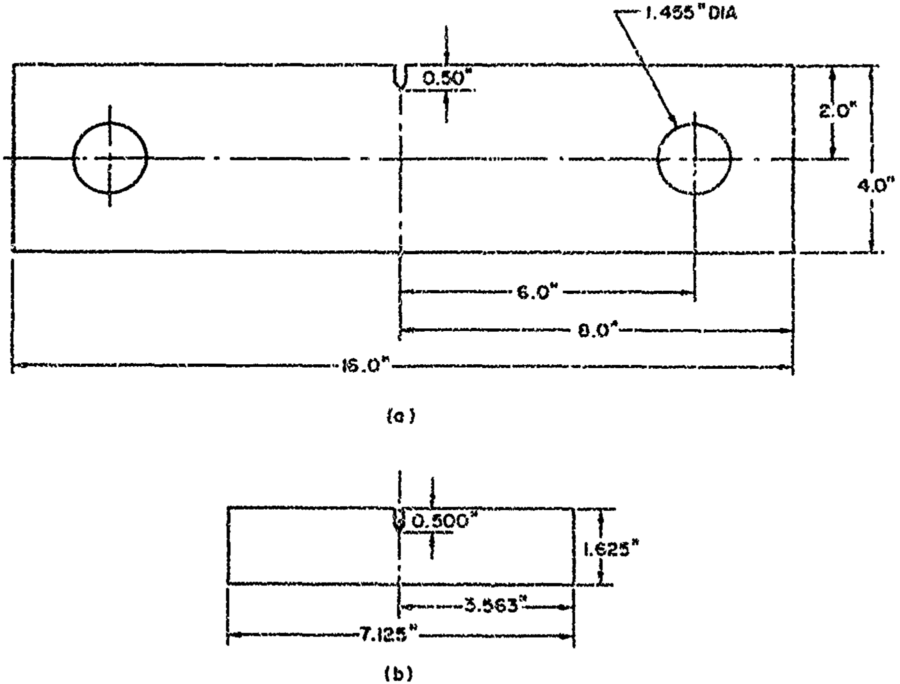

Fig. B1 — Geometries of (a) SEN specimen for fatigue-crack-growth study and (b) 5/8-in. Dynamic Tear Test. (Conversion factor: 1 in. = 2.54 cm.)

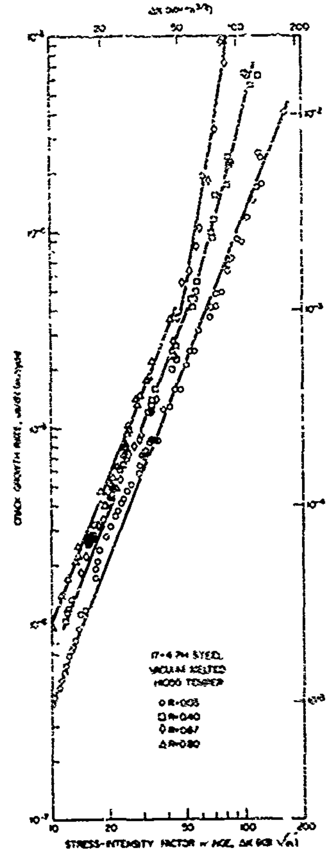

(a)

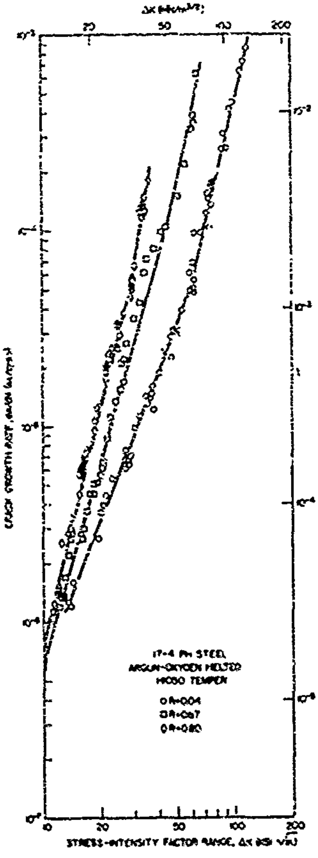

(b)

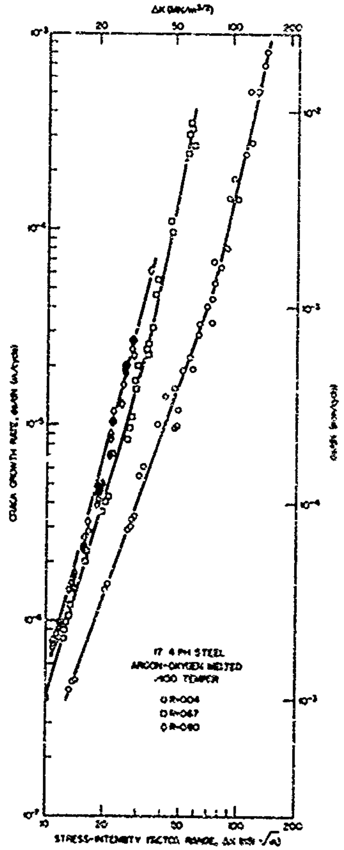

(c)

Fig. B2 — Fatigue crack growth data for (a) VM-H1050 steel, (b) AOM-H1050 steel, and (c) AOM-H1150 steel

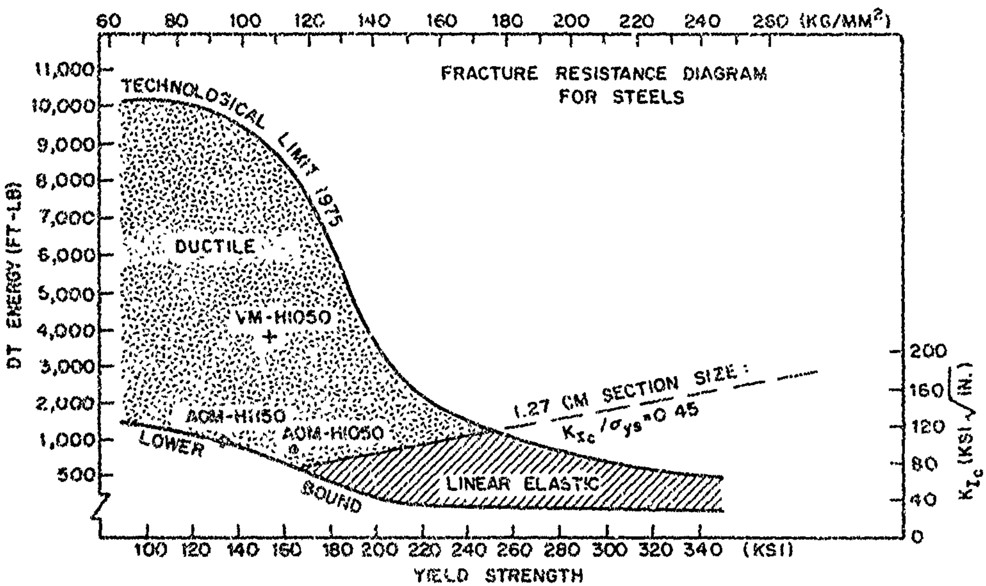

Fig. B3 — Fracture resistance diagram for steels. (Conversion factors: 1 in. = 2.54 cm, 1 ksi$\sqrt{in.}$ = 1.099 MPa$\sqrt{m}$, 1 ksi = 6.89 MPa.)

Fig. B4 — Microcleavage mode of fatigue crack growth in the AOM-H11050 steel. Stereoscopic pair of replica electron fractographs.

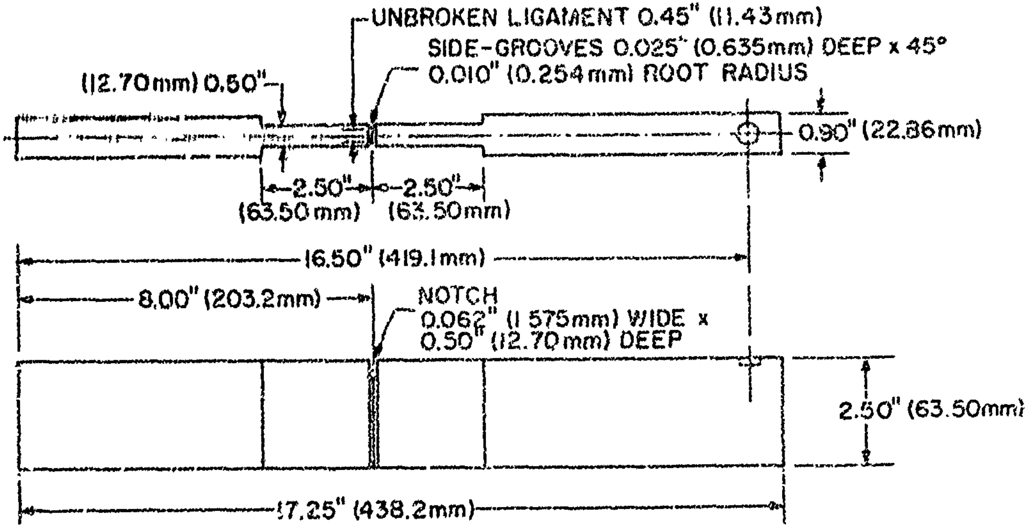

Fig. B5 — Details of the SEN cantilever specimen for corrosion-fatigue crack growth study

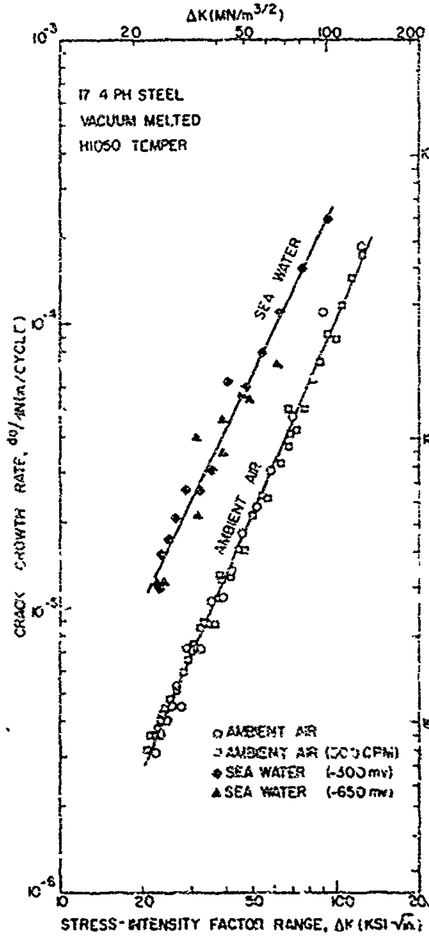

Fig. B6 — Corrosion-fatigue crack growth data for 17-4 PH VM-H1050 steel

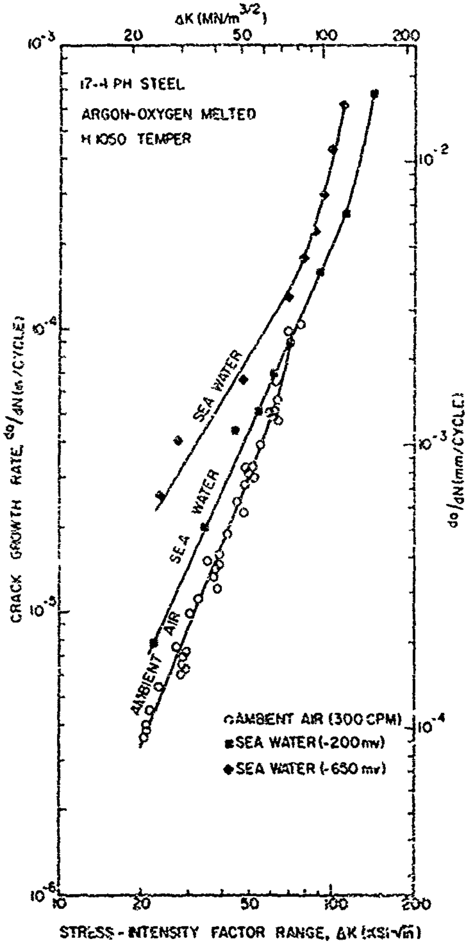

Fig. B7 — Corrosion-fatigue crack growth data for 17-4 PH AOM-H1050 steel

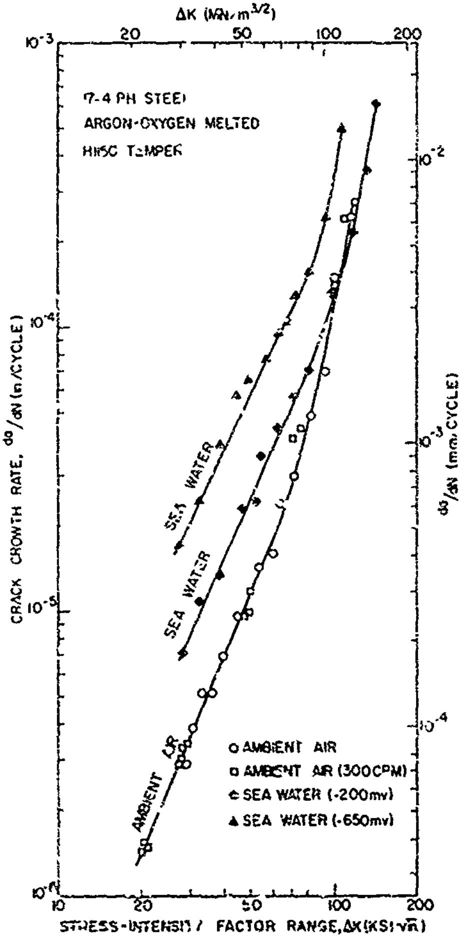

Fig. B8 — Corrosion-fatigue crack growth data for 17-4 PH AOM-H1150 steel

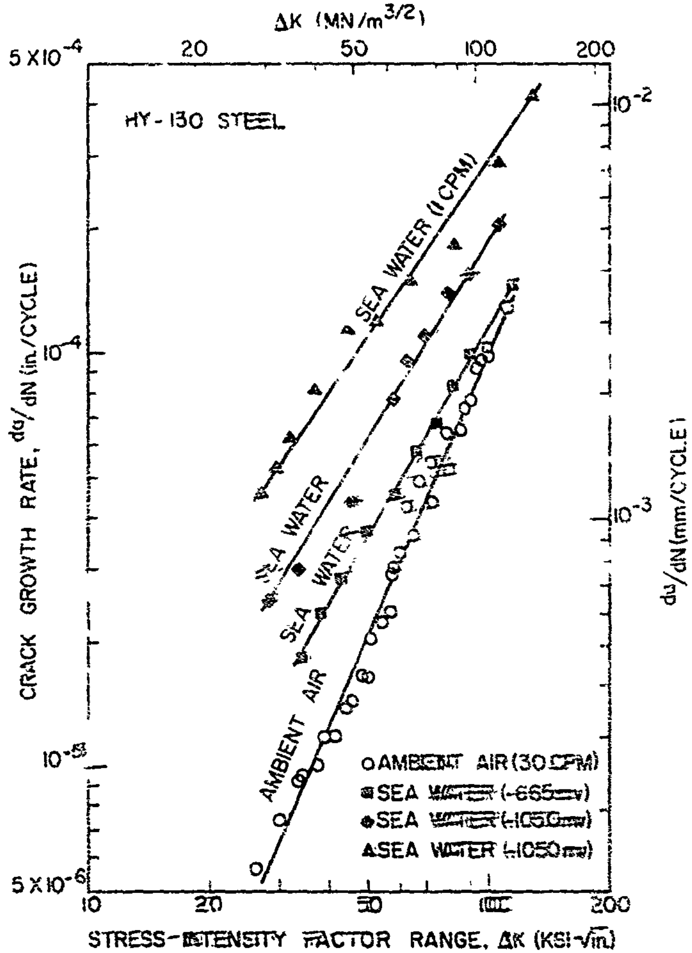

Fig. B9 — Corrosion-fatigue crack growth data for HY-130 steel

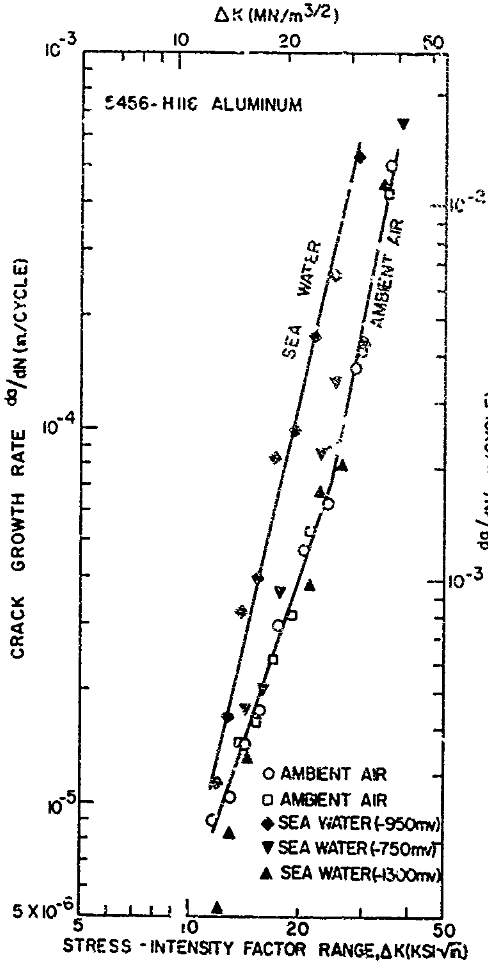

Fig. B11 — Corrosion-fatigue crack growth data for 5456-H116 aluminum alloy

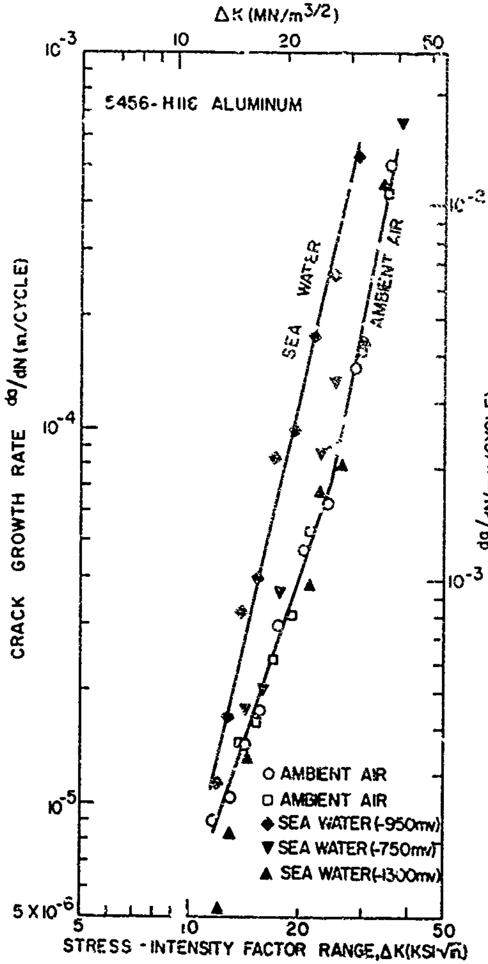

Fig. B11 — Corrosion-fatigue crack growth data for 5456-H116 aluminum alloy

C. Fracture Mechanics Technology/Crack Growth and Electrochemical Protection

Dr. C. T. Fujii

INTRODUCTION

Ships or craft designed for high speed service, such as hydrofoils, will be expected to perform reliably under adverse operating conditions. A real threat to reliable performance, however, is posed by SCC - i.e., the extension of flaws in metals from the combined effects of stress and corrosion. The deleterious synergistic effects of tensile stress and the corrosive ocean environment on structural alloys generally tend to progressively worsen with increasing yield strength. Inadequate background experience in the use of modern high strength alloys in thickness/strength level combinations under hostile marine conditions such as for FCS applications severely restricts attempts to define safe operational limits for such advanced structures. The SCC behavior of candidate alloys for FCS construction needs to be more adequately established to effectively guide material selection, design, and fabrication procedures, as well as aid development of electrochemical protection technology.

The effects of electrochemical potential on the SCC behavior of most alloys are particularly pertinent for naval applications. Increased cathodic potentials may cause crack growth at lower values of K_{Iscc} than under freely corroding conditions, and the magnitude of the effect can be expected to vary with alloy systems. Cathodic protection systems while minimizing corrosion can simultaneously cause increased absorption of hydrogen at the crack-tip which results in an increased SCC sensitivity of the alloy. Thus, electrochemical effects need to be defined accurately to prescribe effective cathodic protection systems for new high strength alloys without significantly lowering the SCC resistance as well as to provide a capability for predicting behavior of galvanically coupled dissimilar alloys as might occur in actual naval structures.

OBJECTIVE

The objective of this subtask was to determine the effect of electrochemical factors on the SCC properties of leading

candidate alloys for fast craft and ships (FCS) applications. The emphasis was on characterizing the SCC behavior of thin-plate materials - one inch or less - utilizing precracked specimens which were tested in 3.5% NaCl solution under freely-corroding and electrochemically coupled (cathodically protected) conditions. Included in the SCC studies were several steels, titanium alloys, and marine aluminum alloys.

SCC TEST METHOD

The cantilever test method employing single-edge-notch (SEN) fatigue-precracked specimens was used to determine the threshold stress-intensity factor for SCC (K_{Iscc}) of selected steels and titanium alloys. The corrodent, 3.5% NaCl solution, was contained in a polyethylene reservoir around the crack and changed daily during the experiment. Tests were conducted for the freely corroding condition of the specimen and for different cathodically polarized conditions by galvanic coupling to appropriate anode materials. The electrochemical potentials of the specimens were measured against an Ag/AgCl reference electrode. A step-load procedure was followed to determine K_{Iscc} values for steel specimens; a single-load-failure criterion was adopted to establish the SCC thresholds for the titanium alloy specimens. At the conclusion of each test, the fracture surfaces of the specimens were examined for confirming evidences of SCC.

ACCOMPLISHMENTS

17-4 PH Steel

An extensive characterization of the SCC behavior of 17-4 PH steel emphasizing the effects of tempering procedures, plate thicknesses, and electrochemical potentials has been completed. The data from cantilever bend tests are summarized in Tables C1 and C2, and graphically compared in Figures C1 and C2. The results show that:

- Increasing yield strength decreases the SCC resistance of the alloy.

- Increasing cathodic polarization decreases SCC resistance of the alloy.

- Metallurgically overaging improves the SCC resistance and flaw tolerance of the alloy.

- The specimen thickness required for determining thickness-independent K_{Iscc} for 17-4 PH steel is considerably less than required for a standard K_{Ic} test.

17-4 PH GMA Weldment

The SCC properties of a 17-4 PH GMA weldment were determined, and the results are summarized in Table C3. Comparison of the SCC behavior of the base and weld metals showed matching properties under cathodically polarized conditions but a measurable decrease of approximately 25% in SCC resistance for the weld metal under freely corroding conditions.

Details of the SCC properties of 17-4 PH steel and GMA weld metal are documented in the publications on these materials listed in the Bibliography.

15-5 PH Steel

The SCC behavior of precracked specimens from thin-plate 15-5 PH steel were determined; and the K_{Iscc} data for 6.4 mm (0.25 in.), 12.7 mm (0.50 in.), and 25.4 mm (1.00 in.) thick plates for the H1050 temper are given in Table C4. Results are similar and comparable to those noted above for 17-4 PH steel.

HY-130 Steel

The SCC properties of two different heats of HY-130 steel in 25.4 mm-thick (1 inch-thick) plate form were determined in 3.5% NaCl solution in the freely corroding and electrochemically coupled conditions. Table C5 summarizes the results obtained. The material has relatively high SCC resistance under freely corroding and limited applied cathodic potentials (coupled to 5086 Al). At higher cathodic potentials, there is a significant decrease in SCC resistance. Details of the SCC experiments of this material are given in Report of NRL Progress of November 1973 (see Bibliography).

Titanium Alloys

Four titanium alloys, each in two plate thicknesses, were characterized under freely corroding and zinc-coupled conditions. The alloys were Ti-6Al-4V (CP grade), Ti-6Al-4V (ELI grade), Ti-6Al-6V-2Sn, and Ti-6Al-2Nb-1Ta-0.8Mo. The results of the SCC tests are summarized in Table C6. All of these alloys exhibited some degree of susceptibility to SCC, but their SCC resistance in salt water is relatively good in comparison to other titanium alloys (such as Ti-7-2-1 and Ti-8-1-1). There appears to be an effect of specimen thickness, B, on the measured K_{Iscc} values. Higher threshold K-values were observed for 6.4 mm (0.25 in.) than 12.7 mm (0.50 in.) specimens for three of the alloys which suggests

lack of crack-tip mechanical constraint in 6.4 mm (0.25 in.) specimens. Metallurgical and yield strength differences between 6.4 mm (0.25 in.) and 12.7 mm (0.50 in.) plates may also have contributed to the observed behavior and perhaps partially explain the performance of the Ti-6Al-6V-2Sn alloy. One notable difference between the SCC behavior of titanium alloys and high strength steels is the relative insensitivity of titanium alloys to applied cathodic potentials as shown by comparison of the freely corroding and Zn-coupled data in Table C6.

Aluminum-Magnesium Alloys

The SCC behavior of two Alcoa Al-Mg alloys - a commercial alloy, 5456-H117, and an experimental alloy, N-H117, was determined in the as-received and aged conditions for susceptibility to cracking in 3.5 percent NaCl solution utilizing double cantilever beam specimens machined from 1-in.-thick plates of the two alloys. The chemical composition of the alloys and the results of the SCC tests are given in Tables C7 and C8, respectively. The results show that the as-received specimens were insensitive to SCC in these tests with the exception of one N-H117 specimen. All of the aged specimens of both alloys were susceptible to SCC. As expected, there is a pronounced tendency to favor SCC in the SL orientation.

SUMMARY DISCUSSION

The work which has been completed has defined the SCC properties of thin plates of several materials which are presently prime candidates for FCS application. These materials include two high-strength stainless steels, a quenched-and-tempered steel, several titanium alloys, and two aluminum alloys. The SCC data obtained for these alloys are some of the most extensive for any thin-plate material obtained to date. All of the high-strength alloys studied were susceptible to a limited degree to SCC. The variation in SCC resistance was shown to be influenced by yield strength, electrochemical potential, and metallurgical variables. The relative influence of each factor varied with alloy system and can be qualitatively described as follows:

- Steels - increasing yield strength and increasing negative potentials decreased SCC resistance.

- Titanium alloys - increasing yield strength generally decreased SCC resistance, but the freely-corroding SCC properties were not affected by an applied negative potential.

- Aluminum alloys - overaging high-magnesium marine aluminum alloys decreases SCC resistance. The SCC properties

of wrought aluminum alloys are highly orientation dependent and are minimal in the short-transverse direction.

The tabulated data for these three types of materials offer a more quantitative basis for comparisons of the effects of temper, potential, plate thickness, and alloy system on the SCC properties in a saline environment. For engineering or structural applications, the comparison of SCC properties is facilitated by a graphical summary of valid data in the format of a Ratio Analysis Diagram (RAD). Figure C3 is a RAD for SCC of steels in laboratory salt water (approximately 3.5 percent NaCl solution) where the ordinate is the critical stress-intensity factor for SCC, K_{Iscc}, and the abscissa is the yield strength, σ_y, of the steel. For purposes of discussing the significance and utility of the K_{Iscc} data of a given alloy, 17-4 PH results are included in Fig. C3. The SCC envelope, the shaded region, was constructed using most of the available SCC data determined for a wide variety of steels by several laboratories. Visual confirmation of crack growth was imposed as a requirement before the K_{Iscc} data were included to define the boundary limits of the envelope. The older forging grade steels would be representative of material in the lower regions of the envelope. The newer weldable steels of improved quality would generally fall in the higher range of the envelope. The system of constant K_{Iscc}/σ_y ratio lines divides the diagram into three ratio zones - high, intermediate, and low. These zones may also be regarded as levels of resistance to SCC. The transition from high to intermediate and low SCC resistance is relatively sharp as indicated by the general slope of the envelope. For specimens with sufficient mechanical constraint to assure applicability of linear elastic fracture mechanics, the ratios are directly relatable to critical flaw sizes for SCC and are most useful for predicting structural performance when applied in this context. The SCC problem is much less severe for high ratio than low ratio material because of its inherently higher flaw tolerance. Thus, under constant applied stress conditions, high ratio material will tolerate larger preexisting cracks before succumbing to SCC. The 17-4 PH data in Fig. C3 show that for the freely-corroding condition this alloy has relatively "high" SCC resistance at yield strengths below approximately 1034 MPa (150 ksi) and an "intermediate" level of SCC resistance at higher yield strengths. Cathodic polarization of the specimen to the zinc potential (-1.0V vs. Ag/AgCl) reduces the SCC resistance to "intermediate" and "low" levels for the indicated yield strength range of 827 to 1241 MPa (120 to 180 ksi). The advantages of low yield strength and the disadvantages of Zn-coupling on the SCC properties of 17-4 PH steel in comparison to other commercial steels are thus clearly evident in Fig. C3.

K_{Iscc} data for other alloy systems may similarly be displayed in the format of RAD's for purposes of rating the SCC behavior of alloys.

TABLE C1. SCC PROPERTIES OF 17-4 PH STEEL IN 3.5% NaCl SOLUTION

TEMPER	σ_y		K_{Ix} Air		K_{Iscc} FC* (-0.3V)•		K_{Iscc} 5086 Al (-0.8V)		K_{Iscc} Zn (-1.0V)		K_{Iscc} Mg (-1.3V)		K_{Iscc} Pot.* (-1.3V)	
	MPa	(ksi)	MPa$\sqrt{m}$	(ksi$\sqrt{in.}$)	MPa$\sqrt{m}$	(ksi$\sqrt{in.}$)	MPa$\sqrt{m}$	(ksi$\sqrt{in.}$)	MPa$\sqrt{m}$	(ksi$\sqrt{in.}$)	MPa$\sqrt{m}$	(ksi$\sqrt{in.}$)	MPa$\sqrt{m}$	(ksi$\sqrt{in.}$)
H900	1220	(177)	124	(113)	87	(79)	59	(54)	33	(30)	29	(26)	31	(28)
H975	1117	(162)	160	(146)	112	(102)	84	(76)	49	(45)	35	(32)	33	(30)
H1025	1082	(157)	173	(157)	122	(111)	98	(89)	58	(53)	38	(35)	40	(36)
H1075	1041	(151)	182	(166)	135	(123)	113	(103)	71	(65)	44	(40)	43	(39)
H1150	827	(120)	187	(170)	143	(130)	127	(116)	85	(77)	48	(44)	45	(41)
H1150M	627	(91)	130	(118)	107	(97)	102	(93)	110	(100)	99	(90)	-	-

*FC - freely corroding, Pot. - potentiostated

•Potential as measured against Ag AgCl reference electrode

TABLE C2. Effect of Specimen Thickness, B, on K_{Iscc} of 17-4 PH Steel*

PLATE THICKNESS		DIMENSIONS ‡						K_{Iscc}, $MPa\sqrt{m}$ ($ksi\sqrt{in.}$)					
		B		W		a		FC (-03V)		5086 Al (-0.8V)		Zn (-1.0V)	
mm	(in.)	mm	(in.)	mm	(in.)	mm	(in.)						
5.1	(0.20)	5.1	(0.20)	9.7	(0.38)	5.1	(0.20)	93	(85)	71	(65)	48	(44)
								88	(80)	64	(58)	44	(40)
7.9	(0.31)	7.8	(0.31)	16.0	(0.63)	8.6	(0.34)	118	(107)	95	(86)	58	(53)
								104	(95)	86	(78)	53	(48)
9.5	(0.37)	9.5	(0.37)	18.8	(0.74)	10.2	(0.40)	116	(106)	93	(85)	60	(55)
								122	(111)	93	(85)	60	(55)
15.9	(0.63)	15.9	(0.63)	31.8	(1.25)	16.8	(0.66)	124	(113)	104	(95)	54	(49)
								132	(120)	100	(91)	59	(54)
25.4	(1.00)	18.6	(0.73)	25.4	(1.00)	13.2	(0.52)	116	(103)	96	(87)	58	(53)
								110	(100)	98	(89)	60	(55)

*H1050 Temper, $\bar{\sigma}_y$ = 1089 MPa (158 ksi)

‡ WOL Cantilever Specimen

TABLE C3. SCC PROPERTIES OF 17-4 PH BASE ALLOY AND GMA WELDMENT IN 3.5% NaCl SOLUTION

MATERIAL	σ_y MPa	(ksi)	K_{Iscc}, MPa$\sqrt{m}$ (ksi$\sqrt{in.}$) FC* (-0.3V)‡		Zn (-1.0V)		Mg (-1.3V)	
Base Alloy	1020	(148)	132	(120)	71	(65)	47	(43)
Weldment	1014	(147)	102	(93)	71	(65)	56	(51)

*FC = Freely Corroding

‡Specimen potential vs. Ag/AgCl reference electrode

TABLE C4. SCC PROPERTIES OF THIN-PLATE 15-5 PH STEEL IN 3.5% NaCl SOLUTION

Plate Thickness mm	Plate Thickness (in.)	Yield Strength MPa	Yield Strength (ksi)	Dimensions[a] B mm	B (in.)	W mm	W (in.)	a mm	a (in.)	K_{Ix} All MPa $\sqrt{m}$	K_{Ix} All (ksi $\sqrt{in.}$)	K_{Iscc}, MPa $\sqrt{m}$ (ksi $\sqrt{in.}$) FC* (-0.5V)+		5086Al (-0.8V)		Zn (-1.0V)	
6.6	(0.26)	1082	(157)	6.6	(0.26)	12.4	(0.49)	6.6	(0.26)	108	(98)	93 100	(85) (91)	77 07	(70) (79)	62 57	(56) (52)
12.7	(0.50)	1103	(160)	12.7	(0.50)	25.4	(1.00)	12.7	(0.50)	140	(127)	131 136	(119) (124)	101 110	(92) (100)	56 55	(51) (50)
25.4	(1.00)	1089	(158)	19.1	(0.75)	26.7	(1.05)	12.7	(0.50)	143	(130)	138 13[illegible]	(126) (125)	116 114	(106) (104)	56 54	(51) (49)

[a]SEN Cantilever Specimen

*FC = freely corroding

+Potential in volts vs. Ag/AgCl reference electrode

TABLE C5. SCC PROPERTIES OF FREELY-CORRODING AND COUPLED HY-130 STEEL PLATE IN 3.5% NaCl SOLUTION

Material	σ_y MPa	σ_y (ksi)	Electrochemical Condition	K_{Iscc} MPa$\sqrt{m}$	K_{Iscc} (ksi$\sqrt{in.}$)
Heat A - as received 25.4 mm (1-inch-thick) plate	896	(130)	Freely Corroding	142	(129)
	896	(130)	Coupled to 5083 Al	145	(132)
	896	(130)	Coupled to Zn	118	(107)
	896	(130)	Coupled to Mg	89	(81)
Heat B - as received 25.4 mm (1-inch-thick) plate	945	(137)	Freely Corroding	142	(129)
	945	(137)	Coupled to 5086 Al	145	(132)
	945	(137)	Coupled to Zn	107	(97)
	945	(137)	Coupled to Mg	95	(86)

Cantilever Specimen Dimensions: B = 20.3 mm (0.8 in.), W = 25.4 mm (1.0 in.), a = 6.4 mm (0.25 in.)

TABLE C6. SCC PROPERTIES OF THIN-PLATE TITANIUM ALLOYS IN 3.5% NaCl SOLUTION

Ti Alloy	Plate Code	Plate Thickness		σ_y		K_{Ix} Air		K_{Iscc} FC*		Zn	
		mm	(in)	MPa	(ksi)	$MPa\sqrt{m}$	$(ksi\sqrt{in.})$	$MPa\sqrt{m}$	$(ksi\sqrt{in.})$	$MPa\sqrt{m}$	$(ksi\sqrt{in.})$
6Al-4V (CP)	R49 C	6.4	(0.25)	972	(141)	52	(47)	48	(44)	48	(44)
	R49 D	12.7	(0.50)	993	(144)	41	(37)	32	(29)	32	(29)
6Al-4V (ELI)	R50 C	6.4	(0.25)	938	(136)	63	(57)	55	(50)	52	(47)
	R50 D	12.7	(0.50)	945	(137)	56	(51)	46	(42)	43	(39)
6Al-6V-2Sn	R51 C	6.4	(0.25)	1076	(156)	33	(30)	25	(23)	25	(23)
	R51 D	12.7	(0.50)	1042	(151)	37	(34)	29	(26)	26	(24)
6Al-2Nb-1Ta-0.8Mo	R32	6.4	(0.25)	896	(130)	92	(84)	76	(69)	82	(75)
	R31	12.7	(0.50)	876	(127)	65	(59)	53	(48)	52	(47)

*Potential of specimen vs. Ag/AgCl reference
FC (freely corroding) = -0.3 to -0.5 V
Zn (coupled to Zn) = -1.0 to -1.1 V

SEN SCC Specimen Dimensions mm(in.)

6.4mm plate: B = 6.9(0.27), W = 25.4(1.0), a = 12.7(0.5)
12.7mm plate: B = 13.7(0.54), W = 25.4(1.0), a = 12.7(0.5)

where B = Thickness, W = Height, a = Crack length.

TABLE C7. CHEMICAL ANALYSIS OF ALLOYS

Alloy	Mg	Mn	Cr	Fe	Si	Zn	Ti	Be	Zr
5456-H117	5.0	0.7	0.15	$(0.40_{Max}$	Fe+Si)	0.25_{Max}	0.20_{Max}	-	-
N-H117	7.7	0.4	0.13	0.08	0.12	0.02	0.02	0.001	0.07

TABLE C8. Stress Corrosion Susceptibility of Two 5000-Series Aluminum Alloys

MATERIAL	σ_y MPa	σ_y (ksi)	CRACK PATH	$K_{Initial}$ MPa$\sqrt{m}$	$K_{Initial}$ (ksi$\sqrt{in.}$)	K_{Ix} MPa$\sqrt{m}$	K_{Ix} (ksi$\sqrt{in.}$)	K_{Iscc} MPa$\sqrt{m}$	K_{Iscc} (ksi$\sqrt{in.}$)	REMARKS
5456-H117 (as-received)	221	(32)	SL	57	(52)	31	(28)	No CG*		3 tests - no evidence of SCC
			TL	41	(37)	CB*		No CG		3 tests - no evidence of SCC
			LT	38	(53)	CB		No CG		3 tests - no evidence of SCC
5456-H117 (aged)	221	(32)	SL	48	(44)	31	(28)	26	(24)	2 tests - CG/SCC confirmed
			TL	36	(33)	CB		CG		3 tests - SCC confirmed
			LT	37	(34)	CB		CG		3 tests - SCC confirmed
N-H117 (as-received)	241	(35)	SL	46	(42)	35	(32)	15	(14)	CG/SCC confirmed
			SL	48	(44)	35	(32)	No CG		No evidence of SCC
			SL	42	(38)	38	(35)	No CG		No evidence of SCC
			TL	42	(38)	CB		No CG		3 tests - no SCC
			LT	36	(33)	CB		No CG		3 tests - no SCC
N-H117 (aged)	249	(36)	SL	63	(57)	33	(30)	16	(15)	3 tests - CG/SCC confirmed
			TL	38	(35)	CB		CG		3 tests - SCC confirmed
			LT	43	(39)	CB		CG		3 tests - SCC confirmed

* CB = Crack Branched
* CG = Crack Growth

Confirmation of SCC by visual examination of fracture surfaces.

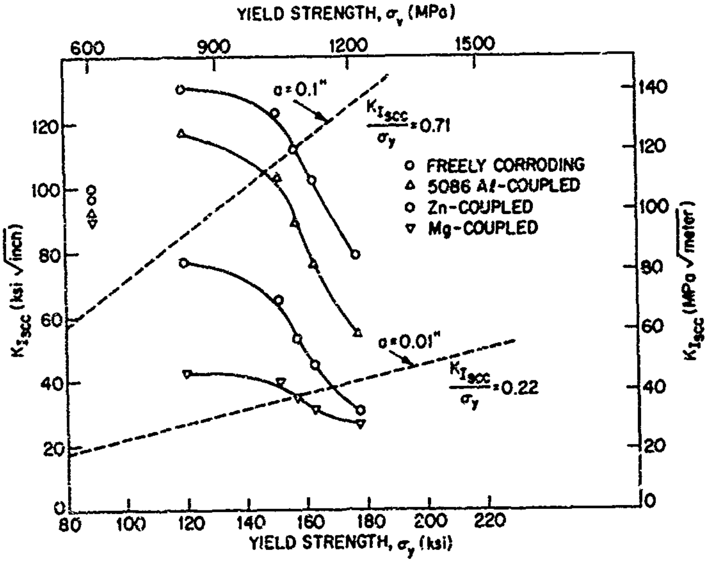

Fig. C1 — K_{Iscc} data for 17-4 PH steel of different yield strengths under four electrochemical conditions. (Conversion factors: 1 ksi = 6.895 MPa, 1 ksi$\sqrt{in.}$ = 1.099 MPa$\sqrt{m}$, 1$\sqrt{in.}$ = 1.594$\sqrt{cm}$, 1 in. = 2.54 cm.)

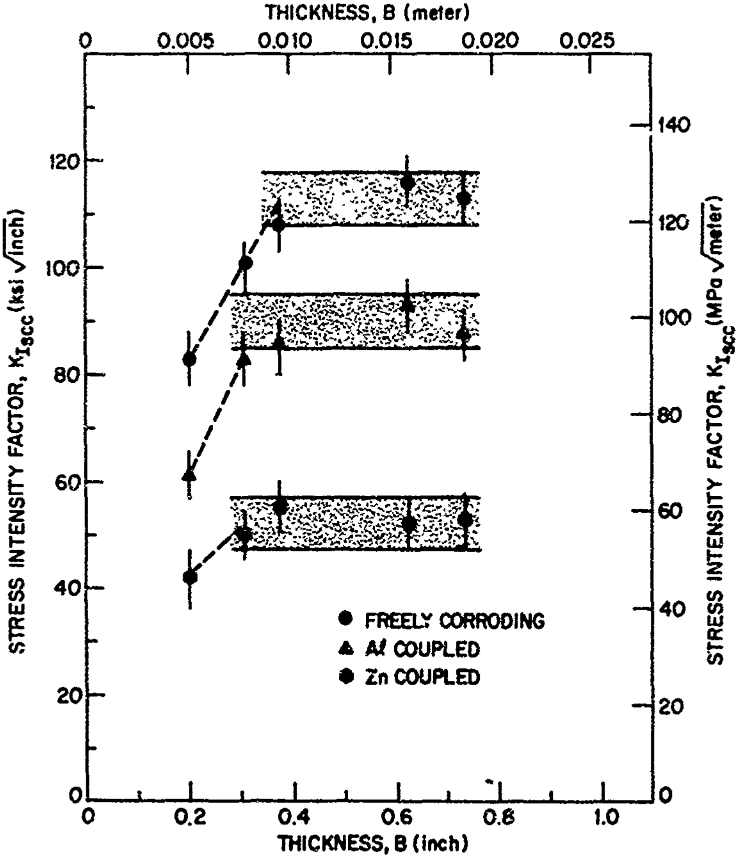

Fig. C2 — The effect of specimen thickness on the measured value of K_{Iscc} for the H1050 temper 17-4 PH steel under three electrochemical conditions

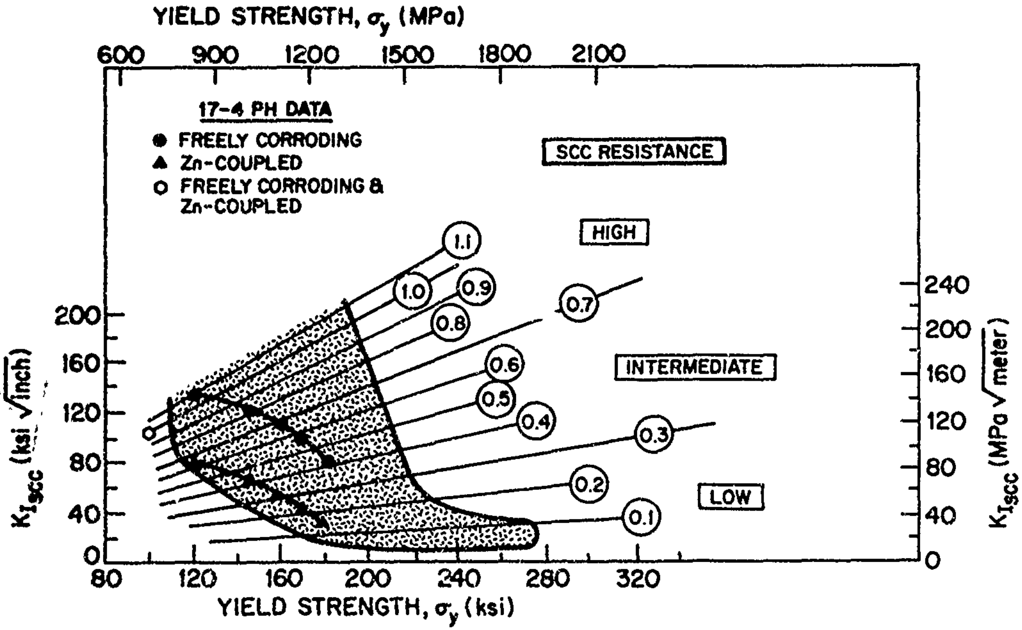

Fig. C3 — Ratio Analysis Diagram for SCC of steels with ratio zoning and superposition of 17-4 PH data

D. Advanced Composites

Dr. J. V. Gauchel and Miss A. M. Sullivan

SUMMARY

The use of composites in "weight critical" Naval vehicles such as the patrol craft hydrofoil is dependent on the development of reliability data for the failure of these materials in a marine environment. The recent recognition of fiber-reinforced composites as a new and valuable class of structural materials is not yet supported by a broad base of reliability data such as has been accumulated on wood, steel, aluminum, etc. over a period of many years. For the most part the data which exists has been derived from short-term laboratory tests and sheds only a little light on the long-term response of the composites to stress in a marine environment.

The principal accomplishment of this subtask has been to determine the effect of long-term exposure to water on the basic fiber-controlled properties of tensile strength, tensile modulus, and fracture toughness of model graphite-reinforced epoxy resin matrix composites systems. While this study has shown that graphite-epoxy composites are extremely stable in a marine environment, it has also determined that they are brittle materials sensitive to crack propagation. It has also demonstrated that the level of quality control in the processing of these materials must be improved before reproducible design data on the effects of matrix and fiber composition can be obtained.

ACCOMPLISHMENTS

The major achievements of this subtask were to monitor the degradation caused by long-term exposure to water of the tensile strength, tensile modulus, and fracture energy of graphite fiber-reinforced epoxy matrix composites, to evaluate the effect of laminate geometry on this degradation, to examine the feasibility of using linear elastic fracture mechanics (LEFM) as a measure of the resistance of composite materials to fast crack growth, and to determine the role of fabrication in the variability of the mechanical properties of composite systems.

it has been shown (D1,D2) that the brittle nature of these materials allows use of LEFM as a model for their failure. Values for the notch sensitivity, K_q, of double notched tensile specimens of each system investigated were evaluated as a function of relative crack length. The results indicated that over a range of relative crack length from 0.2 to 0.6 the notch sensitivity was independent of crack length (Figure D1). The results suggest that LEFM may be a useful method for comparing the resistance of both composites and metallic systems to fast crack growth (Figure D2).

Fabrication-induced variability in composite materials is introduced through differences in fabrication techniques from fabricator to fabricator and by differences in the time-temperature history of the starting prepreg materials (Tables D7 and D8). During the course of this investigation, the variability induced by fabrication masked any effect of compositional parameters on the measured physical properties. This observed variability caused a reevaluation of the fabrication techniques required to manufacture a reproducible laminate. A laboratory vacuum-release method developed previously (D3) for making void-free adhesive bonds was modified for use with a composite system. While this technique is not feasible for the manufacture of large components, it did demonstrate that void-free composites could be produced.

An exploratory investigation was undertaken to assess the suitability of the fracture mechanics parameter K_c for determining the fracture resistance of fiber-reinforced metal-matrix composite materials. In linear elastic fracture mechanics, K_c applies to thin-sheet material essentially under conditions of plane stress where small amount of crack growth occurs prior to instability and final separation. The matter of concern was whether the inhomogeneous nature of metal-matrix composites was sufficient to invalidate the use of traditional methods which were derived for homogeneous metals. The investigations revealed that the inability to predict failure mechanisms, which were different in metal-matrix composites than high-strength metals, and the variation of elastic modulus as a function of orientation of test specimens with respect to fiber direction were the major problem areas in conducting experimental work with these composites. Because of this, it was concluded that fracture resistance as measured by K_c is unlikely to provide reliable characterization for metal-matrix composite materials.

DISCUSSION

The composites industry continues to produce new materials that show potential as components in high performance

it has been shown (D1,D2) that the brittle nature of these materials allows use of LEFM as a model for their failure. Values for the notch sensitivity, K_q, of double notched tensile specimens of each system investigated were evaluated as a function of relative crack length. The results indicated that over a range of relative crack length from 0.2 to 0.6 the notch sensitivity was independent of crack length (Figure D1). The results suggest that LEFM may be a useful method for comparing the resistance of both composites and metallic systems to fast crack growth (Figure D2).

Fabrication-induced variability in composite materials is introduced through differences in fabrication techniques from fabricator to fabricator and by differences in the time-temperature history of the starting prepreg materials (Tables D7 and D8). During the course of this investigation, the variability induced by fabrication masked any effect of compositional parameters on the measured physical properties. This observed variability caused a reevaluation of the fabrication techniques required to manufacture a reproducible laminate. A laboratory vacuum-release method developed previously (D3) for making void-free adhesive bonds was modified for use with a composite system. While this technique is not feasible for the manufacture of large components, it did demonstrate that void-free composites could be produced.

An exploratory investigation was undertaken to assess the suitability of the fracture mechanics parameter K_c for determining the fracture resistance of fiber-reinforced metal-matrix composite materials. In linear elastic fracture mechanics, K_c applies to thin-sheet material essentially under conditions of plane stress where small amount of crack growth occurs prior to instability and final separation. The matter of concern was whether the inhomogeneous nature of metal-matrix composites was sufficient to invalidate the use of traditional methods which were derived for homogeneous metals. The investigations revealed that the inability to predict failure mechanisms, which were different in metal-matrix composites than high-strength metals, and the variation of elastic modulus as a function of orientation of test specimens with respect to fiber direction were the major problem areas in conducting experimental work with these composites. Because of this, it was concluded that fracture resistance as measured by K_c is unlikely to provide reliable characterization for metal-matrix composite materials.

DISCUSSION

The composites industry continues to produce new materials that show potential as components in high performance

Naval systems. Unfortunately, the materials are being developed and modified faster than information on the effect of long-term exposure to a marine environment on their mechanical properties can be generated. This program, as conceived, emphasized the evaluation of reliability criteria for organic-matrix composite system. Of special interest was the determination of the effects of matrix changes on the long-term environmental stability of this material. However, it soon became evident that the use of graphite fiber-reinforced epoxy resin matrix composites as structural materials in high-performance Naval vessels would not be limited by the intrinsic hydrolytic stability of the materials but rather by their brittle nature and by the inability to consistently manufacture reliable laminates.

Of the two problem areas, improving the reproducibility of the fabrication process is the most readily solvable. In fact, recent developments in dielectric analysis and C-13 NMR spectroscopy have given the fabricator powerful tools for overcoming the two major areas of variability - improper cure and variability of the input prepreg.

Improving the toughness of graphite-reinforced systems will require a larger effort. Studies are currently underway to determine the effect of a flexible interlayer between the fiber and the matrix in increasing the toughness of composite systems. Hybridization of the fiber system and increasing toughness by use of stacking sequence designed with integral crack stoppers are also being evaluated. Hopefully, these attempts will result in composites with increased resistance to fast crack propagation.

As of the present date, what is available to the design engineer are materials with good average mechanical properties intrinsically stable in a water environment, but with a variability that causes large penalties in design allowables. These penalties reduce the attractiveness of graphite-reinforced organic systems and cause design engineers to be reluctant to specify their uses.

This study has been able to identify some of the problem areas of organic-matrix composites. It has shown that the graphite system is intrinsically stable in a water environment. The effect of laminate geometry on mechanical properties has been investigated and found to be predictable from considerations of the failure mode and number of load-bearing plies. Linear elastic fracture mechanics has been shown to be a useful method for evaluating the fracture resistance of composite systems. Lastly, this study has documented the need for increased work in the area of fabrication in order to develop reproducible laminated composites.

REFERENCES

D1. D. C. Philips, "The Fracture Mechanisms of Carbon Fibre Laminates," Journal of Composite Materials, Vol. 8 (April 1974), p. 130.

D2. J. F. Mandell, F. J. McGarry, S. S. Wang and J. Im, "Stress Intensity Factors for Anisotropic Fracture for Anisotropic Fracture Test Specimens of Several Geometries," Journal of Composite Materials, Vol. 8 (April 1974), p. 106.

D3. Bascom, W. D. and Romans, J. B., Ind. Eng. Chem. Pred. Research and Development, Vol. 17 (1968), p. 172.

TABLE D1. MATERIALS

Fibers	
HMS	Hercules Corporation
Modmor II	Whittaker Corporation
Thornel 400	Union Carbide
Resins	
DER332	Dow Chemical Company
Nadic Methyl Anhydride (NMA)	Allied Chemical Company
Benyl Dimethylamine (BDMA)	Eastman Chemical Company
DER332	Dow Chemical Company
Metaphenylenediamine (MPDA)	Shell Chemical Company

TABLE D2. PROPERTIES OF CONTROLLED GRAPHITE-EPOXY SYSTEMS

Fiber	Matrix	Orientation	Modulus (MPax10^3)	Modulus (msi)	Strength (MPa)	Strength (ksi)	K_Q (MPa$\sqrt{m}$)	K_Q (ksi·in.$^{1/2}$)
HMS	DER332/NMA/BDMA	$90_2,0_2,90_2$	73.7	10.6	448	65.0	-	-
		90,0,90,0,90	86.9	12.6	652	94.6	22.9	20.8
		$90_2,0_4,90_2$	100.0	14.5	718	104.2	-	-
HMS	DER332/MPDA	90,0,90,0,90	79.3	11.5	661	95.8	26.3	23.9
Thornel 400	DER332/NMA/BDMA	$90_2,0_2,90_2$	43.6	6.32	472	68.5	28.1	25.6
		90,0,90,0,90	55.7	8.08	618	89.6	27.3	25.3
		$90_2,0_4,90_2$	65.4	9.48	672	97.4	41.4	37.7
Thornel 400	DER332/MPDA	$90_2,0_2,90_2$	47.8	6.94	476	69.0	26.6	24.2
		90,0,90,0,90	59.8	8.67	561	81.4	30.2	27.5
		$90_2,0_4,90_2$	65.2	9.46	703	102.0	33.7	30.7
Modmor II	DER332/NMA/BDMA	$90_2,0_2,90_2$	49.6	7.19	410	59.5	20.8	18.9
		90,0,90,0,90	59.0	8.56	477	69.2	19.5	17.7
		$90_2,0_4,90_2$	69.8	10.13	609	88.3	36.8	33.5
Modmor II	DER332/MPDA	$90_3,0_2,90_2$	45.7	6.63	[illegible]	63.1	26.8	24.4
		90,0,90,0,90	58.6	8.50	514	74.6	23.4	21.3
		$90_2,0_4,90_2$	70.3	10.20	708	103.7	40.4	36.8

TABLE D3. EFFECT OF IMMERSION ON THE RELATIVE STRENGTH OF GRAPHITE-EPOXY COMPOSITES

Fiber	Matrix	Orientation	Immersion Time 2 months	6 months	12 months
HMS	DER332/NMA/BDMA	$90_2,0_2,90_2$	1.07	1.03	1.23
		$90,0,90,0,90$	1.04	.98	.94
		$90_2,0_4,90_2$	.90	.92	.99
HMS	DER332/MPDA	$90,0,90,0,90$	1.09	.91	-
Thornel 400	DER332/NMA/BDMA	$90_2,0_2,90_2$	1.03	.94	1.10
		$90,0,90,0,90$	1.06	.92	1.06
		$90_2,0_4,90_2$	1.32	1.05	1.09
Thornel 400	DER332/MPDA	$90_2,0_2,90_2$	1.08	1.03	1.03
		$90,0,90,0,90$	.92	.95	1.03
		$90_2,0_4,90_2$	.97	1.08	1.02
Modmor II	DER332/NMA/BDMA	$90_2,0_2,90_2$	1.00	.99	.97
		$90,0,90,0,90$	1.03	1.13	1.16
		$90_2,0_4,90_2$	.91	1.01	1.03
Modmor II	DER332/MPDA	$90_2,0_2,90$	1.01	1.04	.91
		$90,0,90,0,90$	1.01	.97	1.03
		$90_2,0_4,90_2$	.99	.98	.97

TABLE D4. EFFECT OF IMMERSION ON THE RELATIVE MODULUS OF GRAPHITE-EPOXY COMPOSITES

Fiber	Matrix	Orientation	Immersion Time 2 months	6 months	12 months
HMS	DER332/NMA/BDMA	$90_2,0_2,90_2$	-	1.07	1.07
		90,0,90,0,90	.85	1.06	.91
		$90_2,0_4,90_2$	.83	.94	.96
HMS	DER332/MPDA	90,0,90,0,90	1.02	1.10	1.04
Thornel 400	DER332/NMA/BDMA	$90_2,0_2,90_2$	1.00	1.08	1.20
		90,0,90,0,90	.92	.98	1.02
		$90_2,0_4,90_2$	1.06	1.07	1.06
Thornel 400	DER332/MPDA	$90_2,0_2,90_2$	1.07	.99	1.05
		90,0,90,0,90	.95	.95	1.02
		$90_2,0_4,90_2$	1.05	1.00	1.14
Modmor II	DER332/NMA/BDMA	$90_2,0_2,90_2$	.96	.97	.92
		90,0,90,0,90	.94	.95	.94
		$90_2,0_4,90_2$	1.05	.73	.75
Modmor II	DER332/MPDA	$90_2,0_2,90_2$	1.05	1.04	.91
		90,0,90,0,90	.99	.93	1.09
		$90_2,0_4,90_2$	1.02	1.00	1.03

TABLE D5. EFFECT OF IMMERSION ON THE RELATIVE TOUGHNESS OF GRAPHITE-EPOXY COMPOSITES

Fiber	Matrix	Orientation	Immersion Time 2 months	6 months	12 months
HMS	DER332/[illegible]/BDMA	$90_2,0_2,90_2$	–	–	–
		90,0,90,0,90	.90	–	1.01
		$90_2,0_4,90_2$	–	–	–
HMS	DER332/MPDA	90,0,90,0,90	1.03	1.19	1.16
Thornel 400	DER332/NMA/BDMA	$90_2,0_2,90_2$	.94	1.01	1.01
		90,0,90,0,90	1.03	.94	1.01
		$90_2,0_4,90_2$	1.06	1.13	1.14
Thornel 400	DER332/MPDA	$90_2,0_2,90_2$	1.03	1.06	.83
		90,0,90,0,90	.94	.96	.69
		$90_2,0_4,90_2$	.93	1.17	1.23
Modmor II	DER332/NMA/BDMA	$90_2,0_2,90_2$	1.04	1.03	1.12
		90,0,90,0,90	1.04	1.08	1.37
		$90_2,0_4,90_2$	.82	.89	.75
Modmor II	DER332/MPDA	$90_2,0_2,90_2$	.95	.94	.94
		90,0,90,0,90	.98	1.05	1.00
		$90_2,0_4,90_2$	.99	.93	.88

TABLE D7. EFFECT OF FABRICATOR ON PROPERTIES OF GRAPHITE REINFORCED COMPOSITES

Fabricator	Strength (MPa)	Strength (psi)	Notch Toughness (MPa)	Notch Toughness (psi · in.$^{1/2}$)	ϕ_f
A	718.9	104,271	273.0	39,588	62
B	517.4	75,038	159.5	23,133	64

EFFECT OF PREPREG CURE ON PROPERTIES OF GRAPHITE COMPOSITES

Plate	Strength (MPa)	Strength (psi)	K_Q (MPa$\sqrt{m}$)	K_Q (psi · in.$^{1/2}$)
C*	428.1	62,085	10.1	9,195
D*	409.3	59,364	20.6	18,717

*Plate C contained prepreg which had a greater than average degree of cure prior to fabrication. The prepreg was still within the manufacturers stated life of the system. Plate D was manufactured from prepreg with the standard degree of cure.

TABLE D7. EFFECT OF FABRICATOR ON PROPERTIES OF GRAPHITE REINFORCED COMPOSITES

Fabricator	Strength (MPa)	Strength (psi)	Notch Toughness (MPa)	Notch Toughness ($psi \cdot in.^{1/2}$)	ϕ_f
A	718.9	104,271	273.0	39,588	62
B	517.4	75,038	159.5	23,133	64

EFFECT OF PREPREG CURE ON PROPERTIES OF GRAPHITE COMPOSITES

Plate	Strength (MPa)	Strength (psi)	K_Q ($MPa\sqrt{m}$)	K_Q ($psi \cdot in.^{1/2}$)
C*	428.1	62,085	10.1	9,195
D*	409.3	59,364	20.6	18,717

*Plate C contained prepreg which had a greater than average degree of cure prior to fabrication. The prepreg was still within the manufacturers stated life of the system. Plate D was manufactured from prepreg with the standard degree of cure.

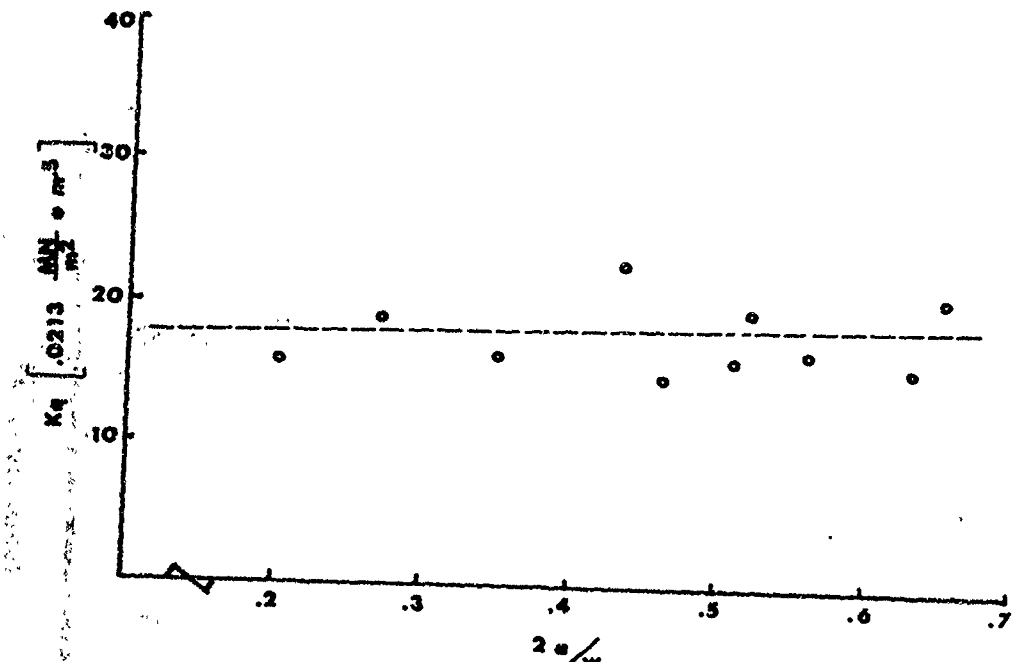

Fig. D1 — Notch sensitivity versus relative crack length for a typical graphite-epoxy composite. (Conversion factor: 1 ksi$\sqrt{\text{in.}}$ = 1.099 MPa$\sqrt{\text{m}}$.)

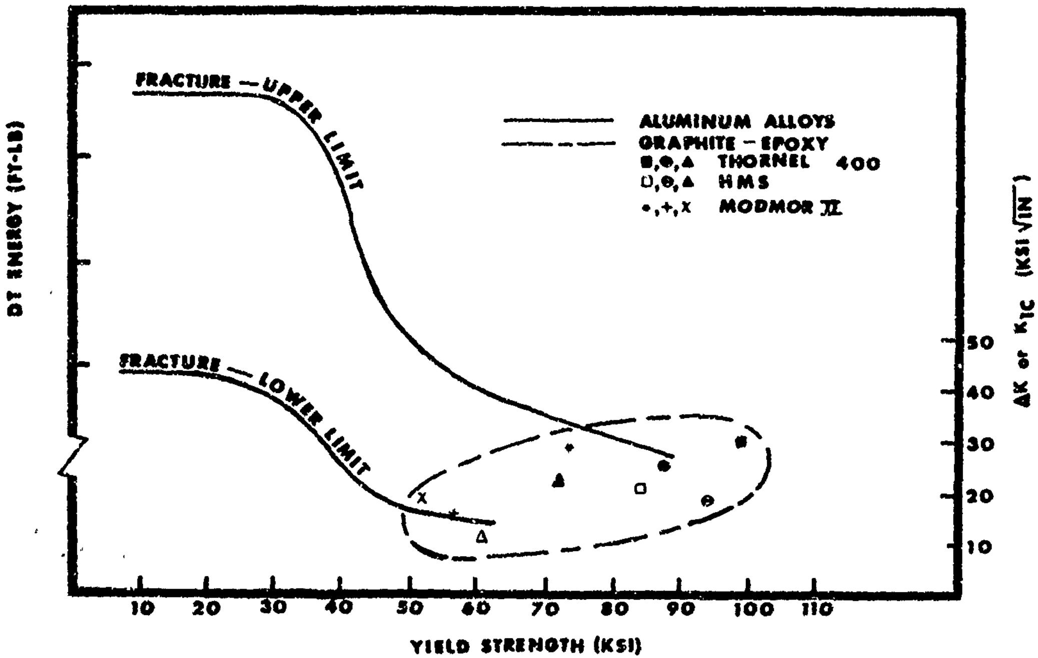

Fig. D2 — Ratio Analysis Diagram for aluminum comparing fracture properties of composites with range of fracture properties of commercial aluminum alloys. (Conversion factors: 1 ksi = 6.895 MPa, 1 ksi$\sqrt{\text{in.}}$ = 1.095 MPa$\sqrt{\text{m}}$, 1 ft-lb = 1.356 Nm.)

E. Bonding Technology

Dr. W. D. Bascom

Organic matrix composites and structural adhesives are among the materials being considered for use in FCS. Reliability criteria must be developed for these materials to (1) assess their suitability for FCS and (2) to be part of the data base for SI technology. As with high-strength metals, reliability testing is based on fracture mechanics principles and in fact, because composites and structural adhesive joints show so little ductility, their failure can be characterized by linear elastic fracture mechanics (LEFM). The state-of-the-art of LEFM testing of composites and adhesives is, however, still developmental and not yet ready for unqualified engineering applications. Indeed, the principal accomplishments of this subtask have been advancements in LEFM testing methodology especially with respect to structural adhesives.

Two general comments should be made about the use of composites and structural adhesives in FCS before summarizing the work on LEFM testing. First, there should be considerable caution in the use of graphite/epoxy composites. Although these materials have high modulus and are not especially sensitive to moisture (Figs. E11,E12), they have an inordinately low toughness (Fig. E13) and therefore would be susceptible to flaw growth. Secondly, the use of structural adhesives in metal joining for FCS construction is not presently warranted because of their extreme moisture sensitivity (Fig. E1 and Table E2). Possible means of correcting or circumventing these problems are discussed in the text.

The advances made here in structural adhesive fracture testing for reliability criteria were to (1) establish the existence of a bond thickness-temperature effect (Figs. E14, E15) and (2) demonstrate a dramatic reduction in toughness in joints subject to combined tensile and shear stresses (Figs. E6,E7). These effects had not been previously known and add considerable complexity to adhesive fracture testing. It was possible in this work to identify the micromechanics of the bond thickness and combined stress effects, and this information may eventually help in reducing the complexity of fracture testing these materials.

ACCOMPLISHMENTS

The reliability of structures bonded with high-performance adhesives is determined by the resistance of flaws in the bond line to propagate by combined conditions of stress and environment. Test methods for the fracture reliability of adhesives based on linear elastic fracture mechanics (LEFM) had been developed prior to this program (Ref. E1 and E2). These methods were used and significantly extended in the work of this subtask to determine the effect of joint geometry (bond thickness and bond angle), environment and adhesive composition on bond reliability.

A survey was made of the fracture resistance of commercial structural adhesives now used in aerospace construction and presumably suitable for FCS. The fracture energies ($\mathscr{J}_{Ic}$) measured in opening mode (cleavage, mode-I) are presented in Fig. E1. Clearly, the commercially formulated adhesives overcome the very low toughness of the base epoxy resins from which they are derived.

A relatively simple elastomer-epoxy resin composition was formulated that effectively modeled the fracture behavior of the commercial adhesives. In this formulation the elastomer is dispersed as 2-5μ particles in the epoxy resin matrix. This morphology gives high toughness with a minimum loss in the tensile strength and modulus of the base epoxy resin. This "model" structural adhesive along with selected commercial adhesives were used in subsequent testing.

The effects of bond thickness on adhesive fracture were determined using the model adhesive and the mode-I (cleavage) specimen illustrated in Fig. E2A. The results plotted in Fig. E3 are characterized by a maximum in fracture energy at about 20-30 mils (0.051-0.076 cm) bond thickness. Note the following: (a) the toughness of the epoxy resin has been increased 30-40X by the incorporation of the dispersed elastomeric phase, (b) the steep decline in toughness as the bond thickness is reduced below the maximum point, and (c) in this region below the maximum joint, fracture is stable, i.e., the crack is driven by the machine instead of jumping unstably ahead of the crossheads.

The bond thickness-adhesive toughness relationship of the model adhesive undergoes a marked, systematic change with temperature. The results shown in Fig. E4 indicate that the maximum in toughness shifts to higher bond thicknesses with increasing temperature. This data can be used to show the change in fracture energy with temperature at a fixed bond thickness. For example, at the 10 mil (0.025 cm) thickness frequently recommended by adhesive suppliers the plot in Fig. E5 shows a strong maximum at 25°C (ambient).

The stress conditions of mode-I testing simulate only peel-type loading, yet many joints are designed to avoid peeling loads as much as possible in favor of shear loads. Therefore, it is important to characterize adhesive fracture in combined tensile and shear loading. The test specimens used for this purpose in this work are illustrated in Figs. E2B and E2C. Results using the "scarf-joint" specimen with a bond angle (ϕ) of 45° (Fig. E2B) are given in Table E1. The adhesive fracture toughness ($\mathscr{J}_{(I,II)c}45$) of the commercial and the model structural adhesives in this combined stress condition were generally 10X less than the corresponding mode-I toughness ($\mathscr{J}_{Ic}$). This was not the case for the base epoxy resin for which the fracture energy was about the same in both loading conditions.

Tests were conducted to determine the influence of bond angle on adhesive fracture using both the scarf-joint and the dual-loaded specimens (Figs. E2B and E2C, respectively). In the latter configuration, shear and tensile loads can be imposed simultaneously and their ratio determines an effective bond angle. The results using both specimens are given in Figs. E6 and E7 and indicate a complex relationship between bond angle and adhesive toughness.

The moisture sensitivity of resin/metal adhesive bonds is well documented (Ref. E3). Procedures for testing the stress-corrosion cracking of adhesive joints have been developed (Ref. E4) in which the specimen in Fig. 2A is static loaded in water. A "threshold" critical stress-corrosion fracture energy, $\mathscr{J}_{Iscc}$, is determined below which there is essentially no crack growth.

Efforts to determine $\mathscr{J}_{Iscc}$ in the work of this subtask were largely unsuccessful due to experimental difficulties. Although the results obtained at other laboratories are undoubtedly valid, it became clear that there are fundamental problems associated with the test. Accordingly, the work was transferred to 6.1 funding (NAVAIR 022-06-001). In replacement, time-to-failure tests were conducted on static loaded aluminum-epoxy resin butt-joint specimens. Data typical of these tests obtained using an unmodified epoxy resin are given in Fig. E8 and show the usual exponential decay in survival time characteristic of metal/resin bonds.

Post-failure examination of the butt-joint fracture surfaces revealed fracture markings from which the critical flaw size could be estimated. This dimension combined with the failure stress was used to compute the critical fracture energy, $\mathscr{J}_{c}$. In Table E2, values of $\mathscr{J}_{c}$ are listed for various loading conditions and environments. Note especially that

the critical fracture energy, - - the criterion determining bond reliability is characteristic of stress-corrosion failure, $\mathscr{G}_{Iscc}$, even when the relative humidity was as low as 45 percent (ambient). Only when the bond was kept essentially anhydrous by surrounding it with a dessicant or in dynamic, rising-load testing was the failure criteria determined by $\mathscr{G}_{Ic}$, the fracture toughness of the adhesive resin.

DISCUSSION

It is quite clear that the limiting factor in the reliability of state-of-the-art adhesives is their moisture resistance. In Fig. E1, the stress-corrosion fracture toughness of the aluminum adhesive bonds are 2X to 10X less than the fracture toughness of the adhesives themselves; and judging from the results in Table E2, bond failure occurs by stress-corrosion even at ambient humidity. Only under nearly anhydrous conditions or when a joint is subject to a sudden increase in load does the "dry" toughness control joint strength. Because of this moisture sensitivity, structural adhesives are presently unsuited for use in marine environments and thus are not candidates for FCS construction. Improvements in bond SCC reliability are on the horizon, notably new surface treatments for metals and the combined use of adhesives with spot welding, i.e., weldbond. These technologies are still developmental and even when developed, engineering and reliability experience will be required before they can be considered for FCS. Work on the SCC of adhesive bonds is continuing here with emphasis on improving the test method for $\mathscr{G}_{Iscc}$ (NAVAIR WR 022-06-001, NRL 61C02-21) and improved moisture resistant adhesives (V/STOL-DLF, NAVAIR WF 54-593-202, NRL 61C04-10).

Establishing reliability criteria for bonding is further complicated by the fact that an adhesive joint is in many respects a structure; and unlike a monolithic material, e.g., a steel plate, its fracture behavior has certain geometric aspects such as bond thickness and bond angle. One of the accomplishments in this subtask has been to demonstrate the importance of these effects.

The dramatic effect of bond thickness on adhesive fracture had not been realized prior to this work and has important implications with respect to joint design. In the results for cleavage toughness ($\mathscr{G}_{Ic}$) at ambient temperature (Fig. E3), the optimum thickness would not be at the maximum but at the highest value of $\mathscr{G}_{Ic}$ that would also assure stable crack propagation, i.e., ~ 0.025 cm (0.010 in.). The data also indicate the importance of maintaining close tolerances on bond thickness. The steep decline in $\mathscr{G}_{Ic}$ imposes a severe penalty on joint strength

if the thickness is only a few mils under specification or a joint subject to catastropic failure (unstable crack propagation) if the thickness is over specification. Temperature changes can have a large effect on joint toughness as indicated in Figs. E4 and E5. The latter indicates a severe temperature dependence typical of an adhesive formulated to have high peel strength in a narrow temperature range near ambient. Adhesive formulations have been developed with high strength over wide temperature ranges although usually at a sacrifice in toughness and/or processability.

The most surprising result of this work is the effect of stress-condition (bond angle) on adhesive fracture. Simply stated, the high toughness of structural adhesives in peel loading (i.e., $\mathscr{T}_{Ic}$) is essentially lost at other loading conditions. This does not mean that adhesive joints are strongest in peel: Actually, there is a significant increase in joint strength as the bond angle is increased. On the other hand, the strength of structural adhesives presently available could be increased by more than a factor of two if the toughness they presently have in mode-I fracture could be translated into other loading modes, i.e., scarf-joints, lap-shear joints, etc.

The effect of stress-condition on adhesive fracture revealed in Table E1 and Fig. E7 indicates the need for a major change in the test methodology for adhesive joint reliability criteria. Heretofore, it had been assumed that cleavage testing for adhesive $\mathscr{T}_{Ic}$ was sufficient since opening-mode (mode-I) is generally the lowest fracture energy and therefore a sufficient criterion for design purposes. Although this assumption is usually true for monolithic specimens, it is clearly not the case for a bonded joint which, as indicated above, must be viewed as a structure and not as a monolithic element. The error in assuming that $\mathscr{T}_{Ic}$ is a sufficient criterion for joint design can be appreciated by considering the nylon-epoxy adhesive and using the $\mathscr{T}_{Ic}$ (Table E1) as the failure criterion. The predicted strength of a scarf-joint ($\phi = 45^\circ$) using this adhesive would be about 3X the actual strength.

Based on the results of this study, complete fracture characterization of a structural adhesive must include: (a) $\mathscr{T}_c$ determinations at bond angles from 0° ($\mathscr{T}_{Ic}$) to 90° ($\mathscr{T}_{IIc}$ - pure shear), (b) the effect of bond thickness to establish the thickness for maximum $\mathscr{T}_c$ and its rate of change around the maximum point, and (c) the effect of temperature on the bond angle and thickness dependencies. These requirements represent a rather formidable testing program for a given adhesive especially if SCC testing

is required in addition. In order to simplify the effort, there is a need to establish analytical relationships between fracture toughness and joint geometry.

Part of the work of this subtask was devoted to identifying the micromechanics of adhesive failure. The details of the work are reported elsewhere (Ref. E4-E8), but the general conclusions have a bearing on the analytical relationships needed to simplify adhesive fracture testing. Essentially, the micromechanics studies demonstrated the importance of the crack-tip deformation zone in determining adhesive fracture behavior. The diameter of the zone, indicated by $2r_y$ in Fig. E9, is related to the fracture toughness, $\mathscr{J}_c$, yield strength, σ_y, and yield strain, ϵ_y of the adhesive resin by

$$\mathscr{J}_c = Z\ \sigma_y\ \epsilon_y\ r_y \qquad [1]$$

where Z is a constant determined by the stress condition on the joint. The significance of equation 1 is that for a wide range of resins used as structural adhesives the yield properties, σ_y and ϵ_y, are not greatly different; and so the zone size, r_y, is the principal factor in determining resin toughness. Indeed, when an adhesive formulator toughens a basic epoxy resin by the addition of elastomers or other agents, it is the r_y parameter being affected. Furthermore, the effect of bond thickness and possibly bond angle on adhesive $\mathscr{J}_c$ can be understood in terms of the crack-tip deformation zone. For example, the maximum in $\mathscr{J}_c$ (in both mode-I (Fig. E3) and combined mode fracture occurs when the zone diameter, $2r_y$, and the bond thickness are about equal and that the decline in toughness to either side of the maximum can be attributed to changes in the restraint on resin deformation at the crack tip by the stiff metal adherends. The possibility exists that some quantitative relationship exists between bond thickness r_y and adhesive $\mathscr{J}_c$ which if developed would permit calculation of the $\mathscr{J}_c$-bond thickness dependence.

The effects of stress-condition (bond angle) on adhesive failure micromechanics are more complex than the bond thickness effects. Indeed, the results of the study here have raised some fundamental questions about the crack-tip stress field under combined stress loading and the response of the formulated resins to these stress fields. Work on this problem is continuing under 6.1 funding (NRL Problem 61C02-21), but it is clear that the development of analytical relationships between bond angle and adhesive fracture toughness are very distant.

REFERENCES

E1. Ripling, E. J., Mostovoy, S. and Corten, H. T., J. of Adhesion 3, 107 (1971).

E2. Ripling, E. J., Mostovoy, S. and Bersch, C., J. of Adhesion 3, 145 (1971).

E3. Minford, J. D., in Treatise on Adhesion and Adhesives, R. L. Patrick, ed., Vol. 3, Dekker, N.Y., 1973, p. 79.

E4. Bascom, W. D., Timmons, C. O. and Jones, R. L., J. Mat. Sci. 10, 1037 (1975).

E5. Bascom, W. D., Cottington, R. L., Jones, R. L., and Peyser, P., J. Appl. Polym. Sci., 19, 2595 (1975).

E6. Bascom, W. D., Jones, R. L. and Timmons, C. O., in Adhesion Science and Technology, Plenum Press, 1975.

E7. Bascom, W. D., Hunston, D. L. and Timmons, C. O., in preparation.

E8. Bascom, W. D. and Patrick, R. L., Adhesives Age, p. 25, Oct. 1974.

TABLE E1. CLEAVAGE-MODE VS. MIXED-MODE ADHESIVE FRACTURE TOUGHNESS

Adhesive Resin	Fracture Energy (J/m^2) Cleavage $\mathcal{G}_{Ic}$	Cleavage + Shear $\mathcal{G}_{(I,II)c}^{45°}$
Unmodified Epoxy[a]	116	140
CTBN-Epoxy[b]		
10% CTBN	3500	110
30% CTBN	2200	110
Commercial		
Elastomer-Epoxy	2300	870
Nylon-Epoxy	6100	750
ME 329[c]	630	55
AF 243[d]	860	220

[a] Hexahydrophthalic anhydride - DGEBA

[b] Piperidine - DGEBA

[c] Narmco Materials, Inc.

[d] 3M co.

TABLE E2. FAILURE CRITERIA FOR EPOXY[a] - ALUMINUM BONDS IN DIFFERENT ENVIRONMENTAL CONDITIONS

Environment	Loading[b]	Failure Criteria $\mathscr{J}_c\left(\frac{\text{in.-lbs.}}{\text{in.}^2}\right)^d$	
Water	static	0.05 - 0.1	stress-corrosion cracking
50% RH	static	0.05 - 0.1	stress-corrosion cracking
<2% RH	static	~ 1.0	adhesive fracture
58% RH	dynamic[c] (0.05 in./min)	~ 1.0	adhesive fracture

a. Unmodified, amino-cured

b. Static loads of 4000 to 10,000 psi

c. Failure loads ~ 10,000 psi

d. 1 in.-lb./in.^{2} = 175.3 J/m^2

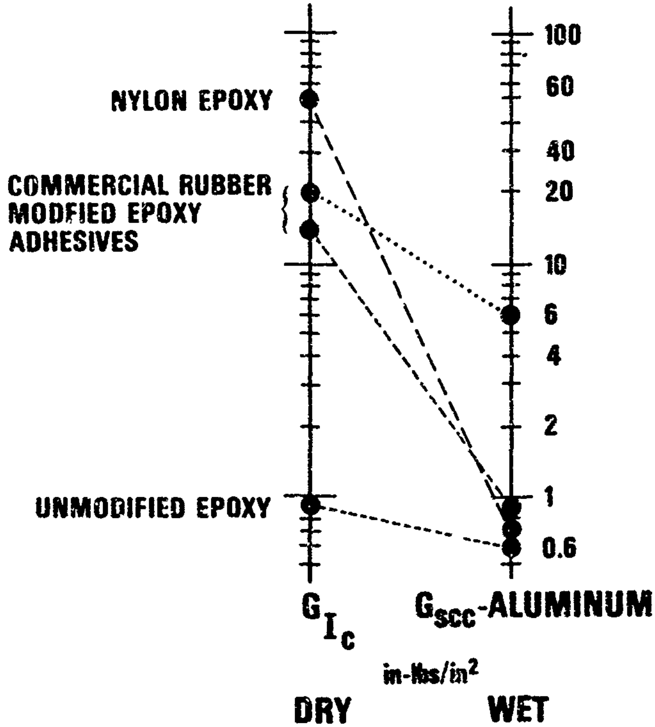

Fig. E1 — Fracture toughness ranking of resins and adhesives. Note the substantial increase in toughness achieved by formulating the epoxy resins with rubber. (1 in.-lb/in.^{2} = 175.3 J/m^2.)

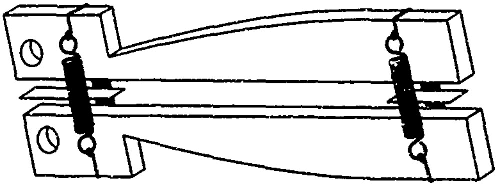

Fig. E2(a) — Tapered double cantilever beam specimens used for opening-mode adhesive fracture

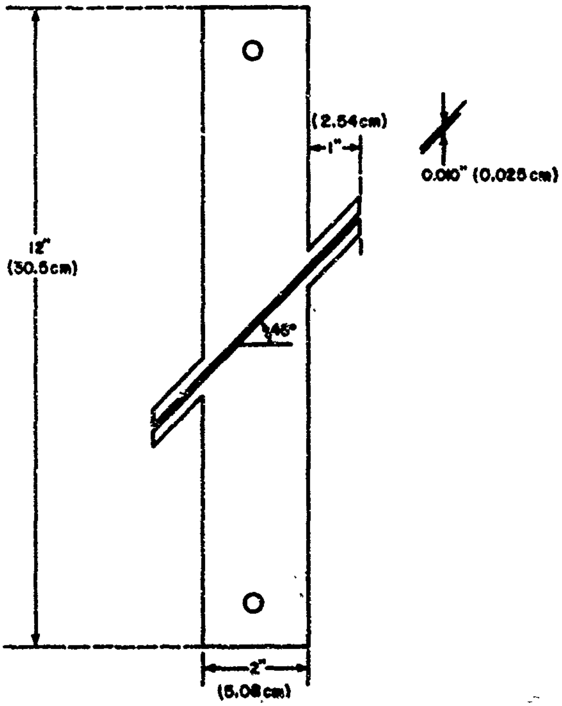

Fig. E2(b) — "Scarf-joint" test specimen for mixed-mode adhesive fracture

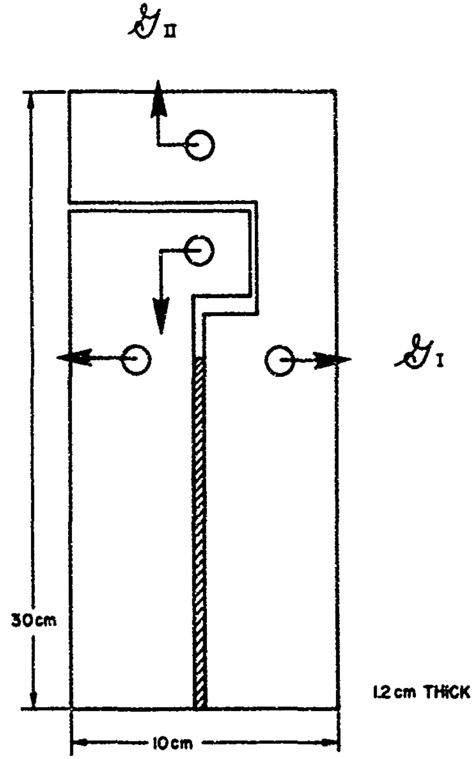

Fig. E2(c) — Specimen configuration used for mixed-mode adhesive fracture tests

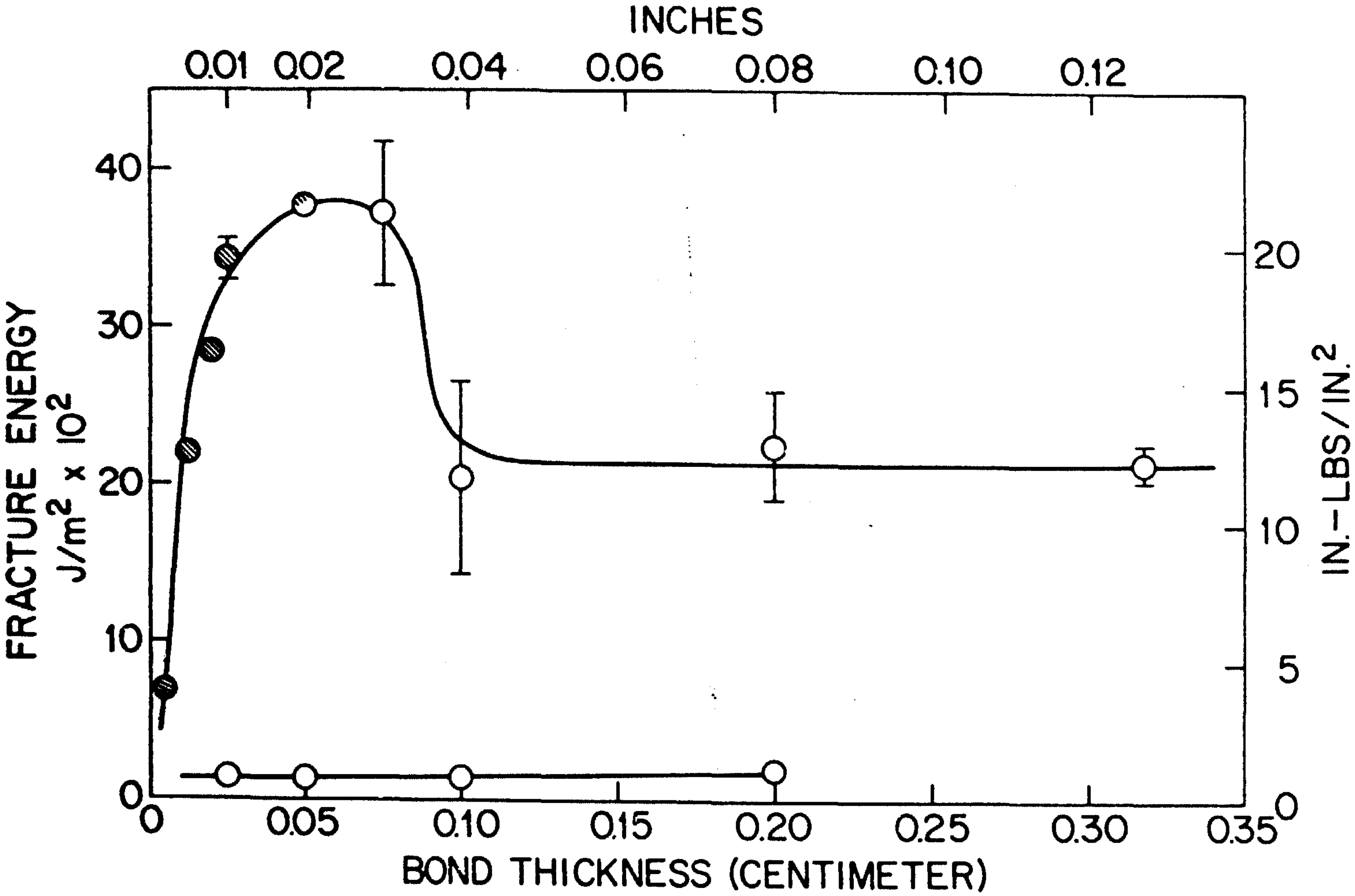

Fig. E3 — **Effect of bond thickness on opening mode adhesive fracture toughness. Lower curve is for an unmodified epoxy. Upper curve is for a rubber-modified epoxy adhesive.**

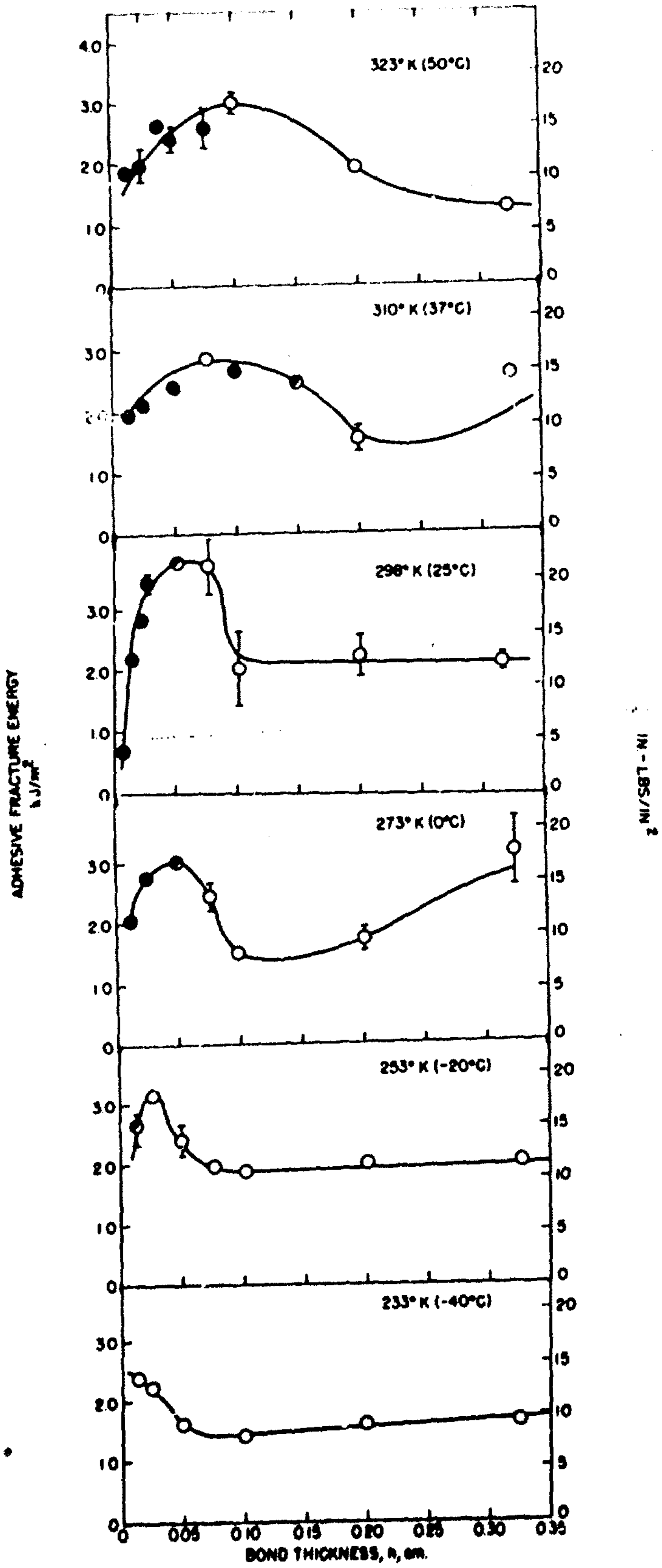

Fig. E4 — Combined temperature and bond thickness dependence of adhesive fracture toughness

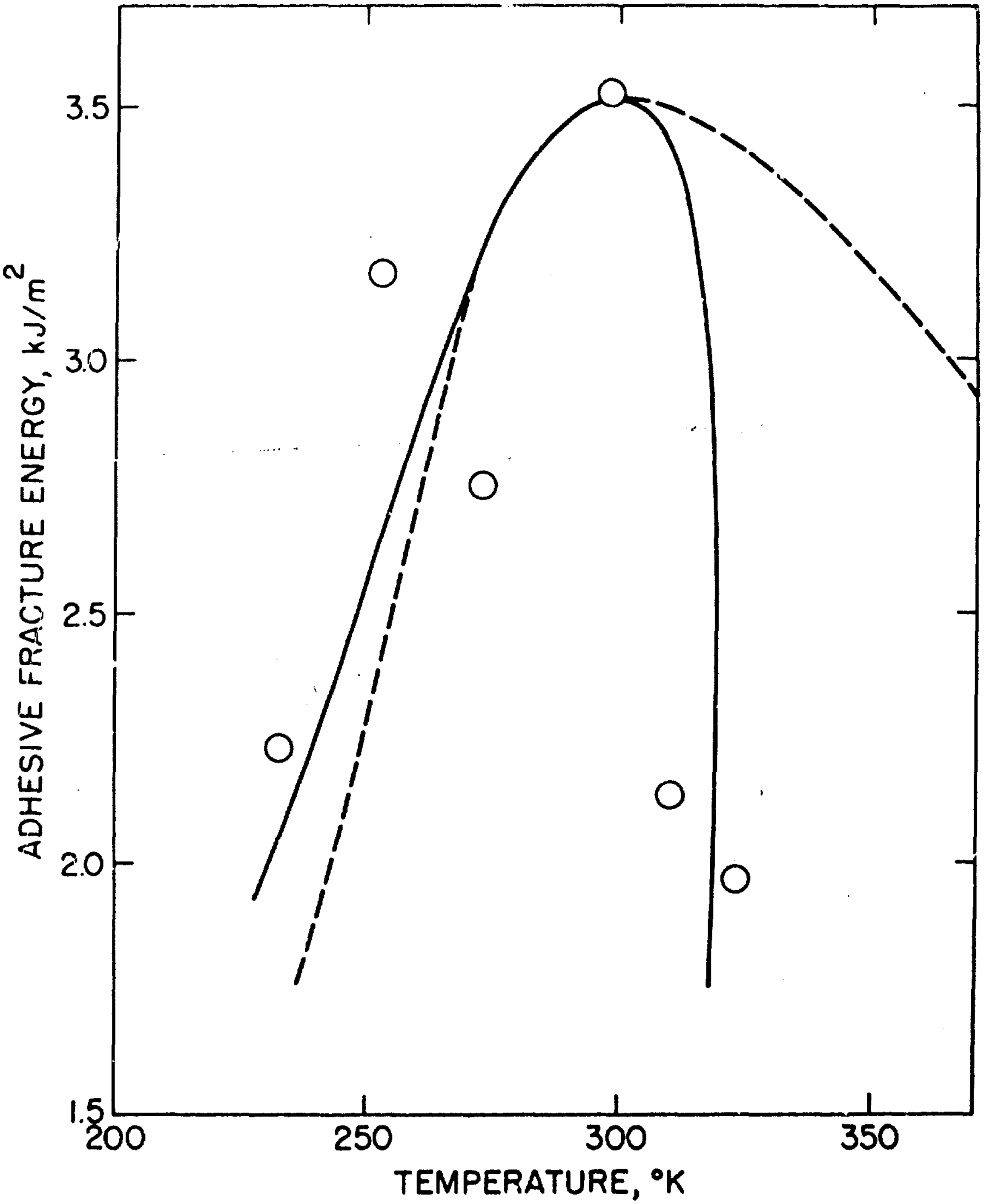

Fig. E5 — Effect of temperature on adhesive toughness at constant bond thickness. Solid line is for a commercial epoxy-rubber adhesive; open circles are for a "model" structural adhesive.

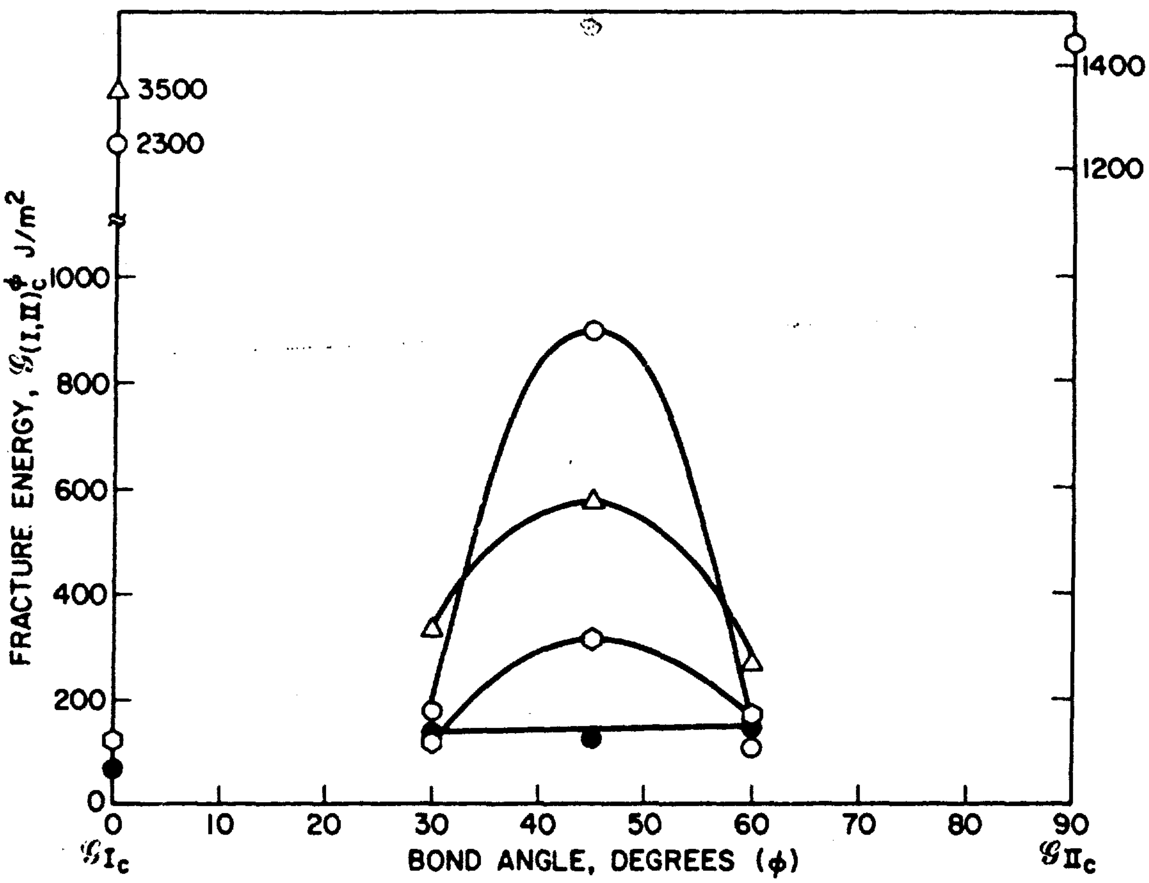

Fig. E6 — Effect of bond angle on adhesive fracture toughness of unmodified epoxy resins, ●, ⬡; and rubber-modified resins, ○, Δ

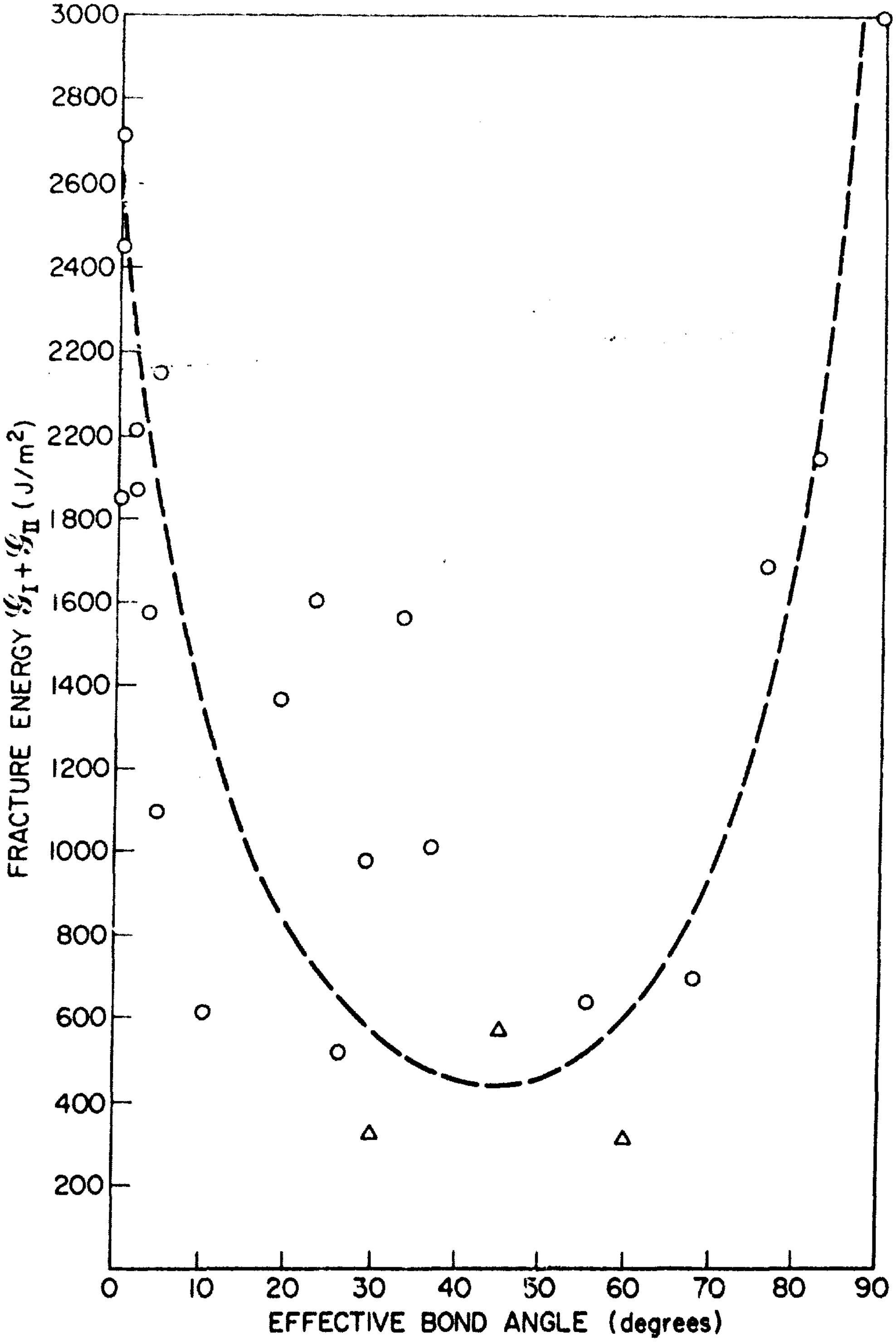

Fig. E7 — Effect of bond angle on the adhesive fracture toughness of a rubber-modified epoxy resin

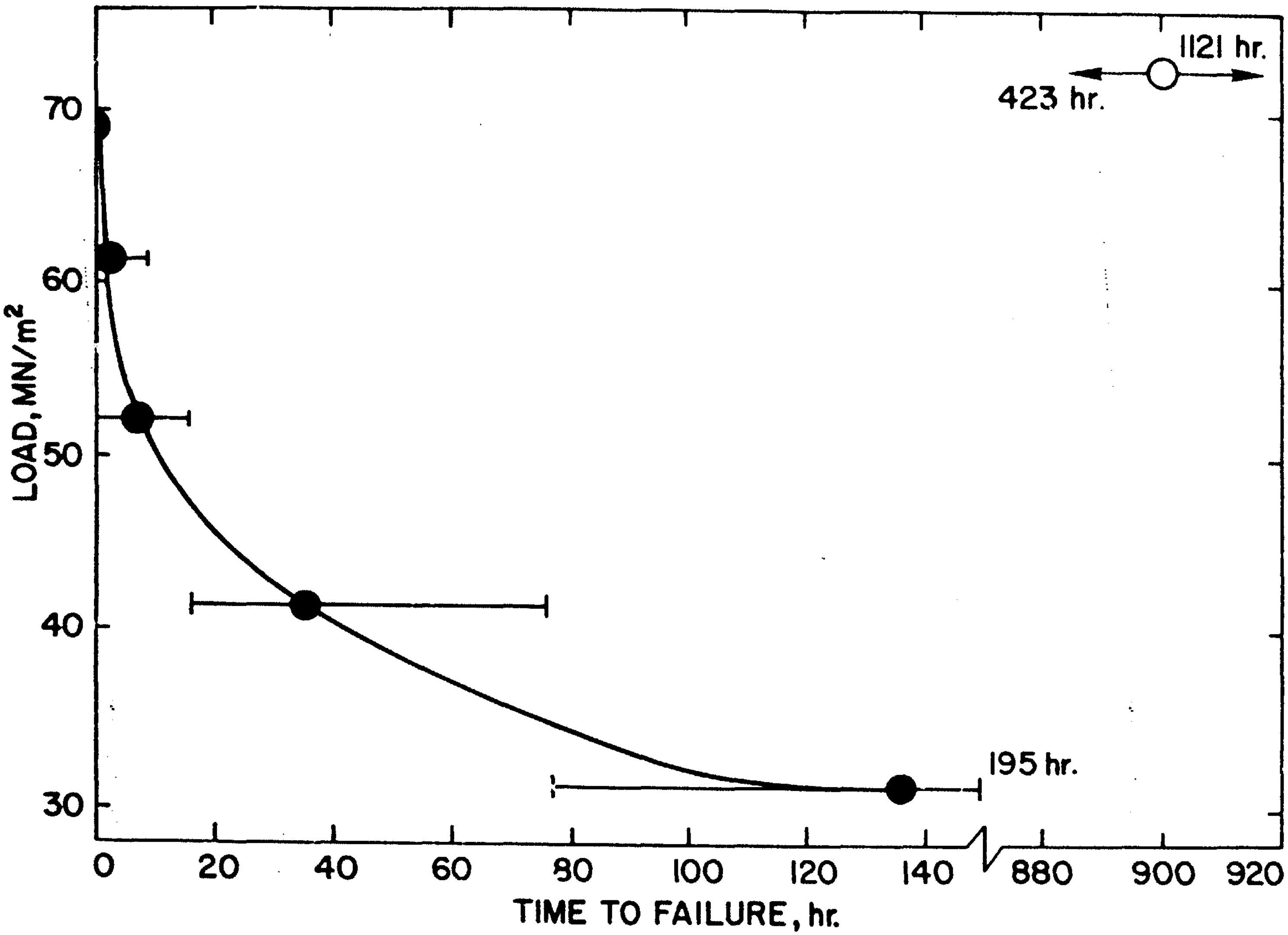

Fig. E8 — Time-to-failure vs. static load for epoxy-aluminum butt joints. Note the considerable durability when the bond is kept below ambient humidity. (open circle)

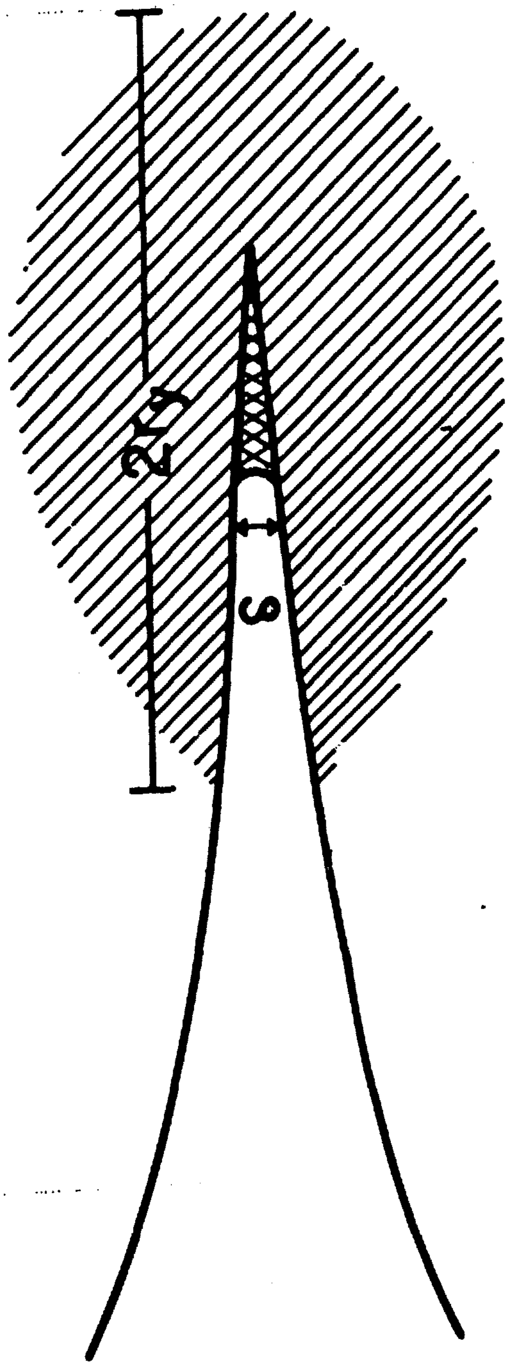

Fig. E9 — Schematic of the crack tip deformation zone characteristic of resin fracture

F. Technology Transfer

Throughout the DLF program a significant effort was made to make use of existing SI technology and of the technology developed in the program to impact existing hardware development programs and to acquaint Navy designers and engineers with SI technology. These efforts were primarily directed at the NATO Patrol Hydrofoil Missile (PHM) program, specifically at the strut and foil structure of this craft. Other activities by NRL personnel to advance the use of SI technology include many consulting activities, courses held at the Naval Ship Engineering Center, publication of a standard method of test for stress-corrosion cracking of metals (1), and participation on ASTM committees to accomplish the same standard at that level.

The major return on investment in the DLF program was the benefits which accrued to the PHM NATO Hydrofoil Program. Early in the program, problem areas concerned with cracking processes due to combined loading and environmental effects in the 17-4 PH strut/foil system were identified. The PHM office and The Boeing Company were informed of the results of the investigation, with the result that NRL and Boeing cooperated to find the optimum way to utilize 17-4 PH steel for the strut/foil. In the earlier part of the program, the potential problems were of the type that require a great deal of maintenance and repair, rather than being short-term catastrophic fracture problems. In later developments, a heat-treatment schedule which results in brittle weld metal was suggested for the struts and foils.

The DLF program concentrated on 17-4 PH steel at a strength level of 1034 MPa (150 ksi), which has demonstrated a susceptibility to cracking in a similar application on the prototype hydrofoil TUCUMCARI. The initial selection of 17-4 PH steel for the PHM in preference to HY-130 and other steels was made primarily on the basis of some experience with 17-4 PH and other contending materials for which extensive data pertaining to crack growth and fracture were not available. To correct this deficiency, a program was initiated to assemble and analyze the data required to define the crack tolerance of 17-4 PH steel in the seawater environment.

The SCC-RAD, Fig. 1, was used to analyze the potential for catastrophic fracture and for crack growth by seawater; stress-corrosion cracking and additional studies of fatigue and corrosion fatigue and electrochemical coupling with other materials were also made. Data zones defining the fast fracture, SCC, and electrochemical coupling properties of vacuum-melted 17-4 PH steel are presented on the RAD in Fig. 1. The data include NRL test results and data from Boeing Company reports. The NRL test materials were heat treated over a range of temperatures which include the condition originally planned for use on the PHM project (H-1050 temper).

Fast fracture is not expected to be a problem for vacuum-melted 17-4 PH steel in the H-1050 temper; however, the air-melted materials have unacceptably low fracture properties. The SCC properties of 17-4 PH steel are very low, which is an indication that crack growth can be expected at reasonable operating loads. An even more severe problem is electrochemical coupling of the strut/foil assembly with the aluminum hull or with other metals. Such coupling results in accelerated flaw growth at lower K_I values, as shown by the coupling zone on the RAD; this translates to a lower expected load requirement to cause crack growth.

A more important item which grew out of the DLF efforts in the 17-4 problem area was that steps are being taken to assure that the same problems are not repeated in similar structures. One approach was to design a strut/foil system for the PHM with HY-130 steel, in which the contractor was required to formulate a plan to prevent or control crack growth and fracture. This plan, called the Hydrofoil Structural Integrity Program (HSIP), was the first such required for Navy structures. Under the DLF project, NRL personnel served on the Navy review board and on Navy/contractor teams to implement the HSIP for the PHM strut/foil system. While the HY-130 strut/foil system was not built, the design was the first to incorporate formal SI plans and served as a valuable learning exercise for both Navy and contractor personnel. Future fast craft and ships will require similar treatment, so that an obvious need is standard documents, spelling out how and where SI technology should be applied; NRL personnel are presently participating in efforts to accomplish the standardization of SI documents.

Of more significance is the experience of follow-on PHM ship design, which is currently ongoing. As a result of studies and interactions with Boeing and the PHM project office, the heat-treat schedule for the 17-4 PH struts and foils for the follow-on production ships was changed to the H1100 temper. In the design of new struts and foils, base

metal and weld metal specifications included a minimum DT energy of 2712 Nm (2000 ft-lbs) (standard 1-in. DT) or 339 Nm (250 ft-lbs) (standard 5/8-in. DT) and a yield strength in the range of 896-1034 MPa (130-150 ksi). Additional requirements placed on the weld metal qualification program was that each candidate weld metal be capable of withstanding an applied stress-intensity of 110 $MPa\sqrt{m}$ (100 $ksi\sqrt{in.}$ in a salt water environment for a period of 500 hrs., i.e., $K_{Iscc} \geq$ 110 $MPa\sqrt{m}$ (100 $ksi\sqrt{in.}$). These requirements were imposed to assure damage tolerance from one-time impact type loading and to enable maintenance and inspection intervals to be established on the basis of expected flaw growth resistance. These requirements for the use of SI technology were engendered by the participation of NRL personnel on the design review boards for struts and foils and an awareness of the potential problems identified in the course of the DLF program.

Another approach to technology transfer was a series of informal seminars conducted at the Naval Ship Engineering Center for the personnel involved with materials and structures. The course which was entitled, "Principles for Fracture-Safe Design of Naval Structures," consisted of 13 1-hr. seminars, 11 of which were presented by NRL speakers under the DLF program. The information ranged from theoretical fracture mechanics concepts to applications of technology for defining fracture, fatigue, and environmentally assisted crack growth in high-performance ship and submarine structures. In this format, the background technology and the information generated under the DLF task were disseminated to the primary users in the quickest and most efficient way possible. Appendix B contains an outline of the subject matter presented.

Standardization of test methods is an essential part of implementation of SI technology. Its main objective is to ensure uniformity of test results whether the test is being performed by laboratories, materials' producers, or builders, and for SI technology, the issue is the most crucial. Properties of metals that pertain to crack growth and fracture often are determined by processing or chemistry variables that are difficult to control in standard mill products; more important is the necessity to specify minimum property requirements and to conduct small scale tests for quality control.

Problems in determining materials' properties are the frequent dependence of the test result on the test piece dimensions and on the test procedure used, and the use of inappropriate test methods for defining the property in question. One contribution to the technology was the

drafting of a standard test method for determining the parameter, K_{Iscc}, by cantilever-bend test methods. The standard was published as NRL Report 7865 (1) and has already been specified in the PHM project for qualification of weld procedures to be used in 17-4 PH and 15-5 PH on the production ships. Additional efforts are currently underway in the ASTM Committee on Fracture (E-24) to standardize the procedure using several methods; the NRL report is serving as the baseline document in a round-robin program to evaluate the cantilever-bend test method.

The results of the work on adhesive bond and graphite-resin composites have been widely disseminated within the Navy, the other armed services, industry including aerospace and resin manufacturers, and the academic community. A list of publications and presentations is attached. Notable among the presentations is the NAVAIR-NRL Tutorial on Fracture Behavior of Structural Adhesive Bonds which was organized to acquaint Air Force, Army and NASA personnel on the fracture mechanics of structural adhesive joint design. Subsequent to this meeting the Air Force initiated a program on advanced design airframe structures using adhesives and composite materials. The program includes the use of fracture design criteria for adhesive joints and because of the DLF program results the Air Force is specifically addressing the problems of bond thickness effect and mixed-mode loading. The DLF work on adhesive fracture has had impact on adhesive testing by the Army, the 3M Company and the Locktite Corporation and on the adhesive fracture design program of NASA.

The fundamental significance of the adhesive fracture work has been brought before the scientific community through publications in refereed journals and presentations at scientific meetings and at universities. Strong interest has been expressed by researchers working on related problems of polymer fracture at the University of Utah, University of Pittsburgh, Lehigh University and the British Ministry of Defense. Similar interest in adhesive bond fracture mechanics has been expressed by workers at Auburn University, MIT, University of Illinois and the University of Delaware. In addition, the results of the adhesive studies now constitute a major segment of a continuing engineering course on adhesion taught at George Washington University by NRL personnel.

Finally, it should be noted that many of the techniques and concepts developed under the DLF program on adhesives and composites have been carried into a new program at NRL on high temperature resins for V/STOL aircraft.

REFERENCES

1. R. W. Judy, Jr., and R. J. Goode, "Standard Method of Test for Plane Strain Stress-Corrosion-Cracking Resistance of Metallic Materials," NRL Report 7865, Mar. 17, 1975.

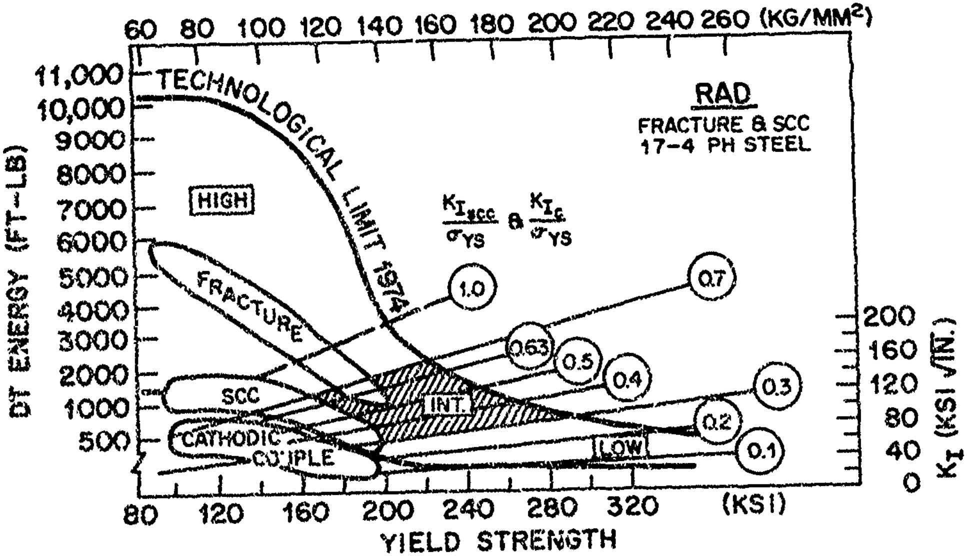

Fig. F-1 — Fracture resistance and SCC resistance of 17-4 PH steels shown on the SCC-RAD. The zones for SCC show the open circuit condition and the condition of electrochemical coupling to aluminum, zinc, and magnesium.

G. BIBLIOGRAPHY

Journal Publications

R. W. Judy, Jr. and R. J. Goode, "R-Curve Characterization and Analysis of Fractures in High-Strength Structural Metals," ASM Metals Engineering Quarterly, Vol. 13, No. 4, pp. 27-35, Nov. 19, 1973

R. J. Goode and R. W. Judy, Jr., "Fracture-Safe Assurance Aspects for Advanced Surface Ships," Conference Proceedings of Symposium of The Technical Cooperation Program at the British Welding Research Association, Cambridge, England, 11-13 June 1973

C. T. Fujii, "Electrochemical Aspects of Stress-Corrosion Cracking - Recent Studies on High-Strength Steels," Lead Article in Report of NRL Progress, pp. 21-28, June 1974

C. A. Griffis, "Elastic-Plastic Fracture Toughness: A Comparison of J Integral and Critical Crack Opening Displacement Characterizations," Transactions of the ASME, J. of Pressure Vessel Technology, Vol. 97, Series J, No. 4, pp. 278-283, November 1975

W. D. Bascom, "Adhesive Fracture Behavior of Elastomer-Modified Epoxy Resins," 30th Anniversary Tech. Conf., Reinforced Plastics/Composites Institute, The Society of the Plastics Industry, 22-D, p. 1, 1975

W. D. Bascom, C. O. Timmons and R. L. Jones, "Apparent Interfacial Failure in Mixed-Mode Adhesive Fracture," J. Materials Sci. 10, 1037 (1975)

W. D. Bascom, R. L. Jones and C. O. Timmons, "Mixed-Mode Fracture of Structural Adhesives," in Adhesion Science and Technology, Vol. 9B, L. H. Lee, ed., Plenum Press, p. 501, 1975

W. D. Bascom, R. L. Cottington, R. L. Jones and P. Peyser, "The Fracture of Epoxy and Elastomer-Modified Epoxy Polymers in Bulk and as Adhesives," J. Appl. Polym. Sci. 19, 2545 (1975)

W. D. Bascom and R. L. Cottington, "Effect of Temperature on the Adhesive Fracture Behavior of an Elastomer-Epoxy Resin," J. of Adhesion 7, 333 (1976)

W. D. Bascom, S. T. Gadomski, C. M. Henderson and R. L. Jones, "Fracture Markings on Stress-Corroded Epoxy/Aluminum Butt Joints" (Pending)

W. D. Bascom, R. L. Cottington and C. O. Timmons, "Fracture Design Criteria for Structural Adhesive Bonding - Promise and Problems," Naval Engineers Journal, in press

C. A. Griffis and G. R. Yoder, "Initial Crack Extension in Two Intermediate-Strength Aluminum Alloys," Trans. of ASME, J. of Engineering Materials Technology (pending)

R. W. Judy, Jr., C. A. Griffis, and R. J. Goode, "Fracture Resistance of Thin-Section Aluminum by Dynamic Tear Test Methods," ASM Metals Engineering Quarterly (pending)

P. Shahinian and R. W. Judy, Jr., "Stress Corrosion Crack Growth in Surface-Cracked Panels of High-Strength Steel," (pending publication by ASTM)

C. T. Fujii, "Stress-Corrosion Cracking Properties of 17-4 PH Steel" (pending publication by ASTM)

Technical Presentations

T. W. Crooker, "Recent Studies of Subcritical Crack Growth Behavior of Naval Structural Materials," Seminar at Air Force Flight Dynamics Laboratory, Wright-Patterson AFB, Ohio, Feb. 9, 1973

R. W. Judy, Jr. and R. J. Goode, "Procedures for Design of High-Performance Surface Ships Against Structural Failure by Crack Extension Processes," The Second Ship Structures Workshop, "Structures Research Program for the Hull Subsystem of High-Performance Ships," Naval Ship Research and Development Center, Bethesda, Md., Feb. 13-14, 1973

R. J. Goode and R. W. Judy, Jr., "Application of Principles for Fracture-Safe Design for Aluminum and Titanium Alloys," Catholic University Workshop - "Analysis and Design of Cylindrical Shells Under Pressure," Washington, D.C., June 4, 1973

R. J. Goode and R. W. Judy, Jr., "Fracture-Safe Assurance Aspects for Advanced Surface Ships," Symposium of The Technical Cooperation Program at the British Welding Research Association, Cambridge, England, 11-13 June 1973

W. D. Bascom and C. O. Timmons, "Mechanically Focused Interfacial Failure of Adhesive Bonds," Gordon Res. Conf., New Hampton, N.H., Aug. 20, 1973

R. W. Judy, Jr., "Introduction to Fracture-Safe Design Problems - Linear Elastic Fracture Mechanics," Seminar at the Naval Ship Engineering Center, Hyattsville, Md., Sept. 11, 1973

R. W. Judy, Jr., "Definition of Principal Engineering Fracture Test Methods and Significance of Each," Seminar at the Naval Ship Engineering Center, Hyattsville, Md., Sept. 18, 1973

R. W. Judy, Jr., "RAD Procedures for Fracture-Safe Design With High and Ultrahigh Strength Steels," Seminar at the Naval Ship Engineering Center, Hyattsville, Md., Oct. 16, 1973

R. W. Judy, Jr., "Effects of Stress-Corrosion Cracking on Structural Integrity," Seminar at the Naval Ship Engineering Center, Hyattsville, Md., Oct. 30, 1973

W. D. Bascom, "Mechanically Focused Interfacial Failure," Univ. of Wash., St. Louis, Mo., Nov. 29, 1973

T. W. Crooker, "Effects of Natural Seawater and Electrochemical Potential on Fatigue-Crack Growth in 17-4 PH Steels," ASTM Committee E-09 on Fatigue, Bal Harbor, Fla., Dec. 3-5, 1973

T. W. Crooker, "Environmental Aspects of Fracture Mechanics," 1974 WESTEC Conference, Los Angeles, Calif., Mar. 11-15, 1974

W. D. Bascom, "Fracture Behavior of Elastomer-Modified Epoxy Adhesives," Symp. at State-of-the-Art, Inc., Pittsburgh, Pa., May 14, 1974

C. A. Griffis, "Adoption of the J Integral for Fracture Analysis in 2024 and 7005 Aluminum Alloys," Metals Properties Council Semi-Annual Meeting, National Academy of Sciences, Washington, D.C., July 18, 1974

W. D. Bascom, R. L. Cottington, R. L. Jones and P. Peyser, "The Fracture of Epoxy and Elastomer-Modified Epoxy Polymers in Bulk and as Adhesives," ACS Meeting, Atlantic City, N.J., September 1974

W. D. Bascom, "Fracture of Epoxies and Elastomer-Modified Epoxies in Bulk and as Adhesives," 5th Akron Polymer Conf. - Adhesion of Elastomers, Univ. of Akron, Ohio, September 1974

R. W. Judy, Jr., "Crack Growth and Fracture in High-Strength Metals," University of Miami, Miami, Fla., Jan. 27, 1975

W. D. Bascom, "Polyphase Adhesives," 2nd Ann. Symp., Adhesion and Adhesives, Univ. of Pittsburgh, Pa., Feb. 18, 1975

W. D. Bascom, "Adhesive Fracture of Elastomer-Modified Epoxy Resins," Society of the Plastics Industry, Washington, D.C., February 1975

R. W. Judy, Jr., C. A. Griffis, and R. J. Goode, "Fracture Resistance of Thin-Section Aluminum by Dynamic Tear Test Methods," 1975 WESTEC Conference, Los Angeles, Calif., Mar. 10-13, 1975

W. D. Bascom, "Apparent Interfacial Failure of Epoxy Adhesive Resins," 3M Company, St. Paul, Minn., March 12, 1975

W. D. Bascom, "Mixed-Mode Fracture of Structural Adhesives," Symp. on Science and Technology of Adhesion, 169th ACS Meeting, Phil., Pa., April 7, 1975

W. D. Bascom, "Adhesive Fracture," 1975 Design Eng. Conf., ASME, New York, N.Y., April 21, 1975

W. D. Bascom, "Adhesive Fracture Behavior," Union Carbide Corp., Bound Brook, N.J., May 15, 1975

C. A. Griffis, "Elastic-Plastic Fracture Toughness: A Comparison of J Integral and Critical Crack Opening Displacement Characterizations," Second National Congress on Pressure Vessels and Piping Technology, San Francisco, Calif., June 23-27, 1975

P. Shahinian and R. W. Judy, Jr., "Stress-Corrosion Crack Growth in Surface-Cracked Panels of High-Strength Steel," 78th Annual Meeting of ASTM Committee G-01 on Stress Corrosion, Montreal, Canada, June 23-27, 1975

C. T. Fujii, "Stress-Corrosion-Cracking Properties of 17-4 PH Steel," ASTM 78th Annual Meeting, Symposium on Stress Corrosion, Montreal, Canada, June 23-27, 1975

W. D. Bascom, "Adhesive Fracture of Epoxy and Elastomer Epoxy Resins," 4th AMMRC Materials Tech. Conf., Advs. in Joining Technology, Boston, Mass., 17 Sept. 1975

NRL Reports

R. W. Judy, Jr. and R. J. Goode, "Ductile Fracture Equation for High-Strength Structural Metals," NRL Report 7557, April 3, 1973

R. W. Judy, Jr. and C. A. Griffis, "Fracture Extension Resistance of Aluminum Alloys in Thin Sections," NRL Report 7627, Oct. 12, 1973

R. W. Judy, Jr., C. T. Fujii, and R. J. Goode, "Properties of 17-4 PH Steel," NRL Report 7639, Dec. 18, 1973

R. W. Judy, Jr. and R. J. Goode, "Prevention and Control of Subcritical Crack Growth in High-Strength Metals," NRL Report 7780, Aug. 2, 1974

R. W. Judy, Jr. and R. J. Goode, "Standard Method of Test for Plane Strain Stress-Corrosion-Cracking Resistance of Metallic Materials," NRL Report 7865, March 17, 1975

Memorandum Reports

W. R. Cares and T. W. Crooker, "Fatigue-Crack Growth of Ti-6Al-2Cb-1Ta-0.8Mo Alloy in Air and Natural Seawater Environments," NRL Memorandum Report 2617, June 1973

T. W. Crooker and W. R. Cares, "An Exploratory Investigation of Corrosion-Fatigue Crack Growth in HY-130 Base Plate," NRL Memorandum Report 2660, October 1973

F. D. Bogar and C. T. Fujii, "Stress-Corrosion-Cracking Properties of Two Aluminum-Magnesium Alloys," NRL Memorandum Report 2724, January 1974

T. R. Tucker and C. T. Fujii, "Acoustic Emissions and Stress-Corrosion Cracking in High-Strength Alloys," NRL Memorandum Report 2879, August 1974

Correspondence

R. W. Judy, Jr., T. W. Crooker, C. T. Fujii, and W. D. Bascom, "Progress Report - Reliability Criteria for Advances Structural Materials Fast Craft and Ships," Letter Report 6382-5N:RWJ:svs of 15 Jan. 1973

R. W. Judy, Jr., C. A. Griffis, and R. J. Goode, "Fracture Resistance of Thin-Section Materials," Letter Report 6382-41H: RWJ:svs of 2 April 1973

R. W. Judy, Jr., R. J. Goode, and C. T. Fujii, "Investigations of Materials for PHM Strut and Foil Applications," Letter Report 6382-59N:RWJ:svs of 25 April 1973

A. M. Sullivan and J. Stoop, "Fracture Resistance K_c of the Metal Matrix Composite: Aluminum-Boron, "Letter Report 6383-93N:AMS:rp of 18 June 1973

W. R. Cares and T. W. Crooker, "Corrosion-Fatigue Crack Propagation in Ti-6Al-2Cb-1Ta-0.8Mo in Natural Seawater," Letter Report 6384-97N:TWC:rp of 25 June 1973

R. W. Judy, Jr., T. W. Crooker, C. T. Fujii, A. M. Sullivan, J. V. Gauchel, and W. D. Bascom, "Annual Report - Reliability Criteria for Advanced Structural Materials/Fast Craft and Ships," Letter Report 6382-101N:RWJ:svs of 13 July 1973

R. W. Judy, Jr., C. A. Griffis, and R. J. Goode, "Fracture Resistance of a Thin-Section Titanium Alloy," Letter Report 6382-128N:RWJ:mr of 6 September 1973

T. W. Crooker and W. R. Cares, "Preliminary Results of Corrosion-Fatigue Crack Propagation Studies on 17-4 PH Steels in Natural Seawater," Letter Report 6384-132N:TWC:mr of 10 September 1973

R. W. Judy, Jr., "Fracture Resistance Tests of 17-4 PH Weld Metals," Letter Report 6382-146N:RWJ:mr of 26 September 1973

W. R. Cares and T. W. Crooker, "Corrosion-Fatigue Crack Propagation in HY-130 Steel in Natural Seawater," Letter Report 6384-150N:TWC:mr of 27 September 1973

C. T. Fujii, "SCC Properties of Freely Corroding and Coupled 5Ni-Cr-Mo Steel Plate in 3-1/2% NaCl Solution," NRL ltr 6385-175N:CTF:clt of 20 November 1973

F. D. Bogar and C. T. Fujii, "Stress-Corrosion-Cracking Properties of Two Aluminum-Magnesium Alloys," Letter Report 6385-185N:FDB:clt of 6 December 1973

T. W. Crooker, "Progress Report - Reliability Criteria for Advanced Structural Materials/Fast Craft and Ships," Letter Report 6382-9N:TWC:mr of 17 January 1974

R. W. Judy, Jr. and C. A. Griffis, "Characterization of Thin-Section Aluminum Alloys by Structural Element Tests," Letter Report 6382-21N:RWJ:mr of 29 January 1974

R. W. Judy, Jr. and R. J. Goode, "Fracture Resistance of Titanium Alloys Ti-6Al-4V and Ti-6Al-6V-2.5Sn in Thin Sections," Letter Report 6382-23N:RWJ:mr of 14 Feb. 1974

D. F. Hasson and T. W. Crooker, "Fatigue-Crack Growth Resistance of Air-Melted and Vacuum-Melted 17-4 PH Steels," Letter Report 6384-29N:TWC:mr of 25 Feb. 1974

R. W. Judy, Jr., "Stress Corrosion Crack Growth in Part-Through Cracked Specimens for 17-4 PH Steel," Letter Report 6382-50N:RWJ:mr of 27 March 1974

R. W. Judy, Jr., "Fracture Properties of Heat Treated Weld Metal of 17-4 PH Steels," Letter Report 6382-91N:RWJ:mr of 10 May 1974

T. W. Crooker, D. F. Hasson, and G. R. Yoder, "Fractographic Observations of Fatigue-Crack Growth in Air-Melted and Vacuum Melted 17-4 PH Steels," Letter Report 6384-114N:TWC:mr of 18 June 1974

R. W. Judy, Jr. and C. A. Griffis, "Fracture Resistance Tests of 17-4 PH Direct-Aged Weld Metal Samples," Letter Report 6382-118N:RWJ:mr of 11 June 1974

T. R. Tucker and C. T. Fujii, "Acoustic Emissions and Stress-Corrosion Cracking in High-Strength Alloys," Letter Report 6385-144N:CTF:svs of 26 July 1974

R. W. Judy, Jr. and R. J. Goode, "Fracture Resistance Properties of Thin-Section Steels," Letter Report 6382-183N:RWJ:mr of 26 September 1974

R. W. Judy, Jr., "Fracture Resistance Properties of HY-180 Steel for Aircraft/Fast Craft and Ship Applications," Letter Report 6382-6N:RWJ:cm of 9 January 1975

C. T. Fujii, "Stress-Corrosion-Cracking Properties of a 17-4 PH Steel GMA Weldment," Letter Report 6385-5N:CTF:svs of 13 January 1975

C. T. Fujii, "Specimen Geometry Effects on Stress-Corrosion-Cracking Testing," Letter Report 6385-56N:CTF:svs of 6 May 1975

C. T. Fujii, "Stress-Corrosion-Cracking Properties of 17-4 PH Steel," Letter Report 6385-61N:CTF:svs of 9 May 1975

Report of NRL Progress

C. T. Fujii and R. L. Newbegin, "Electrochemical Protection Technology/Marine Environment Crack Growth," Report of NRL Progress, pp. 47-48, Aug. 1973

F. D. Bogar, "Effect of Applied Cathodic Potentials on the Stress Corrosion Cracking of Ti-8Al-1Mo-1V Alloy in 3.5% NaCl Solution," Report of NRL Progress, pp. 45-46, Nov. 1973

C. T. Fujii, "SCC Properties of Freely Corroding and Coupled 5Ni-Cr-Mo Steel Plate in 3-1/2% NaCl Solution," Report of NRL Progress, pp. 47-48, Nov. 1973

C. T. Fujii, "Electrochemical Aspects of Stress-Corrosion Cracking - Recent SCC Studies on High-Strength Steels," Report NRL Progress (Lead Article), pp. 21-28, June 1974

J. A. Smith, "Studies on the Cracking Kinetics of Quench and Tempered Steel," Report of NRL Progress, Aug. 1974

C. T. Fujii, "Stress Corrosion Cracking Properties of a 17-4 PH Steel GMA Weldment," Report of NRL Progress, submitted for publication, Jan. 1975

C. T. Fujii, "Specimen Geometry Effects on Stress Corrosion Cracking Testing," Report of NRL Progress, pp. 26-28, May 1975

APPENDIX

PRINCIPLES FOR FRACTURE-SAFE DESIGN OF NAVAL STRUCTURES

Outline of Short Course - NAVSHIPENGCEN

SESSION NO.

1. **Introduction to Fracture-Safe Design Problems - Linear Elastic Fracture Mechanics**

   Concepts of classical linear elastic fracture mechanics and mechanical constraint will be presented in simplified graphical form; laboratory test specimens and procedures will be described.

   Reference: ASTM STP 381, 410

2. **Definition of Principal Engineering Fracture Test Methods and Significance of Each**

   An overview is presented of the general design features of principal engineering fracture toughness tests, including the Charpy V-notch (C_V), Robertson Crack Arrest, Drop-Weight (DW), Dynamic Tear (DT) and K_{Ic}. The role of these tests in interpreting the brittle-ductile transition will be described, and comparisons of crucial features required for accurate definition of specific fracture states will be made for the different test methods.

   Reference: NRL Reports 6957, 6975

3. **Fracture Control Procedures for Low and Intermediate Strength Steels - Fracture Analysis Diagram**

   Procedures for fracture control within plane strain, elastic-plastic and plastic fracture states will be discussed, and their application to solution of engineering problems will be presented for steels featuring temperature transition behavior.

   Reference: NRL Reports 6957, 5920

4. **Role of Mechanical Constraint With Respect to Fracture-Safe Assurance**

   Thickness-induced mechanical constraint expands the temperature regime that defines brittle behavior and shifts the brittle-ductile transition to higher temperatures within well-defined limits. Comparisons

of K_{Ic} and DT energy toughness trends will be made, and the significance of statistical variations in toughness will be discussed.

Reference: NRL Reports 6957, 6913

5. Metallurgical Aspects of Fracture for Low and Intermediate Strength Steels

Metallurgical factors such as chemical composition and heat treatment influence significantly the fracture resistance characteristics of temperature transition steels. These effects will be discussed as they relate to critical aspects of temperature transition features for selected steels.

Reference: NRL Reports 6975, 6900

6. RAD Procedures for Fracture-Safe Design With High and Ultrahigh Strength Steels

The fracture mechanics concepts for defining the three fracture states (linear elastic, elastic-plastic, plastic) will be presented. Application of RAD procedures to the trade-offs between materials, design refinement, and inspection procedures will be emphasized.

Reference: NRL Report 7406

7. RAD Procedures for Fracture-Safe Design With Non-Ferrous Materials

Fracture mechanics concepts developed in prior lectures will be applied to high-strength titanium and aluminum alloy systems.

Reference: NRL Report 7281

8. Effects of Stress-Corrosion Cracking on Structural Integrity

Procedures based on linear elastic fracture mechanics concepts for establishing the stress-corrosion-cracking resistance (K_{Iscc}) of structural metals will be described. RAD procedures for interpretation of the K_{Iscc} test results for stress-corrosion cracking will be presented.

Reference: NRL Report 7371

9. Basic Aspects of Fatigue Crack Propagation

Basic laws governing fatigue crack growth in terms of linear elastic fracture mechanics parameters will be presented.

Reference: NRL Report 7422

10. Application of Fatigue Crack Growth Technology to Design of Naval Structures

A presentation of Navy fatigue problems and design of structures for finite life cycles based on crack growth laws will be made.

11. NAVSHIPENGCEN Structures Department Presentation

12. NAVSHIPENGCEN Structures Department Presentation

13. Application of Code Requirements to Fracture-Safe Assurance

ASTM, ABS, MIL Specifications and ASME Boiler and Pressure Vessel Code will be reviewed. Emphasis will be placed on the ability of codes to define a fixed level of toughness. The question of sufficient toughness versus structural performance requirements will be considered.

Reference: NRL Report 7406, WRC Bulletin 186

14. Review of Course